Wen, Cindy, Margolis, Michael, Dai, Rujia, Zhang, Pan, Przytycki, Pawel F., Vo, Daniel D., Bhattacharya, Arjun, Matoba, Nana, Tang, Miao, Jiao, Chuan, Kim, Minsoo, Tsai, Ellen, Hoh, Celine, Aygün, Nil, Walker, Rebecca L., Chatzinakos, Christos, Clarke, Declan, Pratt, Henry, Peters, Mette A., Gerstein, Mark, Daskalakis, Nikolaos P., Weng, Zhiping, Jaffe, Andrew E., Kleinman, Joel E., Hyde, Thomas M., Weinberger, Daniel R., Bray, Nicholas J. , Sestan, Nenad, Geschwind, Daniel H., Roeder, Kathryn, Gusev, Alexander, Pasaniuc, Bogdan, Stein, Jason L., Love, Michael I., Pollard, Katherine S., Liu, Chunyu, Gandal, Michael J., Akbarian, Schahram, Abyzov, Alexej, Ahituv, Nadav, Arasappan, Dhivya, Almagro Armenteros, Jose Juan, Beliveau, Brian J., Bendl, Jaroslav, Berretta, Sabina, Bharadwaj, Rahul A., Bicks, Lucy, Brennand, Kristen, Capauto, Davide, Champagne, Frances A., Chatterjee, Tanima, Chatzinakos, Chris, Chen, Yuhang, Chen, H. Isaac, Cheng, Yuyan, Cheng, Lijun, Chess, Andrew, Chien, Jo-fan, Chu, Zhiyuan, Clement, Ashley, Collado-Torres, Leonardo, Cooper, Gregory M., Crawford, Gregory E., Davila-Velderrain, Jose, Deep-Soboslay, Amy, Deng, Chengyu, DiPietro, Christopher P., Dracheva, Stella, Drusinsky, Shiron, Duan, Ziheng, Duong, Duc, Dursun, Cagatay, Eagles, Nicholas J., Edelstein, Jonathan, Emani, Prashant S., Fullard, John F., Galani, Kiki, Galeev, Timur, Gaynor, Sophia, Girdhar, Kiran, Goes, Fernando S., Greenleaf, William, Grundman, Jennifer, Guo, Hanmin, Guo, Qiuyu, Gupta, Chirag, Hadas, Yoav, Hallmayer, Joachim, Han, Xikun, Haroutunian, Vahram, Hawken, Natalie, He, Chuan, Henry, Ella, Hicks, Stephanie C., Ho, Marcus, Ho, Li-Lun, Hoffman, Gabriel E., Huang, Yiling, Huuki-Myers, Louise A., Hwang, Ahyeon, Iatrou, Artemis, Inoue, Fumitaka, Jajoo, Aarti, Jensen, Matthew, Jiang, Lihua, Jin, Peng, Jin, Ting, Jops, Connor, Jourdon, Alexandre, Kawaguchi, Riki, Kellis, Manolis, Kleopoulos, Steven P., Kozlenkov, Alex, Kriegstein, Arnold, Kundaje, Anshul, Kundu, Soumya, Lee, Cheyu, Lee, Donghoon, Li, Junhao, Li, Mingfeng, Lin, Xiao, Liu, Shuang, Liu, Jason, Liu, Jianyin, Liu, Shuang, Lou, Shaoke, Loupe, Jacob M., Lu, Dan, Ma, Shaojie, Ma, Liang, Mariani, Jessica, Martinowich, Keri, Maynard, Kristen R., Mazariegos, Samantha, Meng, Ran, Myers, Richard M., Micallef, Courtney, Mikhailova, Tatiana, Ming, Guo-li, Mohammadi, Shahin, Monte, Emma, Montgomery, Kelsey S., Moore, Jill E., Moran, Jennifer R., Mukamel, Eran A., Nairn, Angus C., Nemeroff, Charles B., Ni, Pengyu, Norton, Scott, Nowakowski, Tomasz, Omberg, Larsson, Page, Stephanie C., Park, Saejeong, Patowary, Ashok, Pattni, Reenal, Pertea, Geo, Phalke, Nishigandha, Pinto, Dalila, Pjanic, Milos, Pochareddy, Sirisha, Pollen, Alex, Purmann, Carolin, Qin, Zhaohui S., Qu, Ping-Ping, Quintero, Diana, Raj, Towfique, Rajagopalan, Ananya S., Reach, Sarah, Reimonn, Thomas, Ressler, Kerry J., Ross, Deanna, Roussos, Panos, Rozowsky, Joel, Ruth, Misir, Ruzicka, W. Brad, Sanders, Stephan J., Schneider, Juliane M., Scuderi, Soraya, Sebra, Robert, Seyfried, Nicholas, Shao, Zhiping, Shedd, Nicole, Shieh, Annie W., Shin, Joo Heon, Skarica, Mario, Snijders, Clara, Song, Hongjun, State, Matthew W., Steyert, Marilyn, Subburaju, Sivan, Sudhof, Thomas, Snyder, Michael, Tao, Ran, Therrien, Karen, Tsai, Li-Huei, Urban, Alexander E., Vaccarino, Flora M., van Bakel, Harm, Voloudakis, Georgios, Wamsley, Brie, Wang, Tao, Wang, Sidney H., Wang, Daifeng, Wang, Yifan, Warrell, Jonathan, Wei, Yu, Weimer, Annika K., Whalen, Sean, White, Kevin P., Willsey, A. Jeremy, Won, Hyejung, Wong, Wing, Wu, Hao, Wu, Feinan, Wuchty, Stefan, Wylie, Dennis, Xu, Siwei, Yap, Chloe X., Zeng, Biao, Zhang, Chunling, Zhang, Bin, Zhang, Ji[illegible]g, Yanqiong, Zhou, Xiao, Ziffra, Ryan, Zeier, Zane R. and Zintel, Trisha M. 2024. Cross-ancestry a[illegible]ene, isoform, and splicing regulation in the developing human brain. Science 384 (6698) , eadh0829. 10.1126/science.adh0829

Cross-ancestry atlas of gene, isoform, and splicing regulation in the developing human brain

Authors: Cindy Wen[1,2,3], Michael Margolis[2,3], Rujia Dai[4], Pan Zhang[2,3], Pawel F. Przytycki[5], Daniel D. Vo[2,3,6,7], Arjun Bhattacharya[8,9], Nana Matoba[10,11], Miao Tang[6,7], Chuan Jiao[4], Minsoo Kim[2,3], Ellen Tsai[2,3], Celine Hoh[2,3], Nil Aygün[10,11], Rebecca L. Walker[1,2,3], Christos Chatzinakos[12,13,14], Declan Clarke[15], Henry Pratt[16], PsychENCODE Consortium, Mette A. Peters[17], Mark Gerstein[15,18,19,20], Nikolaos P. Daskalakis[12,13,14], Zhiping Weng[16], Andrew E. Jaffe[21,22,23,24,25,26,27], Joel E. Kleinman[21,22], Thomas M. Hyde[21,22,28], Daniel R. Weinberger[21,22,23,24,28], Nicholas J. Bray[29], Nenad Sestan[30,31], Daniel H. Geschwind[3,32,33], Kathryn Roeder[34,35], Alexander Gusev[36,37,38,39], Bogdan Pasaniuc[1,3,8,33,40], Jason L. Stein[10,11], Michael I. Love[10,41], Katherine S. Pollard[5,42,43], Chunyu Liu[4,44*], Michael J. Gandal[1,2,3,6,7*]

Affiliations:

[1]*Interdepartmental Program in Bioinformatics, University of California, Los Angeles; Los Angeles, CA, 90095, USA*
[2]*Department of Psychiatry, David Geffen School of Medicine, University of California, Los Angeles; Los Angeles, CA, 90095, USA*
[3]*Department of Human Genetics, David Geffen School of Medicine, University of California, Los Angeles; Los Angeles, CA, 90095, USA*
[4]*Department of Psychiatry, SUNY Upstate Medical University; Syracuse, NY, 13210, USA*
[5]*Gladstone Institute of Data Science and Biotechnology; San Francisco, CA, 94158, USA*
[6]*Department of Psychiatry, Perelman School of Medicine, University of Pennsylvania; Philadelphia, PA, 19104, USA*
[7]*Lifespan Brain Institute, The Children's Hospital of Philadelphia; Philadelphia, PA, 19104, USA*
[8]*Department of Pathology and Laboratory Medicine, David Geffen School of Medicine, University of California, Los Angeles; Los Angeles, CA, 90095, USA*
[9]*Institute for Quantitative and Computational Biosciences, David Geffen School of Medicine, University of California, Los Angeles; Los Angeles, CA, 90095, USA*
[10]*Department of Genetics, University of North Carolina at Chapel Hill; Chapel Hill, NC, 27599, USA*
[11]*UNC Neuroscience Center, University of North Carolina at Chapel Hill; Chapel Hill, NC, 27599, USA*
[12]*Department of Psychiatry, Harvard Medical School; Boston, MA, 02215, USA*
[13]*McLean Hospital; Belmont, MA, 02478, USA*
[14]*Stanley Center for Psychiatric Research, Broad Institute of MIT and Harvard; Cambridge, MA, 02142, USA*
[15]*Department of Molecular Biophysics and Biochemistry, Yale University; New Haven, CT, 06520, USA*
[16]*Program in Bioinformatics and Integrative Biology, University of Massachusetts Medical School; Worcester, MA, 01605, USA*
[17]*CNS Data Coordination Group, Sage Bionetworks; Seattle, WA, 98109, USA*
[18]*Program in Computational Biology and Bioinformatics, Yale University; New Haven, CT, 06520, USA*
[19]*Department of Computer Science, Yale University; New Haven, CT, 06520, USA*
[20]*Department of Statistics and Data Science, Yale University; New Haven, CT, 06520, USA*
[21]*Lieber Institute for Brain Development; Baltimore, MD, 21205, USA*
[22]*Department of Psychiatry & Behavioral Sciences, Johns Hopkins University School of Medicine; Baltimore, MD, 21205, USA*
[23]*Department of Neuroscience, Johns Hopkins University School of Medicine; Baltimore, MD, 21205, USA*
[24]*Department of Genetic Medicine, Johns Hopkins University School of Medicine; Baltimore, MD, 21205, USA*
[25]*Department of Mental Health, Johns Hopkins Bloomberg School of Public Health; Baltimore, MD, 21205, USA*
[26]*Department of Biostatistics, Johns Hopkins Bloomberg School of Public Health; Baltimore, MD, 21205, USA*
[27]*Neumora Therapeutics; Watertown, MA, 02472, USA*
[28]*Department of Neurology, Johns Hopkins University School of Medicine; Baltimore, MD, 21205, USA*
[29]*MRC Centre for Neuropsychiatric Genetics & Genomics, Division of Psychological Medicine & Clinical Neurosciences, Cardiff University School of Medicine; Cardiff, CF24 4HQ, UK*
[30]*Department of Comparative Medicine, Yale University School of Medicine; New Haven, CT, 06520, USA*
[31]*Department of Neuroscience, Yale University School of Medicine; New Haven, CT, 06520, USA*
[32]*Program in Neurogenetics, Department of Neurology, David Geffen School of Medicine, University of California, Los Angeles; Los Angeles, CA, 90095, USA*
[33]*Institute for Precision Health, University of California, Los Angeles; Los Angeles, CA, 90095, USA*

[34]*Department of Statistics & Data Science, Carnegie Mellon University; Pittsburgh, PA, 15213, USA*
[35]*Computational Biology Department, Carnegie Mellon University; Pittsburgh, PA, 15213, USA*
[36]*Department of Medical Oncology, Division of Population Sciences, Dana-Farber Cancer Institute; Boston, MA, 02215, USA*
[37]*Broad Institute of MIT and Harvard; Cambridge, MA, 02142, USA*
[38]*Harvard Medical School; Boston, MA, 02215, USA*
[39]*Division of Genetics, Brigham and Women's Hospital; Boston, MA, 02215, USA*
[40]*Department of Computational Medicine, David Geffen School of Medicine, University of California, Los Angeles; Los Angeles, CA, 90095, USA*
[41]*Department of Biostatistics, University of North Carolina at Chapel Hill; Chapel Hill, NC, 27599, USA*
[42]*Department of Epidemiology & Biostatistics, University of California, San Francisco; San Francisco, CA, 94158, USA*
[43]*Chan Zuckerberg Biohub; San Francisco, CA, 94158, USA*
[44]*Center for Medical Genetics & Hunan Key Laboratory of Medical Genetics, School of Life Sciences, Central South University; Changsha, Hunan, 410008, China*

Abstract:

Neuropsychiatric genome-wide association (GWAS) studies, including for autism, schizophrenia, and bipolar disorder, are strongly enriched for genomic regulatory elements in the developing brain. However, prioritizing candidate risk genes and mechanisms is challenging without a unified regulatory atlas. Across 672 diverse developing human brain samples, we identified 15,752 genes harboring gene, isoform, and/or splicing quantitative trait loci (xQTLs) and mapped 3,739 QTLs to cellular contexts. Gene expression heritability drops during brain development, likely reflecting both increasing cellular heterogeneity as well as intrinsic properties of neurons as they mature. Isoform-level regulation, particularly in the second trimester, mediated the largest proportion of GWAS heritability. Via colocalization, we prioritized candidate mechanisms for ~60% of GWAS loci across disorders, exceeding adult brain findings. Finally, we contextualized results within gene/isoform co-expression networks, revealing the comprehensive landscape of genetic regulation in development and disease.

One-sentence Summary:

This study provides xQTL maps of the developing human brain and uncovers candidate neuropsychiatric risk mechanisms.

Main Text

Thousands of genetic risk loci have been robustly associated with neurodevelopmental and psychiatric disorders by large-scale genome-wide association studies (GWAS) (*1*, *2*). However, as most associated GWAS variants reside within non-coding regions of the human genome, often in large linkage disequilibrium (LD) blocks, the true underlying causal variant(s) and their target gene(s) remain largely unknown. Consequently, the critical defining obstacle of the post-GWAS era is to pinpoint the specific, locus-level molecular impact of GWAS variants at scale (*3*). As risk loci are enriched in regulatory regions of the human genome (*4–6*), one major approach to address this challenge has been to connect risk variants with tissue-specific reference panels of gene expression quantitative trait loci (eQTLs), through statistical colocalization, transcriptome-wide association (TWAS), and related approaches (*7–9*). This has prompted several large-scale efforts (*10–16*) to generate comprehensive functional genomic compendia connecting population-level allelic variation with gene expression profiles in the human brain. Yet, while these resources have provided biologically interpretable and meaningful annotations for dozens of neuropsychiatric risk loci, the majority remain mechanistically unannotated (*15*, *17*).

Gene regulation is highly dependent on the specific underlying developmental stage, tissue, and cellular context (*7*, *17–20*), and increasing evidence implicates the developing human brain in the genetic risk for neuropsychiatric disorders, including autism spectrum disorder (ASD) and schizophrenia (SCZ) (*21–23*). Consequently, several efforts have begun to characterize the genetic control of gene expression during human brain development, finding that gene regulation is tightly controlled during brain development and enriched for neuropsychiatric risk (*11*, *12*, *24–28*). However, as these studies are individually small, the power to pinpoint the developmental timing or elucidate the full extent of gene regulation in the developing human brain has been limited.

The regulation of transcript-isoform structure and diversity, through alternative local splicing and differences in transcriptional start and termination sites, is also known to be a mechanism critical for human brain development that is implicated in disease pathogenesis (*14*, *29–32*). Indeed, relative to other tissues and species, the landscape of alternative splicing is particularly extensive in the human brain, and its regulation is notably distinct from that of gene expression (*16*, *33*). While individual studies have begun to investigate splicing and isoform QTLs (s/iso-QTLs) in the developing brain (*24*, *25*), a lack of uniform data processing has precluded a systematic characterization of these critical mechanisms and their potential relationships with genetic risk factors for neuropsychiatric disorders.

To address these critical gaps, here we present a comprehensive investigation into the genetic regulation of the transcriptome during human brain development by uniformly processing data from 672 distinct samples spanning 4-39 post-conception weeks (PCW), most of which are within the first and second trimesters. The full integrated dataset is highly diverse, comprising several major continental ancestries including European (EUR; 45%), Hispanic/Latino (AMR; 25%), African (AFR; 22%), and East Asian/Southeast Asian (EA/SEA; 8%). This well-powered, cross-ancestry resource provides an extensive view of the developmental timing and regulatory landscape of human brain development at gene, isoform, and splicing levels. We observed a substantial drop in the heritability of gene expression and local splicing with development, particularly from 10 to 18 PCW). Yet, psychiatric GWAS signals were more concentrated within the second trimester. We found that isoform-level regulation mediated substantially more psychiatric GWAS heritability than gene regulation. We prioritized candidate risk genes and molecular mechanisms for ~60% of GWAS loci across five neuropsychiatric disorders, with ~2-fold more colocalizations observed compared with larger adult brain functional genomic reference panels. Finally, we contextualized these risk mechanisms within a comprehensive set of gene and isoform-level co-expression networks across fetal brain development. Results can be visualized at devbrainhub.gandallab.org.

Large-Scale Functional Genomic Interrogation of Human Brain Development

Here, we present a comprehensive investigation of gene expression, splicing, and isoform regulation during human brain development by integrating data across five individual cohorts (*12*, *24–27*) (**Fig. S1**) comprising 672 distinct donors. Following uniform data processing, including imputation into the multi-ancestry TOPMed reference panel (*34*), and strict quality control (*35*) (**Fig. S2**), we retained 654 samples with matched genotype and cortical RNA-sequencing data spanning 4-39 PCW, the majority falling within the first two trimesters (Tri1, N = 216; Tri2, N = 433; **Table S1**). Altogether, our large sample size enabled detection of 10,094 genes with at least one *cis*-eQTL at FDR < 0.05 (termed "eGenes"), following permutation-based and FDR correction for multiple comparisons while accounting for local LD structure **(Fig. 1A**; **Fig. S3**; **Table S1**; (*35*)).

Compared with adult brain eQTL datasets from PsychENCODE (N = 1,387) (*13*, *14*) and GTEx (N = 205) (*16*), we identified 2,488 "fetal-specific" eGenes in this dataset (**Fig. 1B; Table S1**). Among eQTL-eGene pairs conserved between the developing and adult human brain cohorts, we observed substantial consistency in effect size as measured by allelic fold change (GTEx: Spearman rho = 0.93, P < 2.2e-16; PsychENCODE: Spearman rho = 0.89, P < 2.2e-16; **Fig. 1C**; **Fig. S3**). Notably, these 2,488 fetal-specific eGenes were significantly more intolerant to loss-of-function mutations, as measured by the pLI score (*36*), compared with eGenes shared between fetal and adult timepoints (Wilcoxon P < 2e-16; **Fig. S4**), suggesting that these context-specific annotations may be more relevant for interpretation of neuropsychiatric GWAS signals, which are under negative selection (*37*, *38*). These fetal-specific eGenes were enriched for spliceosomal pathways and cell-type-specific marker genes (*39*) for a subtype of ventricular radial glia (OR 3.3, FDR-corrected P = 0.054, Fisher's exact test; **Fig. S4**; **Table S1**).

Dysregulation of RNA splicing has been strongly implicated in complex disease risk (*29*) as well as alterations in brain development (*24*). To systematically investigate RNA splicing regulation in the developing human brain, we used two complementary approaches. First, guided by existing GENCODE reference transcriptome annotations (*40*), we imputed isoform expression from short-read RNA-seq using Salmon (*41*). Second, we profiled local alternative splicing events via LeafCutter (*42*), an annotation-free method that quantifies intron excision ratios. Next, we identified genetic variants that are associated with these isoform- and splicing-level quantitative traits (**Fig. S5**; **Fig. S6**; (*35*)), identifying 11,845 and 7,490 genes harboring a *cis*-isoQTL or sQTL at FDR-corrected P < 0.05 (termed "isoGenes" and "sGenes"; **Table S1**), respectively. Among the identified xQTL containing-genes, 3,740 are shared, and 2,312/1,891 only have QTLs detected at isoform/local splicing levels (**Fig. 1D**). As expected, *cis*-xQTLs are strongly clustered near their target genes' transcription start site (TSS) (**Fig. 1E**) and are correspondingly enriched in functional regions of the genome (**Fig. 1F**; **Table S1**). Of note, e/iso/sQTLs are significantly differentially enriched in promoter and splicing regions (P < 0.05 with Bonferroni correction; **Table S1**). In addition, we observed that isoGenes and sGenes are more intolerant to loss-of-function mutations than eGenes (**Fig. 1G**). To investigate the variant-level overlap among *cis*-e/iso/sQTLs, we calculated the pairwise Storey's pi1 statistic (*43*) that measures the proportion of *cis*-e/iso/sQTLs in the "Discovery" group (permutation qvalue < 0.05) that also exhibit true associations in the "Replication" group (nominal P-values from all association pairs). We found that genetic variants directly associated with RNA splicing (especially isoQTL) capture orthogonal signals from eQTLs (**Fig. 1H**; (*35*)). Lastly, to investigate the potential impact of the different library preparations and sequencing depth of the individual sub-studies, we remapped sQTLs in the Walker (*24*) and HDBR (*27*) datasets using our uniform processing pipeline. We observed a high replication rate of our full sQTL results within each individual dataset (Walker pi1=0.93; HDBR pi1=0.89), indicating that the splicing regulation detected in our combined analysis was robust to these potential technical factors.

We next sought to characterize the extent of allelic heterogeneity in the developing human brain, in which multiple causal variants regulate gene expression at a given locus. Through stepwise conditional QTL mapping (*44*) (**Fig. S3; Table S1;** (*35*)), we identified multiple independent regulatory signals for 3,570 eGenes in the fetal brain, with some exhibiting up to 10 groups of conditionally independent *cis*-eQTL signals. As expected, the primary *cis*-eQTL signal (median -0.0340 kb) was closer to the corresponding target gene's TSS than was the secondary *cis*-eQTL signal (median 0.4820 kb; Wilcoxon rank sum P-value < 2.2e-16). The same was also true for tertiary and higher-rank *cis*-eQTL signals. As an orthogonal

approach, we also performed statistical fine-mapping with SuSiE (*45*), which estimates credible sets (CS) of causal variants. The number of SuSiE-estimated CS was highly concordant with the number of conditionally independent QTL signals for each eGene (Spearman rho 0.66, P-value < 2.2e-16; **Fig. 1I**), indicating that fine-mapping is a complementary approach to conditional QTL mapping for detecting independent regulatory signals. Each CS prioritized a median of 5 SNPs, with 2,423 containing exactly one SNP, which are strong candidates for functional validation (extended data can be accessed at https://doi.org/10.7303/syn50897018.5).

Compared to SNPs and indels, the impact of other classes of genetic variation, such as structural variants, on downstream gene expression remains underexplored. Nevertheless, complex structural variants such as large recurrent inversions have known associations with brain-relevant traits and can impact gene expression extensively (*25*, *46*). To address this, we imputed the genotypes of 17 common (MAF > 0.05) inversions into our uniformly processed fetal brain data and quantified their effects on gene expression across the transcriptome. Longer inversions are more likely to affect downstream gene expression. We found 49 inversion-associated expression quantitative loci (Inv-eQTLs) both in *cis* and in *trans*, for four of the inversions located at 17q21.31, 16p11.2, 7q11.22 and 8p23.1 (**Fig. 1J**; **Fig. S7**; **Table S1**; (*35*)).

Cross-Ancestry Gene Regulation and Fine-mapping

Differences in genetic variation (for example, allele frequency and LD) across ancestries (*47*) have the potential to increase power for statistical fine-mapping (*48*, *49*). After filtering and imputing the genotype data (**Fig. S2**; (*35*)), we inferred genetic ancestries in the fetal brain samples in reference to the 1000 Genomes (*47*). Of the 654 samples, 292 (44.6%) were labeled as "European" (EUR), 164 (25.1%) as "Hispanic/Latino" (AMR), 145 (22.2%) as "African" (AFR), 29 (4.4%) as "Southeast Asian" (SEA), and 24 (3.7%) as "East Asian" (EA) (**Fig. 2A**; **Fig. S1**; **Table S1**). Following the multi-ancestry QTL mapping pipeline, we independently mapped xQTLs in the three largest ancestry groupings: EUR, AMR, and AFR. 986 eGenes were shared between the multi-ancestry dataset and the three ancestry groupings (**Fig. 2B; Table S2**). Among the shared eGene-eQTL pairs between ancestries, we observed a highly consistent effect size measured by allelic fold change (*50*) (AMR-EUR Spearman correlation = 0.97, P-value < 2.2e-16; AFR-EUR Spearman correlation = 0.97, P-value < 2.2e-16; **Fig. 2C**). We then performed statistical fine-mapping separately in the ancestry groupings (*45*), and showed that AFR, despite having the smallest sample size, has on average the smallest credible sets (CS) of causal variants (**Fig. 2D**). Next, we found that the multi-ancestry dataset substantially reduced the CS size. Taking gene *MTFR1* as an example (**Fig. 2E**), we show that the gain in fine-mapping resolution is not solely due to larger sample size, but the potential of multi-ancestry data to leverage distinct patterns of LD. *MTFR1* has complex LD structure in EUR and AMR, reflected in its large CS (EUR n=49, AMR n=57), whereas in AFR, with simpler LD, the CS is only 9 variants. CS sizes are further reduced in multi-ancestry fine-mapping (n=5), and in a *trans*-ancestry fine-mapping framework that leverages functional annotation (*51*, *52*) (n=3). With these results, we highlight the promise of multi-ancestry data in refining statistical fine-mapping.

Trimester-Specific Genetic Regulation

Previous work has implicated the mid-fetal period of human brain development as a critical window convergently impacted by multiple distinct rare genetic risk factors for ASD and SCZ (*21–23*). Although common variant-mediated gene regulation is also known to be dependent on developmental context, this has not been systematically evaluated in the developing human brain. To address this critical gap, we conducted trimester-specific analyses to investigate the specificity of genetic regulation during distinct periods of brain development. We called QTLs after first separating samples into similarly powered trimester 1 (4-13 PCW; EUR, N = 143) and trimester 2 (14-26 PCW; EUR, N = 145) windows, although there were too few samples in trimester 3 (N = 4) to conduct a similar analysis. We identified almost two-fold more trimester 1 eGenes ('Tri1'; n=4,211) than Tri2 (n=2,220), with 1,261 eGenes shared between the two trimesters (**Fig. 3A-B; Fig. S8; Table S3**). Splicing regulation showed a similar pattern with >2 fold more sGenes in Tri1 (n=5,312) than Tri2 (n=2,318; **Fig. 3A**).

To further explore this unexpected result, we next calculated the *cis*-window SNP-based heritability (*cis*-h^2_{SNP}) for gene expression -- a related measure that is more robust to sample size variation -- in Tri1 and Tri2 samples, as well as in adult samples from PsychENCODE (N = 1,387). Mirroring eQTL results, we found that *cis* heritability drops significantly from Tri1 to Tri2, with higher *cis*-h^2_{SNP} in both Tri1 and Tri2 compared with adult brain samples (all P's < 2.2e-8, Wilcoxon; **Fig. 3C**; **Table S3**). We next sought to determine whether a particular developmental inflection point could contextualize this drop in heritability. To address this, we rank ordered samples by PCW, and performed a sliding window analysis of *cis*-h^2_{SNP} across development in equally powered batches (N = 150). We again observed a striking linear drop in *cis*-h^2_{SNP} across the entire range from 10-18 weeks (**Fig. 3D).** There were no detectable differences in the number of conditionally independent eQTLs (**Fig. S8**), levels of gene expression, or phenotypic variance across Tri1 and Tri2 that could be driving these results (**Fig. S9**). To determine whether these observations extended beyond gene expression, we conducted similar analyses using sQTLs, as local splicing event quantifications are highly distinct from expression (*29*). Here again, we observed a significant drop in local splicing heritability from Tri1 to Tri2 (P<2e-16, Wilcoxon), with a linear drop from 10-18 weeks (**Fig. 3C, D; Fig. S8; Table S3**).

We next sought to investigate potential biological explanations for these observed, stage-specific properties of developmental gene regulation. We first assessed whether Tri1/Tri2 eGenes were differentially enriched among specific gene biotypes, observing a significant shift from non-coding to protein-coding biotypes (chi-square = 37.1, df = 9, P-value = 2.5e-5; **Fig. 3E**). However, the heritability drop remained significant when restricted to protein-coding genes, suggesting that coding-status was not the primary driver of these findings (**Fig. S8**). The 10-20 PCW period is also coincident with a shift in cell-type proportion from neural progenitor cells (NPCs) to distinct classes of migrating and maturing excitatory neurons. As such, we hypothesized that the observed decrease in heritability could reflect genetic regulation in specific cell types as their proportions become more heterogeneous. To assess this, we deconvoluted bulk gene expression using a reference panel of cell-type specific marker genes derived from a meta-analysis of 2.95M single cells/nuclei from the developing human brain (*53*, *54*). As expected, estimated cell-type proportions were highly dynamic during this window, with a notable increase in glutamatergic neurons and a concomitant decrease in progenitor populations (**Fig. 3F; Fig. S8**). Consistent with the cellular heterogeneity hypothesis, proportions of these cell-types were significantly correlated over time with the drop in *cis*-h^2_{SNP} (Dividing_progenitor: R=0.96, FDR=0.005; Glutamatergic: R=-0.94, FDR=0.006, Pearson; **Fig. S8**). However, heritability was calculated using gene expression data corrected for hidden covariates (**Methods; Fig S8**), known to control for cell-type heterogeneity across samples (*7*, *55*), which we verified (**Fig. S8**), suggesting an indirect relationship. As an alternative hypothesis, the drop in heritability could reflect intrinsic properties of neurons as they mature. We tested this by comparing gene expression *cis*-h^2_{SNP} in a matched cohort of cultured primary human neural progenitor cells (phNPCs) and their differentiated neuronal progeny (*56*). Mirroring our findings, we observed significantly greater gene expression *cis*-h^2_{SNP} in phNPCs compared with their differentiated neuron counterparts (**Fig. S8**; P=0.0009, Wilcoxon rank sum test), consistent with a reported >2-fold increase in eGenes (*56*) and ATACseq-defined regulatory elements (*57*) in phNPCs compared with neurons. Altogether, these results underscore the temporally dynamic, context-specific nature of gene regulation in the human brain, likely reflecting the interplay between changing cell-type proportions and intrinsic properties of neuronal maturation.

Temporal and Molecular Specificity of Neuropsychiatric GWAS

To prioritize the potential underlying biological context(s) through which genetic risk is conferred, we next sought to integrate our expanded set of functional genomic annotations with neuropsychiatric GWAS results. Using the well-powered SCZ GWAS as an example, we observed substantial enrichment of test statistics when subsetting to fetal brain *cis* e-, iso-, and sQTLs compared with background variants (**Fig. 4A**). Using stratified LD-score regression (S-LDSC (*6*, *58*)), we next sought to estimate the degree to which SNP-based heritability was enriched among these xQTLs. We generated continuous

annotations for genetic variants based on fine-mapping posterior probabilities (*59*) and found SCZ GWAS signals to be highly enriched among fetal brain regulatory elements -- more so than in the adult brain (**Fig. 4B**; **Table S4**; (*35*)). When jointly modeling fetal brain e-, iso-, and sQTLs, we observed that splicing and isoform QTLs captured greater enrichment than eQTLs (**Fig. S10**; **Table S4**; (*35*)). These observations were consistent when extending across multiple neuropsychiatric GWAS as well as within trimester-specific annotations (**Fig. S10**; **Table S4**). Overall, these analyses highlight the critical importance of the fetal brain context -- as well as splicing and isoform regulation -- for interpreting potential mechanisms underlying psychiatric GWAS signals.

Although the S-LDSC results clearly demonstrate greater enrichment of SNP heritability among prenatal (relative to postnatal) gene regulatory variants, and splicing/isoform regulation (relative to total gene expression), these analyses are based on small genomic windows centered around top xQTLs. It can be difficult to compare results across annotations that differ substantially in genomic coverage, and it has been hypothesized that the top xQTLs may not overlap strongly with complex traits under negative selection (*37*, *38*). To address these issues, we next leveraged the mediated expression score regression (MESC) framework (*38*) to estimate the proportion of heritability that is mediated by the *cis*-genetic component of assayed genes, isoforms, and introns (h^2_{med}/h^2_g). Notably, while S-LDSC is restricted to a subset of significant xQTLs, MESC estimates enrichments genome-wide, including assayed features with low expression heritability (*38*). We chose five GWAS of brain-relevant neuropsychiatric traits: SCZ, ASD, bipolar disorder (BIP), attention deficit/hyperactivity disorder (ADHD), and major depression disorder (MDD) (*1*, *2*, *60–62*). Across these traits, we consistently observed greater heritability mediated by isoform regulation (isoform h^2_{med}/h^2_g 6.45±1.92%) than that of gene expression (3.15±1.25%) or splicing (2.13±1.74%), although the overall extent of mediation remained small (**Fig. 4C**; **Table S4**; (*35*)). The findings remain consistent after excluding high pLI genes (pLI > 0.9), indicating that these results are not simply a reflection of our observation that genes intolerant to loss-of-function mutations are more likely to harbor isoQTLs than eQTLs (**Fig. S10**). Extending these analyses across trimester-specific annotations, although less well powered, pointed to isoform-regulation in Tri2 as being particularly important, especially for BIP (paired t-test P-value = 0.04 on isoform h2med/h2 across all traits; **Fig. 4D**; **Table S4**). The findings remained consistent when restricting to protein-coding genes and their isoforms, indicating that the results were not biased by the shift of eGene biotype between trimesters (**Fig. S10**). Altogether, our results highlight the importance of fetal isoform expression regulation as a critical mediator of psychiatric GWAS heritability, and the second trimester as the time frame during which genetic risks converge in the developing human brain.

Colocalization and Isoform-level Transcriptome-wide Association Study (isoTWAS)

To move from broad GWAS enrichments to locus-specific risk genes and molecular mechanisms, we next conducted a systematic colocalization analysis using eCAVIAR (*9*), which performs joint probabilistic fine-mapping and estimates the colocalization posterior probability (CLPP) that a given variant is "causal" in both GWAS and xQTL datasets. Across the combined 485 psychiatric GWAS loci, we prioritized 292 (60.2%) with CLPP above the established cutoff of 0.01 (**Fig. 5A**, **B**; **Fig. S11**; **Table S5**; (*35*)). For context, restricting our results to eQTLs in SCZ and BIP, we identified 80 loci with prioritized eQTLs, while a recent, much larger adult brain eQTL study with an effective sample size of 3,154 identified 20 significant colocalizations (CLPP > 0.01) for the two disorders (*15*).

Consistent with heritability enrichment patterns, we observed many more GWAS loci harboring colocalized iso-QTLs and sQTLs, compared to standard eQTLs (**Fig. 5A**, **B**; **Fig. S11**; **Table S5**). To confirm the consistency with previous studies, we identified the well-established neuropsychiatric risk gene *FURIN*, with an isoQTL colocalization observed across both SCZ and BIP (**Fig. 5B**; **Fig. S11)** (*10*). The colocalized variant rs6224 (located at intron 13) is in moderately strong LD (R^2=0.7) with rs4702 (located at the 3'-UTR of *FURIN*) that has been CRISPR-validated as an eQTL (*63*, *64*). Further, we prioritized a candidate common variant mechanism for SCZ at the *SP4* locus, a transcription factor and high-confidence rare variant implicated SCZ risk gene (*1*, *65*). While *SP4* was known to be the target gene in this GWAS locus, variant-to-gene mapping was limited by the lack of an observable *SP4* eQTL signal in adult or fetal brain. Here, we identified a cryptic

splicing event in *SP4* colocalizing with both SCZ and BIP GWAS (**Fig. 5C**; **Fig. S11**). The risk variant rs10276352 (G>A) was identified as an sQTL associated with increased inclusion of a 181 bp cryptic, unannotated exon (chr7:21521120-21521300). The inclusion of this cryptic exon was predicted to introduce a frameshift and premature stop codon between canonical exons 4 and 5, likely resulting in nonsense-mediated decay. The resulting truncated protein, if any, would be missing the zinc finger domain that is critical for *SP4*'s DNA-binding activity (**Fig. 5C**).

Other candidate disease mechanisms prioritized by these analyses include: downregulation of the $GABA_A$-receptor subunit *GABRA2* in SCZ (eQTL: rs514733, CLPP=0.32; **Fig. 5B**; **Table S5**), providing genetic evidence for GABAergic dysfunction hypothesized to contribute to disease pathophysiology (*66*); in BIP, splicing dysregulation of *ADCY2* (top colocalization sQTL: rs11750832, CLPP=0.97; **Fig. S11**; **Table S5**), which encodes adenylate cyclase, a cell membrane-bound enzyme regulating cAMP signaling and a target of the mood stabilizer lithium (*67*); splicing dysregulation in BIP of *SCN2A* (sQTL: rs17183814, CLPP=0.70; **Fig. S11**; **Table S5**), a voltage gated sodium channel subunit with rare variant associations in ASD and epilepsy (*68*, *69*); and in MDD, the dysregulated splicing of *CBLL1* (CLPP=0.43; **Fig. S11**; **Table S5**), a highly constrained E3 ubiquitin-protein ligase and regulator of N6-methyladenosine RNA modification involved in neural-immune activation (*70*).

We next conducted an isoform-centric transcriptome-wide association study (isoTWAS) (*71*), to identify genes and isoforms whose *cis* regulated expression is associated with SCZ risk. isoTWAS identified 536 isoforms across 271 distinct genes with significant isoTWAS associations (Bonferroni-corrected $P < 0.05$ across genes, FWER-corrected $P < 0.05$ across transcripts of the same gene, permutation $P < 0.05$; (*35*)). To leverage local LD and to account for SNP weight correlations, we performed fine-mapping on isoTWAS associations that passed permutation testing (**Fig. 5D**; **Table S5**). This analysis resulted in 129 putatively causal isoforms from 107 distinct genes that fall in 90% credible sets, with 15 of these genes with pLI score > 0.9. Of these, 69 isoforms from 57 distinct genes are within 500 kb of independent GWAS-significant loci (41 distinct GWAS loci with lead GWAS SNP < 5e-8, defined by LD clumping with GWAS P-value used for ranking and a R^2 threshold of 0.2 (*72*)). Comparing isoforms prioritized through isoTWAS and/or isoQTL colocalization revealed 14 isoforms that were prioritized with both methods, including *SLC9C2, KMT2E,* and *ABCB9.* Of note, the relatively low overlap could be due to the low power of probabilistic colocalization methods (*73*). With its increased power, isoTWAS also captured additional notable associations, including genetically mediated upregulation of *HCN1-201*, the dominant isoform of the hyperpolarization-activated cation channel *HCN1*. An additional advantage of isoTWAS over colocalization analyses was the ability to map isoform-level associations outside of GWAS-significant loci, additionally identifying putatively causal 60 isoforms across 50 distinct genes that were found outside a GWAS-significant locus.

When examining results from gene prioritization analyses, we noticed several instances in which a single variant was associated with multiple distinct QTLs and overlapped with disease GWAS signal. For example, rs6769789 was identified as an xQTL for multiple genes on chromosome 3 that colocalized with SCZ GWAS (**Fig. 5B**). Due to pleiotropy, it can be particularly difficult to distinguish whether one (of many potential) molecular effects is the true mediator of the SNP-trait effect. In attempt to address this, we applied MRLocus (*74*), which leverages a Mendelian randomization framework for loci with allelic heterogeneity, using conditionally-independent QTLs for these mediators to further support (or refute) observed gene-to-trait effects. Among 14 TWAS-identified genes with >3 conditionally independent eQTLs, the MRLocus framework provided additional support for 7 genes with FDR<0.2 (**Table S5**; (*35*)). In the pleiotropic rs6769789 locus described above, for example, there was an association between eQTL and GWAS effect sizes among conditionally independent eQTLs for *NT5DC2* (FDR=0.125), providing additional evidence in support of this gene-trait association (**Fig. S12**).

Network-level Contextualization of Developmental Gene Regulation

To identify developmentally relevant transcriptional networks, interrogate them for common and rare genetic risk, and connect that risk with key biological and cellular processes, we performed robust weighted gene co-expression network analysis (rWGCNA) on our dataset, an unsupervised method that clusters genes into modules based on shared patterns of expression (*22*, *75–77*). We constructed networks using gene and isoform-level quantifications across all samples (N = 642), as well as within samples filtered by trimester (Tri1, Tri2) or chromosomal sex (XX, XY). In total, we identified 124 gene and isoform co-expression modules demonstrating enrichment for all major developmental cell types (*39*) and recapitulating early biochemical processes and developmental pathways (**Fig. 6A**; (*35*)). We expanded on previous work (*12*, *18*, *19*, *21*, *22*, *24*) by incorporating an order of magnitude more samples, generating previously unknown isoform-level modules for over 120,000 transcripts, and contextualizing development-wide findings within trimester- and sex-specific contexts.

Overlaying enrichment for common and rare variation within the hierarchical structure defined by co-expression pinpointed groups of modules that harbor most of neurodevelopmental disease risk (**Fig. 6B**; **Fig. S13**; **Table S6**; (*35*)). Broadly, we found that isoform modules were more likely to capture cell-type marker enrichment (two-sided Fisher's exact test on FDR < 0.1 hits, P-value = 8e-5, OR = 2.37), demonstrating the importance of incorporating splicing and isoform expression in a network context. Neuropsychiatric GWAS signals localized within modules enriched for deep layer excitatory, maturing excitatory, and interneuron cell populations, while exhibiting depletion for neural progenitor modules. Rare variation was more likely to be enriched in deep layer excitatory, maturing excitatory, and oligodendrocyte precursor modules, suggesting that most disease-associated variation perturbs the maturation of neuronal cell types (**Fig. S14**).

At the gene level, a group of modules (M1, M2, M3) enriched for chromatin remodeling and histone modification pathways, with hub genes including *EP300*, *EP400*, *ARID1A*, *KMT2E* and *POGZ*, converged with maturing excitatory and inhibitory neuron marker genes and showed strong enrichment for rare variation associated with ASD and developmental delay (DD) (**Fig. 6C**). These modules highly overlapped with the DD- and ASD-risk yellow module described in Walker et al. (*24*), building upon the previously described excitatory neuron enrichment for these disorders. Notably, our analysis partitioned the hub genes of the yellow module into a new group of deep-excitatory synaptic projection modules (M83, M84, M85; **Fig. S15**), which exhibited strong enrichment for cross-disorder common variation and rare variation risk for ASD, epilepsy, and SCZ. Among the strongest genetic risk for SCZ was observed in two groups of interrelated synaptic modules (group 1: M93, M94; group 2: M86, M87, M88; **Fig. S15**), which are enriched for synaptic gene ontologies and excitatory neuron marker genes. A closely related isoform module, M82, captured this SCZ signal and harbored hub transcripts with known risk, like the canonical transcripts of *TRIO* and *SYNGAP1*, as well as multiple transcripts of *ANK3* (**Fig. S15**). Using module preservation analysis on our trimester specific networks, we identified M17 as a first trimester-specific module that shows distinct enrichment for neurodevelopmental disorders (NDD) and ontologies for neurogenesis and DNA binding, with hub genes such as *GREB1L*, *LRP2*, and *CASZ1* (**Fig. S15**).

At the isoform level, M59 was notable for its consistent association with ADHD common variant risk and GO term enrichment for mitochondrial and bioenergetic pathways. Hub genes for this module included multiple proteasome subunit genes (PSMD family), and cell type analysis revealed association with excitatory, microglial, and pericyte populations (**Fig. 6D**). Furthermore, a group of neuronally-enriched modules (M65, M66, M67; **Fig. S15**) displayed robust BIP, education attainment (EA), and SCZ enrichment while harboring high risk hub genes like *MEF2C* and *SATB2* – similar to the prenatally-enriched M37 module described in Li et al (*18*). Of note, distinct transcripts of known ASD risk gene *SOX5* acted as hub genes for two isoform modules, M120 and M122, but M120 alone showed a strong and specific signal for ASD rare variation (**Fig. S15**).

Cell-type Specificity through Module-interaction QTLs

Finally, as gene regulation is often known to occur within cell-type-specific contexts, we leveraged two orthogonal approaches to integrate cellular specificity into our gene regulatory results in the developing human brain. First, we applied

the network-based framework implemented in CellWalker to integrate fetal single-cell chromatin accessibility with eQTL results (*78*), using the largest existing atlas from mid-gestation telencephalon (*79*). Chromatin accessibility complements RNA-seq by providing additional evidence that eQTLs are active regulatory elements. CellWalker mapped 21.7% of eQTL-containing genes to a specific cellular context in the developing human brain, corresponding to 3,739 of the bulk-derived eQTLs (**Fig. 7A**; **Table S7**; (*35*)). Second, we leveraged the fact that co-expression modules capture cell-type-specific processes (**Fig. 6A**) to identify module-interacting eQTL (ieQTLs). To identify such ieQTLs, in which SNP-gene associations are modulated by the levels of a given module, we tested the interaction effect between genotype and module eigengenes on gene and isoform expression (**Fig. 7B**; (*35*)). Across all gene and isoform modules, 8,008 ieQTLs were identified after the permutation test (BH-corrected FDR < 0.05; (*35*)), in which 3,960 ieQTLs were specific to a single module (**Fig. 7C**). To validate the cell-type specificity of module ieQTLs, we examined the sharing between module ieQTLs and eQTLs identified separately within cultured neurons and progenitors (*56*). Using the Storey's pi1 statistic (*43*), we observed substantial concordance between module interacting SNP-gene pairs that are true associations in external neuron/progenitor eQTL datasets (**Fig. 7C**). 40 modules have a pi1 difference greater than 0.2 between neuron and progenitor eQTLs, suggesting cell-type-specific genetic regulation (**Fig. 7C**). Finally, integrating disease GWAS, we identified significant colocalizations (CLPP > 0.01) between ieQTLs and 22 SCZ GWAS loci, 13 of which are not found with bulk *cis*-eQTLs (**Table S5**). For example, we identified a SCZ colocalization with an ieQTL of *BRINP2* and the Tri1 gene module M93 (rs17659437, CLPP = 0.01653) (**Fig. 7D**). M93 is enriched for deep layer excitatory neuron markers (ExD), cross-disorder psychiatric GWAS signal, and synapse-related pathways (**Fig. 7E**), with eigengene expression increasing across development (**Fig. 7F**). Concordantly, this module shows greater pi1 concordance with neuronal compared to progenitor eQTLs (**Fig. 7C**). *BRINP2* is involved in BMP and retinoic acid signaling pathways, both of which play critical roles in brain development and neuropsychiatric disease. In sum, these analyses demonstrate how publicly available data can be used to annotate bulk QTLs to specific cell types, adding further context for detecting gene regulatory variation relevant to neuropsychiatric disease mechanisms in the developing human brain.

Discussion

Here, we presented a broad view of the landscape of gene, isoform, and splicing regulation in the developing human brain, across more than 650 distinct donors. We further provided xQTL maps specific to the first and second trimesters of human brain development, as well as across three genetic ancestries, leveraging the resulting allelic diversity through cross-ancestry fine-mapping to narrow in on underlying candidate causal genetic associations. With this work, we prioritized 2-fold more risk genes and candidate molecular mechanisms for neurodevelopmental and psychiatric disorder GWAS loci compared with much larger adult brain reference panels, highlighting the importance of developmental context when interpreting genetic risk variation. Finally, we built gene and isoform-level co-expression networks to place this polygenic risk within an unsupervised, systems-level developmental and cell-type-specific contextualization.

Our results have several notable implications for future investigations of the functional genomic underpinnings of brain-relevant complex traits and disorders. First, several findings highlight the substantial impact of developmental stage on gene regulation, including a striking drop from 10-18 PCW in *cis*-heritability of gene expression and splicing. As QTL discovery and *cis* heritability are interrelated, this explains why we identified a similar number of eGenes on par with larger adult brain studies. Furthermore, while disease genes tend to be under negative selection, which is inversely related to gene expression heritability (*37*, *38*), our data suggest that this relationship is likely further moderated by developmental stage. Indeed, the fetal brain -- and Tri2, in particular -- harbors greater enrichment for neuropsychiatric GWAS signal than at postnatal timepoints, consistent with results from rare variant enrichment analyses (*22*). There are several potential biological explanations for the observed temporal drop in heritability. On one hand, dynamic changes in neurogenesis and neuronal cell fate specification during this period lead to an increasing diversity of underlying cell-types. As such, this decline could reflect distinct gene regulatory mechanisms specific to unique cell types, especially progenitor and glutamatergic neuronal lineages, as their proportions become more variable. On the other hand, we also find evidence that

heritability is intrinsically higher in neural progenitor cells (phNPCs) compared with their differentiated neuronal counterparts, consistent with a reported larger number of chromatin accessibility peaks in phNPCs (*57*). Both biological explanations likely contribute, and future population-level developmental brain atlases with single cell resolution and multi-omic readouts will be needed to further address this question.

Second, we observed prominent differences in the ability of distinct molecular features to capture neuropsychiatric risk mechanisms. Specifically, isoform-level regulation mediated substantially more neuropsychiatric disease heritability than eQTLs, across several distinct GWAS. Further, iso- and sQTL colocalizations explained many more GWAS loci than standard eQTLs from the fetal or adult brain. Given that isoform quantification requires accurate imputation from short-read RNA-seq, guided by genomic reference annotations which are notably incomplete with respect to the human brain (*80*), we expect these differences to only become further accentuated as our understanding of the landscape of alternative splicing and isoform complexity grows, through the continued adoption of emerging long-read RNA-sequencing technologies.

Third, with the ever-increasing number of available functional genomic reference panels, including from this study, it is becoming increasingly clear that there will soon be multiple potential, prioritized functional genomic mechanisms at a given GWAS locus. This can occur when a GWAS SNP tags a haplotype containing an underlying structural variant (such as an inversion), with multiple pleiotropic effects on *cis* gene regulation. Mendelian randomization-based approaches can help address this challenge but will require larger reference panels capable of capturing the full extent of conditionally independent QTL signals across the transcriptome. Further, while single-cell QTL studies have been heralded of late, they will only exacerbate this issue while lacking the ability to profile splicing and isoform-level regulation which we show to be most high-yield for mechanistic inference.

Finally, given our finding that isoform-level co-expression networks, in particular, recapitulate cell-type-specific biological processes and genetic regulation, future work should continue to build larger bulk-tissue reference panels of the developing human brain guided by more complete, matching isoform-level annotations from long-read sequencing. Greater visibility is needed, especially in the third trimester of brain development, which is critically underrepresented in our sample.

Materials and methods summary

Here, we integrated and uniformly processed genotype and RNA-seq data from five fetal brain datasets (*12*, *24–27*), in total 654 unique samples passing strict quality control. The genotype data were filtered by minor allele frequency (MAF), missingness, and Hardy-Weinberg Equilibrium (HWE). The QC-ed genotype data were imputed on Michigan Imputation Server (*81*) in reference to the multi-ancestry TOPMed dataset (*34*). After imputation, genotype variants of all studies were combined and merged with 1000 Genomes (*47*) to infer ancestry of each subject. RNA-seq reads were aligned to GENCODE v29lift37 (*40*, *82*) via STAR-2.7.3a (*83*). Gene and isoform quantifications were calculated using Salmon v1.0.0 (*41*). QC metrics were calculated using PicardTools. Genes and isoforms with an expression level of TPM > 0.1 in more than 25% of the subjects were included in the analysis. Local splicing was quantified using Leafcutter v0.2.7 (*42*). Introns and intron cluster that passed extensive quality controls, including >50 reads per cluster, >500kb intron length, >0.001 of reads in a cluster support an intron, >5 reads per intron, were included in the analysis.

With the quantifications of gene expression, isoform expression, and local splicing, we next performed *cis*-e/iso/sQTL mapping. Covariates of sample sex, age, top 5 genotype PCs, and hidden components with priors (HCPs) were included in the analysis. QTLs were mapped using FastQTL (*84*), the feature quantifications, and variants within 1Mb of the tested feature. Genes with adjusted beta-approximated permutation P-value < 0.05 were defined as eGenes, isoGenes, and sGenes. Population-specific xQTLs were mapped in EUR, AMR, and AFR samples. Trimester-specific xQTLs were mapped in EUR Tri1 and Tri2 samples. xQTLs were fine-mapped using SuSiE (*45*), and cross-ancestry eQTL was further fine-mapped using PAINTOR (*51*, *52*) while leveraging functional annotations. Gene expression and splicing heritability were estimated using a restricted maximum likelihood (REML) algorithm implemented in Julia (*85*). Cell-type

proportions were estimated for 7 major cell classes with CIBERSORTx (*53*) using a single cell reference panel of meta-analyzed cell-type markers ("metamarkers") from 37 primary fetal brain scRNAseq datasets comprising ~2.95M individual nuclei/cells (*54*).

Stratified LD-score regression (*6*) was applied to investigate the enrichment of neuropsychiatric GWAS heritability among fetal brain QTLs, which were quantitatively annotated based on their probability of being causal using maxCPP (*59*). Mediated Expression Score Regression (MESC) (*38*) was used to estimate the proportion of GWAS heritability mediated by the *cis* genetic component of genes, isoforms, introns, which were further stratified into trimesters. Isoform-level transcriptome-wide association study (isoTWAS) (*71*) framework was applied to identify isoforms whose *cis*-regulated expression is associated with neuropsychiatric GWAS. Statistical colocalization between xQTLs and GWAS was performed using eCAVIAR v2.2 (*9*) and variants with colocalization posterior probability (CLPP) greater than 0.01 were defined as colocalized.

Robust Weighted Gene Co-expression Network Analysis (WGCNA) was performed to identify co-expression modules utilizing gene and isoform quantifications, as well as trimester- and sex-specific quantifications. Module-interacting QTLs (ieQTLs) were identified by testing the interaction effect between genotype and module eigengenes. The enrichment of ieQTLs in neurons and progenitors (*56*) was examined by Storey's pi1 statistic (*43*). CellWalker (*78*) leveraged single-cell RNA-seq and ATAC-seq data to map bulk eQTLs to specific cell types. See the supplementary materials and methods (*35*) for full details.

References and Notes

1. V. Trubetskoy, A. F. Pardiñas, T. Qi, G. Panagiotaropoulou, S. Awasthi, T. B. Bigdeli, J. Bryois, C.-Y. Chen, C. A. Dennison, L. S. Hall, M. Lam, K. Watanabe, O. Frei, T. Ge, J. C. Harwood, F. Koopmans, S. Magnusson, A. L. Richards, J. Sidorenko, Y. Wu, J. Zeng, J. Grove, M. Kim, Z. Li, G. Voloudakis, W. Zhang, M. Adams, I. Agartz, E. G. Atkinson, E. Agerbo, M. Al Eissa, M. Albus, M. Alexander, B. Z. Alizadeh, K. Alptekin, T. D. Als, F. Amin, V. Arolt, M. Arrojo, L. Athanasiu, M. H. Azevedo, S. A. Bacanu, N. J. Bass, M. Begemann, R. A. Belliveau, J. Bene, B. Benyamin, S. E. Bergen, G. Blasi, J. Bobes, S. Bonassi, A. Braun, R. A. Bressan, E. J. Bromet, R. Bruggeman, P. F. Buckley, R. L. Buckner, J. Bybjerg-Grauholm, W. Cahn, M. J. Cairns, M. E. Calkins, V. J. Carr, D. Castle, S. V. Catts, K. D. Chambert, R. C. K. Chan, B. Chaumette, W. Cheng, E. F. C. Cheung, S. A. Chong, D. Cohen, A. Consoli, Q. Cordeiro, J. Costas, C. Curtis, M. Davidson, K. L. Davis, L. de Haan, F. Degenhardt, L. E. DeLisi, D. Demontis, F. Dickerson, D. Dikeos, T. Dinan, S. Djurovic, J. Duan, G. Ducci, F. Dudbridge, J. G. Eriksson, L. Fañanás, S. V. Faraone, A. Fiorentino, A. Forstner, J. Frank, N. B. Freimer, M. Fromer, A. Frustaci, A. Gadelha, G. Genovese, E. S. Gershon, M. Giannitelli, I. Giegling, P. Giusti-Rodríguez, S. Godard, J. I. Goldstein, J. González Peñas, A. González-Pinto, S. Gopal, J. Gratten, M. F. Green, T. A. Greenwood, O. Guillin, S. Gülöksüz, R. E. Gur, R. C. Gur, B. Gutiérrez, E. Hahn, H. Hakonarson, V. Haroutunian, A. M. Hartmann, C. Harvey, C. Hayward, F. A. Henskens, S. Herms, P. Hoffmann, D. P. Howrigan, M. Ikeda, C. Iyegbe, I. Joa, A. Julià, A. K. Kähler, T. Kam-Thong, Y. Kamatani, S. Karachanak-Yankova, O. Kebir, M. C. Keller, B. J. Kelly, A. Khrunin, S.-W. Kim, J. Klovins, N. Kondratiev, B. Konte, J. Kraft, M. Kubo, V. Kučinskas, Z. A. Kučinskiene, A. Kusumawardhani, H. Kuzelova-Ptackova, S. Landi, L. C. Lazzeroni, P. H. Lee, S. E. Legge, D. S. Lehrer, R. Lencer, B. Lerer, M. Li, J. Lieberman, G. A. Light, S. Limborska, C.-M. Liu, J. Lönnqvist, C. M. Loughland, J. Lubinski, J. J. Luykx, A. Lynham, M. Macek Jr, A. Mackinnon, P. K. E. Magnusson, B. S. Maher, W. Maier, D. Malaspina, J. Mallet, S. R. Marder, S. Marsal, A. R. Martin, L. Martorell, M. Mattheisen, R. W. McCarley, C. McDonald, J. J. McGrath, H. Medeiros, S. Meier, B. Melegh, I. Melle, R. I. Mesholam-Gately, A. Metspalu, P. T. Michie, L. Milani, V. Milanova, M. Mitjans, E. Molden, E. Molina, M. D. Molto, V. Mondelli, C. Moreno, C. P. Morley, G. Muntané, K. C. Murphy, I. Myin-Germeys, I. Nenadić, G. Nestadt, L. Nikitina-Zake, C. Noto, K. H. Nuechterlein, N. L. O'Brien, F. A. O'Neill, S.-Y. Oh, A. Olincy, V. K. Ota, C. Pantelis, G. N. Papadimitriou, M. Parellada, T. Paunio, R. Pellegrino, S. Periyasamy, D. O. Perkins, B. Pfuhlmann, O. Pietiläinen, J. Pimm, D. Porteous, J. Powell, D. Quattrone, D. Quested, A. D. Radant, A. Rampino, M. H. Rapaport, A. Rautanen, A. Reichenberg, C. Roe, J. L. Roffman, J. Roth, M. Rothermundt, B. P. F. Rutten, S. Saker-Delye, V. Salomaa, J. Sanjuan, M. L. Santoro, A. Savitz, U. Schall, R. J. Scott, L. J. Seidman, S. I. Sharp, J. Shi, L. J. Siever, E. Sigurdsson, K. Sim, N. Skarabis, P. Slominsky, H.-C. So, J. L. Sobell, E. Söderman, H. J. Stain, N. E. Steen, A. A. Steixner-Kumar, E. Stögmann, W. S. Stone, R. E. Straub, F. Streit, E. Strengman, T. S. Stroup, M. Subramaniam, C. A. Sugar, J. Suvisaari, D. M. Svrakic, N. R. Swerdlow, J. P. Szatkiewicz, T. M. T. Ta, A. Takahashi, C. Terao, F. Thibaut, D. Toncheva, P. A. Tooney, S. Torretta, S. Tosato, G. B. Tura, B. I. Turetsky, A. Üçok, A. Vaaler, T. van Amelsvoort, R. van Winkel, J. Veijola, J. Waddington, H. Walter, A. Waterreus, B. T. Webb, M. Weiser, N. M. Williams, S. H. Witt, B. K. Wormley, J. Q. Wu, Z. Xu, R. Yolken, C. C. Zai, W. Zhou, F. Zhu, F. Zimprich, E. C. Atbaşoğlu, M. Ayub, C. Benner, A. Bertolino, D. W. Black, N. J. Bray, G. Breen, N. G. Buccola, W. F. Byerley, W. J. Chen, C. R. Cloninger, B. Crespo-Facorro, G. Donohoe, R. Freedman, C. Galletly, M. J. Gandal, M. Gennarelli, D. M. Hougaard, H.-G. Hwu, A. V. Jablensky, S. A. McCarroll, J. L. Moran, O. Mors, P. B. Mortensen, B. Müller-Myhsok, A. L. Neil, M. Nordentoft, M. T. Pato, T. L. Petryshen, M. Pirinen, A. E. Pulver, T. G. Schulze, J. M. Silverman, J. W. Smoller, E. A. Stahl, D. W. Tsuang, E. Vilella, S.-H. Wang, S. Xu, Indonesia Schizophrenia Consortium, PsychENCODE, Psychosis Endophenotypes International Consortium, SynGO Consortium, R. Adolfsson, C. Arango, B. T. Baune, S. I. Belangero, A. D. Børglum, D. Braff, E. Bramon, J. D. Buxbaum, D. Campion, J. A. Cervilla, S. Cichon, D. A. Collier, A. Corvin, D. Curtis, M. D. Forti, E. Domenici, H. Ehrenreich, V. Escott-Price, T. Esko, A. H. Fanous, A. Gareeva, M. Gawlik, P. V. Gejman, M. Gill, S. J. Glatt, V. Golimbet, K. S. Hong, C. M. Hultman, S. E. Hyman, N. Iwata, E. G. Jönsson, R. S. Kahn, J. L. Kennedy, E. Khusnutdinova, G. Kirov, J. A. Knowles, M.-O. Krebs, C. Laurent-Levinson, J. Lee, T. Lencz, D. F. Levinson, Q. S. Li, J. Liu, A. K. Malhotra, D. Malhotra, A. McIntosh, A. McQuillin, P. R. Menezes, V. A. Morgan, D. W. Morris, B. J. Mowry, R. M. Murray, V. Nimgaonkar, M. M. Nöthen, R. A. Ophoff, S. A. Paciga, A. Palotie, C. N. Pato, S. Qin, M. Rietschel, B. P. Riley, M. Rivera, D. Rujescu, M. C. Saka, A. R. Sanders, S. G. Schwab, A. Serretti, P. C. Sham, Y. Shi, D. St Clair, H. Stefánsson, K. Stefansson, M. T. Tsuang, J. van Os, M. P. Vawter, D. R. Weinberger, T. Werge, D. B. Wildenauer, X. Yu, W. Yue, P. A. Holmans, A. J. Pocklington, P. Roussos, E. Vassos, M. Verhage, P. M. Visscher, J. Yang, D. Posthuma, O. A. Andreassen, K. S. Kendler, M. J. Owen, N. R. Wray, M. J. Daly, H. Huang, B. M. Neale, P. F. Sullivan, S. Ripke, J. T. R. Walters, M. C. O'Donovan, Schizophrenia Working Group of the Psychiatric Genomics Consortium, Mapping genomic loci implicates genes and synaptic biology in schizophrenia. *Nature* (2022), doi:10.1038/s41586-022-04434-5.

2. J. Grove, S. Ripke, T. D. Als, M. Mattheisen, R. K. Walters, H. Won, J. Pallesen, E. Agerbo, O. A. Andreassen, R. Anney, S. Awashti, R. Belliveau, F. Bettella, J. D. Buxbaum, J. Bybjerg-Grauholm, M. Bækvad-Hansen, F. Cerrato, K. Chambert, J. H. Christensen, C. Churchhouse, K. Dellenvall, D. Demontis, S. De Rubeis, B. Devlin, S. Djurovic, A. L. Dumont, J. I. Goldstein, C. S. Hansen, M. E. Hauberg, M. V. Hollegaard, S. Hope, D. P. Howrigan, H. Huang, C. M. Hultman, L. Klei, J. Maller, J. Martin, A. R. Martin, J. L. Moran, M. Nyegaard, T. Nærland, D. S. Palmer, A. Palotie, C. B. Pedersen, M. G. Pedersen, T. dPoterba, J. B. Poulsen, B. S. Pourcain, P. Qvist, K. Rehnström, A. Reichenberg, J. Reichert, E. B. Robinson, K. Roeder, P. Roussos, E. Saemundsen, S. Sandin, F. K. Satterstrom, G. Davey Smith, H. Stefansson, S. Steinberg, C. R. Stevens, P. F. Sullivan, P. Turley, G. B. Walters, X. Xu, Autism Spectrum Disorder Working Group of the Psychiatric Genomics Consortium, BUPGEN, Major Depressive Disorder Working Group of the Psychiatric Genomics Consortium, 23andMe Research Team, K. Stefansson, D. H. Geschwind, M. Nordentoft, D. M. Hougaard, T. Werge, O. Mors, P. B. Mortensen, B. M. Neale, M. J. Daly, A. D. Børglum, Identification of common genetic risk variants for autism spectrum disorder. *Nat. Genet.* **51**, 431–444 (2019).

3. M. J. Gandal, V. Leppa, H. Won, N. N. Parikshak, D. H. Geschwind, The road to precision psychiatry: translating genetics into disease mechanisms. *Nat. Neurosci.* **19**, 1397–1407 (2016).

4. L. D. Ward, M. Kellis, Evidence of abundant purifying selection in humans for recently acquired regulatory functions. *Science*. **337**, 1675–1678 (2012).

5. M. T. Maurano, R. Humbert, E. Rynes, R. E. Thurman, E. Haugen, H. Wang, A. P. Reynolds, R. Sandstrom, H. Qu, J. Brody, A. Shafer, F. Neri, K. Lee, T. Kutyavin, S. Stehling-Sun, A. K. Johnson, T. K. Canfield, E. Giste, M. Diegel, D. Bates, R. S. Hansen, S. Neph, P. J. Sabo, S. Heimfeld, A. Raubitschek, S. Ziegler, C. Cotsapas, N. Sotoodehnia, I. Glass, S. R. Sunyaev, R. Kaul, J. A. Stamatoyannopoulos, Systematic localization of common disease-associated variation in regulatory DNA. *Science*. **337**, 1190–1195 (2012).

6. H. K. Finucane, B. Bulik-Sullivan, A. Gusev, G. Trynka, Y. Reshef, P.-R. Loh, V. Anttila, H. Xu, C. Zang, K. Farh, S. Ripke, F. R. Day, ReproGen Consortium, Schizophrenia Working Group of the Psychiatric Genomics Consortium, RACI Consortium, S. Purcell, E. Stahl, S. Lindstrom, J. R. B. Perry, Y. Okada, S. Raychaudhuri, M. J. Daly, N. Patterson, B. M. Neale, A. L. Price, Partitioning heritability by functional annotation using genome-wide association summary statistics. *Nat. Genet.* **47**, 1228–1235 (2015).

7. L. M. Hernandez, M. Kim, G. D. Hoftman, J. R. Haney, L. de la Torre-Ubieta, B. Pasaniuc, M. J. Gandal, Transcriptomic Insight Into the Polygenic Mechanisms Underlying Psychiatric Disorders. *Biol. Psychiatry*. **89**, 54–64 (2021).

8. A. Gusev, A. Ko, H. Shi, G. Bhatia, W. Chung, B. W. J. H. Penninx, R. Jansen, E. J. C. de Geus, D. I. Boomsma, F. A. Wright, P. F. Sullivan, E. Nikkola, M. Alvarez, M. Civelek, A. J. Lusis, T. Lehtimäki, E. Raitoharju, M. Kähönen, I. Seppälä, O. T. Raitakari, J. Kuusisto, M. Laakso, A. L. Price, P. Pajukanta, B. Pasaniuc, Integrative approaches for large-scale transcriptome-wide association studies. *Nat. Genet.* **48**, 245–252 (2016).

9. F. Hormozdiari, M. van de Bunt, A. V. Segrè, X. Li, J. W. J. Joo, M. Bilow, J. H. Sul, S. Sankararaman, B. Pasaniuc, E. Eskin, Colocalization of GWAS and eQTL Signals Detects Target Genes. *Am. J. Hum. Genet.* **99**, 1245–1260 (2016).

10. M. Fromer, P. Roussos, S. K. Sieberts, J. S. Johnson, D. H. Kavanagh, T. M. Perumal, D. M. Ruderfer, E. C. Oh, A. Topol, H. R. Shah, L. L. Klei, R. Kramer, D. Pinto, Z. H. Gümüş, A. E. Cicek, K. K. Dang, A. Browne, C. Lu, L. Xie, B. Readhead, E. A. Stahl, J. Xiao, M. Parvizi, T. Hamamsy, J. F. Fullard, Y.-C. Wang, M. C. Mahajan, J. M. J. Derry, J. T. Dudley, S. E. Hemby, B. A. Logsdon, K. Talbot, T. Raj, D. A. Bennett, P. L. De Jager, J. Zhu, B. Zhang, P. F. Sullivan, A. Chess, S. M. Purcell, L. A. Shinobu, L. M. Mangravite, H. Toyoshiba, R. E. Gur, C.-G. Hahn, D. A. Lewis, V. Haroutunian, M. A. Peters, B. K. Lipska, J. D. Buxbaum, E. E. Schadt, K. Hirai, K. Roeder, K. J. Brennand, N. Katsanis, E. Domenici, B. Devlin, P. Sklar, Gene expression elucidates functional impact of polygenic risk for schizophrenia. *Nat. Neurosci.* **19**, 1442–1453 (2016).

11. A. E. Jaffe, R. E. Straub, J. H. Shin, R. Tao, Y. Gao, L. Collado-Torres, T. Kam-Thong, H. S. Xi, J. Quan, Q. Chen, C. Colantuoni, W. S. Ulrich, B. J. Maher, A. Deep-Soboslay, BrainSeq Consortium, A. J. Cross, N. J. Brandon, J. T. Leek,

T. M. Hyde, J. E. Kleinman, D. R. Weinberger, Developmental and genetic regulation of the human cortex transcriptome illuminate schizophrenia pathogenesis. *Nat. Neurosci.* **21**, 1117–1125 (2018).

12. D. M. Werling, S. Pochareddy, J. Choi, J.-Y. An, B. Sheppard, M. Peng, Z. Li, C. Dastmalchi, G. Santpere, A. M. M. Sousa, A. T. N. Tebbenkamp, N. Kaur, F. O. Gulden, M. S. Breen, L. Liang, M. C. Gilson, X. Zhao, S. Dong, L. Klei, A. E. Cicek, J. D. Buxbaum, H. Adle-Biassette, J.-L. Thomas, K. A. Aldinger, D. R. O'Day, I. A. Glass, N. A. Zaitlen, M. E. Talkowski, K. Roeder, M. W. State, B. Devlin, S. J. Sanders, N. Sestan, Whole-Genome and RNA Sequencing Reveal Variation and Transcriptomic Coordination in the Developing Human Prefrontal Cortex. *Cell Rep.* **31**, 107489 (2020).

13. D. Wang, S. Liu, J. Warrell, H. Won, X. Shi, F. C. P. Navarro, D. Clarke, M. Gu, P. Emani, Y. T. Yang, M. Xu, M. J. Gandal, S. Lou, J. Zhang, J. J. Park, C. Yan, S. K. Rhie, K. Manakongtreecheep, H. Zhou, A. Nathan, M. Peters, E. Mattei, D. Fitzgerald, T. Brunetti, J. Moore, Y. Jiang, K. Girdhar, G. E. Hoffman, S. Kalayci, Z. H. Gümüş, G. E. Crawford, PsychENCODE Consortium, P. Roussos, S. Akbarian, A. E. Jaffe, K. P. White, Z. Weng, N. Sestan, D. H. Geschwind, J. A. Knowles, M. B. Gerstein, Comprehensive functional genomic resource and integrative model for the human brain. *Science*. **362** (2018), doi:10.1126/science.aat8464.

14. M. J. Gandal, P. Zhang, E. Hadjimichael, R. L. Walker, C. Chen, S. Liu, H. Won, H. van Bakel, M. Varghese, Y. Wang, A. W. Shieh, J. Haney, S. Parhami, J. Belmont, M. Kim, P. Moran Losada, Z. Khan, J. Mleczko, Y. Xia, R. Dai, D. Wang, Y. T. Yang, M. Xu, K. Fish, P. R. Hof, J. Warrell, D. Fitzgerald, K. White, A. E. Jaffe, PsychENCODE Consortium, M. A. Peters, M. Gerstein, C. Liu, L. M. Iakoucheva, D. Pinto, D. H. Geschwind, Transcriptome-wide isoform-level dysregulation in ASD, schizophrenia, and bipolar disorder. *Science*. **362** (2018), doi:10.1126/science.aat8127.

15. B. Zeng, J. Bendl, R. Kosoy, J. F. Fullard, G. E. Hoffman, P. Roussos, Multi-ancestry eQTL meta-analysis of human brain identifies candidate causal variants for brain-related traits. *Nat. Genet.*, 1–9 (2022).

16. GTEx Consortium, The GTEx Consortium atlas of genetic regulatory effects across human tissues. *Science*. **369**, 1318–1330 (2020).

17. B. D. Umans, A. Battle, Y. Gilad, Where Are the Disease-Associated eQTLs? *Trends Genet.* **37**, 109–124 (2020).

18. M. Li, G. Santpere, Y. Imamura Kawasawa, O. V. Evgrafov, F. O. Gulden, S. Pochareddy, S. M. Sunkin, Z. Li, Y. Shin, Y. Zhu, A. M. M. Sousa, D. M. Werling, R. R. Kitchen, H. J. Kang, M. Pletikos, J. Choi, S. Muchnik, X. Xu, D. Wang, B. Lorente-Galdos, S. Liu, P. Giusti-Rodríguez, H. Won, C. A. de Leeuw, A. F. Pardiñas, BrainSpan Consortium, PsychENCODE Consortium, PsychENCODE Developmental Subgroup, M. Hu, F. Jin, Y. Li, M. J. Owen, M. C. O'Donovan, J. T. R. Walters, D. Posthuma, M. A. Reimers, P. Levitt, D. R. Weinberger, T. M. Hyde, J. E. Kleinman, D. H. Geschwind, M. J. Hawrylycz, M. W. State, S. J. Sanders, P. F. Sullivan, M. B. Gerstein, E. S. Lein, J. A. Knowles, N. Sestan, Integrative functional genomic analysis of human brain development and neuropsychiatric risks. *Science*. **362** (2018), doi:10.1126/science.aat7615.

19. H. J. Kang, Y. I. Kawasawa, F. Cheng, Y. Zhu, X. Xu, M. Li, A. M. M. Sousa, M. Pletikos, K. A. Meyer, G. Sedmak, T. Guennel, Y. Shin, M. B. Johnson, Z. Krsnik, S. Mayer, S. Fertuzinhos, S. Umlauf, S. N. Lisgo, A. Vortmeyer, D. R. Weinberger, S. Mane, T. M. Hyde, A. Huttner, M. Reimers, J. E. Kleinman, N. Sestan, Spatio-temporal transcriptome of the human brain. *Nature*. **478**, 483–489 (2011).

20. C. Colantuoni, B. K. Lipska, T. Ye, T. M. Hyde, R. Tao, J. T. Leek, E. A. Colantuoni, A. G. Elkahloun, M. M. Herman, D. R. Weinberger, J. E. Kleinman, Temporal dynamics and genetic control of transcription in the human prefrontal cortex. *Nature*. **478**, 519–523 (2011).

21. A. J. Willsey, S. J. Sanders, M. Li, S. Dong, A. T. Tebbenkamp, R. A. Muhle, S. K. Reilly, L. Lin, S. Fertuzinhos, J. A. Miller, M. T. Murtha, C. Bichsel, W. Niu, J. Cotney, A. G. Ercan-Sencicek, J. Gockley, A. R. Gupta, W. Han, X. He, E. J. Hoffman, L. Klei, J. Lei, W. Liu, L. Liu, C. Lu, X. Xu, Y. Zhu, S. M. Mane, E. S. Lein, L. Wei, J. P. Noonan, K. Roeder, B. Devlin, N. Sestan, M. W. State, Coexpression networks implicate human midfetal deep cortical projection neurons in the pathogenesis of autism. *Cell*. **155**, 997–1007 (2013).

22. N. N. Parikshak, R. Luo, A. Zhang, H. Won, J. K. Lowe, V. Chandran, S. Horvath, D. H. Geschwind, Integrative functional genomic analyses implicate specific molecular pathways and circuits in autism. *Cell*. **155**, 1008–1021 (2013).

23. S. Gulsuner, T. Walsh, A. C. Watts, M. K. Lee, A. M. Thornton, S. Casadei, C. Rippey, H. Shahin, Consortium on the Genetics of Schizophrenia (COGS), PAARTNERS Study Group, V. L. Nimgaonkar, R. C. P. Go, R. M. Savage, N. R. Swerdlow, R. E. Gur, D. L. Braff, M.-C. King, J. M. McClellan, Spatial and temporal mapping of de novo mutations in schizophrenia to a fetal prefrontal cortical network. *Cell*. **154**, 518–529 (2013).

24. R. L. Walker, G. Ramaswami, C. Hartl, N. Mancuso, M. J. Gandal, L. de la Torre-Ubieta, B. Pasaniuc, J. L. Stein, D. H. Geschwind, Genetic Control of Expression and Splicing in Developing Human Brain Informs Disease Mechanisms. *Cell*. **179**, 750-771.e22 (2019).

25. H. E. O'Brien, E. Hannon, M. J. Hill, C. C. Toste, M. J. Robertson, J. E. Morgan, G. McLaughlin, C. M. Lewis, L. C. Schalkwyk, L. S. Hall, A. F. Pardiñas, M. J. Owen, M. C. O'Donovan, J. Mill, N. J. Bray, Expression quantitative trait loci in the developing human brain and their enrichment in neuropsychiatric disorders. *Genome Biol.* **19**, 194 (2018).

26. A. E. Jaffe, J. Shin, L. Collado-Torres, J. T. Leek, R. Tao, C. Li, Y. Gao, Y. Jia, B. J. Maher, T. M. Hyde, J. E. Kleinman, D. R. Weinberger, Developmental regulation of human cortex transcription and its clinical relevance at single base resolution. *Nat. Neurosci.* **18**, 154–161 (2015).

27. S. J. Lindsay, Y. Xu, S. N. Lisgo, L. F. Harkin, A. J. Copp, D. Gerrelli, G. J. Clowry, A. Talbot, M. J. Keogh, J. Coxhead, M. Santibanez-Koref, P. F. Chinnery, HDBR Expression: A Unique Resource for Global and Individual Gene Expression Studies during Early Human Brain Development. *Front. Neuroanat.* **10**, 86 (2016).

28. R. Birnbaum, A. E. Jaffe, T. M. Hyde, J. E. Kleinman, D. R. Weinberger, Prenatal expression patterns of genes associated with neuropsychiatric disorders. *Am. J. Psychiatry*. **171**, 758–767 (2014).

29. Y. I. Li, B. van de Geijn, A. Raj, D. A. Knowles, A. A. Petti, D. Golan, Y. Gilad, J. K. Pritchard, RNA splicing is a primary link between genetic variation and disease. *Science*. **352**, 600–604 (2016).

30. B. Raj, B. J. Blencowe, Alternative Splicing in the Mammalian Nervous System: Recent Insights into Mechanisms and Functional Roles. *Neuron*. **87**, 14–27 (2015).

31. X. Zhang, M. H. Chen, X. Wu, A. Kodani, J. Fan, R. Doan, M. Ozawa, J. Ma, N. Yoshida, J. F. Reiter, D. L. Black, P. V. Kharchenko, P. A. Sharp, C. A. Walsh, Cell-Type-Specific Alternative Splicing Governs Cell Fate in the Developing Cerebral Cortex. *Cell*. **166**, 1147-1162.e15 (2016).

32. S. M. Weyn-Vanhentenryck, H. Feng, D. Ustianenko, R. Duffié, Q. Yan, M. Jacko, J. C. Martinez, M. Goodwin, X. Zhang, U. Hengst, S. Lomvardas, M. S. Swanson, C. Zhang, Precise temporal regulation of alternative splicing during neural development. *Nat. Commun.* **9** (2018), doi:10.1038/s41467-018-04559-0.

33. D. Garrido-Martín, B. Borsari, M. Calvo, F. Reverter, R. Guigó, Identification and analysis of splicing quantitative trait loci across multiple tissues in the human genome. *Nat. Commun.* **12**, 727 (2021).

34. D. Taliun, D. N. Harris, M. D. Kessler, J. Carlson, Z. A. Szpiech, R. Torres, S. A. G. Taliun, A. Corvelo, S. M. Gogarten, H. M. Kang, A. N. Pitsillides, J. LeFaive, S.-B. Lee, X. Tian, B. L. Browning, S. Das, A.-K. Emde, W. E. Clarke, D. P. Loesch, A. C. Shetty, T. W. Blackwell, A. V. Smith, Q. Wong, X. Liu, M. P. Conomos, D. M. Bobo, F. Aguet, C. Albert, A. Alonso, K. G. Ardlie, D. E. Arking, S. Aslibekyan, P. L. Auer, J. Barnard, R. G. Barr, L. Barwick, L. C. Becker, R. L. Beer, E. J. Benjamin, L. F. Bielak, J. Blangero, M. Boehnke, D. W. Bowden, J. A. Brody, E. G. Burchard, B. E. Cade, J. F. Casella, B. Chalazan, D. I. Chasman, Y.-D. I. Chen, M. H. Cho, S. H. Choi, M. K. Chung, C. B. Clish, A. Correa, J. E. Curran, B. Custer, D. Darbar, M. Daya, M. de Andrade, D. L. DeMeo, S. K. Dutcher, P. T. Ellinor, L. S. Emery, C. Eng, D. Fatkin, T. Fingerlin, L. Forer, M. Fornage, N. Franceschini, C. Fuchsberger, S. M. Fullerton, S. Germer, M. T. Gladwin, D. J. Gottlieb, X. Guo, M. E. Hall, J. He, N. L. Heard-Costa, S. R. Heckbert, M. R. Irvin, J. M. Johnsen, A. D. Johnson, R. Kaplan, S. L. R. Kardia, T. Kelly, S. Kelly, E. E. Kenny, D. P. Kiel, R. Klemmer, B. A. Konkle, C. Kooperberg, A. Köttgen, L. A. Lange, J. Lasky-Su, D. Levy, X. Lin, K.-H. Lin, C. Liu, R. J. F. Loos, L. Garman, R. Gerszten, S. A. Lubitz, K. L. Lunetta, A. C. Y. Mak, A. Manichaikul, A. K. Manning, R. A. Mathias, D.

D. McManus, S. T. McGarvey, J. B. Meigs, D. A. Meyers, J. L. Mikulla, M. A. Minear, B. D. Mitchell, S. Mohanty, M. E. Montasser, C. Montgomery, A. C. Morrison, J. M. Murabito, A. Natale, P. Natarajan, S. C. Nelson, K. E. North, J. R. O'Connell, N. D. Palmer, N. Pankratz, G. M. Peloso, P. A. Peyser, J. Pleiness, W. S. Post, B. M. Psaty, D. C. Rao, S. Redline, A. P. Reiner, D. Roden, J. I. Rotter, I. Ruczinski, C. Sarnowski, S. Schoenherr, D. A. Schwartz, J.-S. Seo, S. Seshadri, V. A. Sheehan, W. H. Sheu, M. B. Shoemaker, N. L. Smith, J. A. Smith, N. Sotoodehnia, A. M. Stilp, W. Tang, K. D. Taylor, M. Telen, T. A. Thornton, R. P. Tracy, D. J. Van Den Berg, R. S. Vasan, K. A. Viaud-Martinez, S. Vrieze, D. E. Weeks, B. S. Weir, S. T. Weiss, L.-C. Weng, C. J. Willer, Y. Zhang, X. Zhao, D. K. Arnett, A. E. Ashley-Koch, K. C. Barnes, E. Boerwinkle, S. Gabriel, R. Gibbs, K. M. Rice, S. S. Rich, E. K. Silverman, P. Qasba, W. Gan, NHLBI Trans-Omics for Precision Medicine (TOPMed) Consortium, G. J. Papanicolaou, D. A. Nickerson, S. R. Browning, M. C. Zody, S. Zöllner, J. G. Wilson, L. A. Cupples, C. C. Laurie, C. E. Jaquish, R. D. Hernandez, T. D. O'Connor, G. R. Abecasis, Sequencing of 53,831 diverse genomes from the NHLBI TOPMed Program. *Nature*. **590**, 290–299 (2021).

35. Materials and methods are available as supplementary materials.

36. M. Lek, K. J. Karczewski, E. V. Minikel, K. E. Samocha, E. Banks, T. Fennell, A. H. O'Donnell-Luria, J. S. Ware, A. J. Hill, B. B. Cummings, T. Tukiainen, D. P. Birnbaum, J. A. Kosmicki, L. E. Duncan, K. Estrada, F. Zhao, J. Zou, E. Pierce-Hoffman, J. Berghout, D. N. Cooper, N. Deflaux, M. DePristo, R. Do, J. Flannick, M. Fromer, L. Gauthier, J. Goldstein, N. Gupta, D. Howrigan, A. Kiezun, M. I. Kurki, A. L. Moonshine, P. Natarajan, L. Orozco, G. M. Peloso, R. Poplin, M. A. Rivas, V. Ruano-Rubio, S. A. Rose, D. M. Ruderfer, K. Shakir, P. D. Stenson, C. Stevens, B. P. Thomas, G. Tiao, M. T. Tusie-Luna, B. Weisburd, H.-H. Won, D. Yu, D. M. Altshuler, D. Ardissino, M. Boehnke, J. Danesh, S. Donnelly, R. Elosua, J. C. Florez, S. B. Gabriel, G. Getz, S. J. Glatt, C. M. Hultman, S. Kathiresan, M. Laakso, S. McCarroll, M. I. McCarthy, D. McGovern, R. McPherson, B. M. Neale, A. Palotie, S. M. Purcell, D. Saleheen, J. M. Scharf, P. Sklar, P. F. Sullivan, J. Tuomilehto, M. T. Tsuang, H. C. Watkins, J. G. Wilson, M. J. Daly, D. G. MacArthur, Exome Aggregation Consortium, Analysis of protein-coding genetic variation in 60,706 humans. *Nature*. **536**, 285–291 (2016).

37. H. Mostafavi, J. P. Spence, S. Naqvi, J. K. Pritchard, Limited overlap of eQTLs and GWAS hits due to systematic differences in discovery. *bioRxiv* (2022), p. 2022.05.07.491045, , doi:10.1101/2022.05.07.491045.

38. D. W. Yao, L. J. O'Connor, A. L. Price, A. Gusev, Quantifying genetic effects on disease mediated by assayed gene expression levels. *Nat. Genet.* **52**, 626–633 (2020).

39. D. Polioudakis, L. de la Torre-Ubieta, J. Langerman, A. G. Elkins, X. Shi, J. L. Stein, C. K. Vuong, S. Nichterwitz, M. Gevorgian, C. K. Opland, D. Lu, W. Connell, E. K. Ruzzo, J. K. Lowe, T. Hadzic, F. I. Hinz, S. Sabri, W. E. Lowry, M. B. Gerstein, K. Plath, D. H. Geschwind, A Single-Cell Transcriptomic Atlas of Human Neocortical Development during Mid-gestation. *Neuron*. **103**, 785-801.e8 (2019).

40. A. Frankish, M. Diekhans, A.-M. Ferreira, R. Johnson, I. Jungreis, J. Loveland, J. M. Mudge, C. Sisu, J. Wright, J. Armstrong, I. Barnes, A. Berry, A. Bignell, S. Carbonell Sala, J. Chrast, F. Cunningham, T. Di Domenico, S. Donaldson, I. T. Fiddes, C. García Girón, J. M. Gonzalez, T. Grego, M. Hardy, T. Hourlier, T. Hunt, O. G. Izuogu, J. Lagarde, F. J. Martin, L. Martínez, S. Mohanan, P. Muir, F. C. P. Navarro, A. Parker, B. Pei, F. Pozo, M. Ruffier, B. M. Schmitt, E. Stapleton, M.-M. Suner, I. Sycheva, B. Uszczynska-Ratajczak, J. Xu, A. Yates, D. Zerbino, Y. Zhang, B. Aken, J. S. Choudhary, M. Gerstein, R. Guigó, T. J. P. Hubbard, M. Kellis, B. Paten, A. Reymond, M. L. Tress, P. Flicek, GENCODE reference annotation for the human and mouse genomes. *Nucleic Acids Res.* **47**, D766–D773 (2019).

41. R. Patro, G. Duggal, M. I. Love, R. A. Irizarry, C. Kingsford, Salmon provides fast and bias-aware quantification of transcript expression. *Nat. Methods*. **14**, 417–419 (2017).

42. Y. I. Li, D. A. Knowles, J. Humphrey, A. N. Barbeira, S. P. Dickinson, H. K. Im, J. K. Pritchard, Annotation-free quantification of RNA splicing using LeafCutter. *Nat. Genet.* **50**, 151–158 (2018).

43. J. D. Storey, R. Tibshirani, Statistical significance for genomewide studies. *Proc. Natl. Acad. Sci. U. S. A.* **100**, 9440–9445 (2003).

44. O. Delaneau, H. Ongen, A. A. Brown, A. Fort, N. I. Panousis, E. T. Dermitzakis, A complete tool set for molecular QTL discovery and analysis. *Nat. Commun.* **8**, 15452 (2017).

45. G. Wang, A. Sarkar, P. Carbonetto, M. Stephens, A simple new approach to variable selection in regression, with application to genetic fine mapping. *J. R. Stat. Soc. Series B Stat. Methodol.* **82**, 1273–1300 (2020).

46. M. A. Ikram, M. Fornage, A. V. Smith, S. Seshadri, R. Schmidt, S. Debette, H. A. Vrooman, S. Sigurdsson, S. Ropele, H. R. Taal, D. O. Mook-Kanamori, L. H. Coker, W. T. Longstreth Jr, W. J. Niessen, A. L. DeStefano, A. Beiser, A. P. Zijdenbos, M. Struchalin, C. R. Jack Jr, F. Rivadeneira, A. G. Uitterlinden, D. S. Knopman, A.-L. Hartikainen, C. E. Pennell, E. Thiering, E. A. P. Steegers, H. Hakonarson, J. Heinrich, L. J. Palmer, M.-R. Jarvelin, M. I. McCarthy, S. F. A. Grant, B. St Pourcain, N. J. Timpson, G. D. Smith, U. Sovio, Early Growth Genetics Consortium, M. A. Nalls, R. Au, A. Hofman, H. Gudnason, A. van der Lugt, T. B. Harris, W. M. Meeks, M. W. Vernooij, M. A. van Buchem, D. Catellier, V. W. V. Jaddoe, V. Gudnason, B. G. Windham, P. A. Wolf, C. M. van Duijn, T. H. Mosley Jr, H. Schmidt, L. J. Launer, M. M. B. Breteler, C. DeCarli, Cohorts for Heart and Aging Research in Genomic Epidemiology Consortium, Common variants at 6q22 and 17q21 are associated with intracranial volume. *Nat. Genet.* **44**, 539–544 (2012).

47. The 1000 Genomes Project Consortium, A. Auton, G. R. Abecasis, D. M. Altshuler (Co-Chair), R. M. Durbin (Co-Chair), G. R. Abecasis, D. R. Bentley, A. Chakravarti, A. G. Clark, P. Donnelly, E. E. Eichler, P. Flicek, S. B. Gabriel, R. A. Gibbs, E. D. Green, M. E. Hurles, B. M. Knoppers, J. O. Korbel, E. S. Lander, C. Lee, H. Lehrach, E. R. Mardis, G. T. Marth, G. A. McVean, D. A. Nickerson, J. P. Schmidt, S. T. Sherry, J. Wang, R. K. Wilson, R. A. Gibbs (Principal, E. Boerwinkle, H. Doddapaneni, Y. Han, V. Korchina, C. Kovar, S. Lee, D. Muzny, J. G. Reid, Y. Zhu, J. Wang (Principal, Y. Chang, Q. Feng, X. Fang, X. Guo, M. Jian, H. Jiang, X. Jin, T. Lan, G. Li, J. Li, Y. Li, S. Liu, X. Liu, Y. Lu, X. Ma, M. Tang, B. Wang, G. Wang, H. Wu, R. Wu, X. Xu, Y. Yin, D. Zhang, W. Zhang, J. Zhao, M. Zhao, X. Zheng, E. S. Lander (Principal, D. M. Altshuler, S. B. Gabriel (Co-Chair), N. Gupta, N. Gharani, L. H. Toji, N. P. Gerry, A. M. Resch, P. Flicek (Principal, J. Barker, L. Clarke, L. Gil, S. E. Hunt, G. Kelman, E. Kulesha, R. Leinonen, W. M. McLaren, R. Radhakrishnan, A. Roa, D. Smirnov, R. E. Smith, I. Streeter, A. Thormann, I. Toneva, B. Vaughan, X. Zheng-Bradley, D. R. Bentley (Principal, R. Grocock, S. Humphray, T. James, Z. Kingsbury, H. Lehrach (Principal, R. Sudbrak (Project L, M. W. Albrecht, V. S. Amstislavskiy, T. A. Borodina, M. Lienhard, F. Mertes, M. Sultan, B. Timmermann, M.-L. Yaspo, E. R. Mardis (Co-Princi, R. K. Wilson (Co-Princi, L. Fulton, R. Fulton, S. T. Sherry (Principal, V. Ananiev, Z. Belaia, D. Beloslyudtsev, N. Bouk, C. Chen, D. Church, R. Cohen, C. Cook, J. Garner, T. Hefferon, M. Kimelman, C. Liu, J. Lopez, P. Meric, C. O'Sullivan, Y. Ostapchuk, L. Phan, S. Ponomarov, V. Schneider, E. Shekhtman, K. Sirotkin, D. Slotta, H. Zhang, G. A. McVean (Principal, R. M. Durbin (Principal, S. Balasubramaniam, J. Burton, P. Danecek, T. M. Keane, A. Kolb-Kokocinski, S. McCarthy, J. Stalker, M. Quail, J. P. Schmidt (Principal, C. J. Davies, J. Gollub, T. Webster, B. Wong, Y. Zhan, A. Auton (Principal, C. L. Campbell, Y. Kong, A. Marcketta, R. A. Gibbs (Principal, F. Yu (Project L, L. Antunes, M. Bainbridge, D. Muzny, A. Sabo, Z. Huang, J. Wang (Principal, L. J. M. Coin, L. Fang, X. Guo, X. Jin, G. Li, Q. Li, Y. Li, Z. Li, H. Lin, B. Liu, R. Luo, H. Shao, Y. Xie, C. Ye, C. Yu, F. Zhang, H. Zheng, H. Zhu, C. Alkan, E. Dal, F. Kahveci, G. T. Marth (Principal, E. P. Garrison (Project L, D. Kural, W.-P. Lee, W. Fung Leong, M. Stromberg, A. N. Ward, J. Wu, M. Zhang, M. J. Daly (Principal, M. A. DePristo (Project L, R. E. Handsaker (Project L, D. M. Altshuler, E. Banks, G. Bhatia, G. del Angel, S. B. Gabriel, G. Genovese, N. Gupta, H. Li, S. Kashin, E. S. Lander, S. A. McCarroll, J. C. Nemesh, R. E. Poplin, S. C. Yoon (Principal, J. Lihm, V. Makarov, A. G. Clark (Principal, S. Gottipati, A. Keinan, J. L. Rodriguez-Flores, J. O. Korbel (Principal, T. Rausch (Project L, M. H. Fritz, A. M. Stütz, P. Flicek (Principal, K. Beal, L. Clarke, A. Datta, J. Herrero, W. M. McLaren, G. R. S. Ritchie, R. E. Smith, D. Zerbino, X. Zheng-Bradley, P. C. Sabeti (Principal, I. Shlyakhter, S. F. Schaffner, J. Vitti, D. N. Cooper (Principal, E. V. Ball, P. D. Stenson, D. R. Bentley (Principal, B. Barnes, M. Bauer, R. Keira Cheetham, A. Cox, M. Eberle, S. Humphray, S. Kahn, L. Murray, J. Peden, R. Shaw, E. E. Kenny (Principal, M. A. Batzer (Principal, M. K. Konkel, J. A. Walker, D. G. MacArthur (Principal, M. Lek, R. Sudbrak (Project L, V. S. Amstislavskiy, R. Herwig, E. R. Mardis (Co-Princi, L. Ding, D. C. Koboldt, D. Larson, K. Ye, S. Gravel, A. Swaroop, E. Chew, T. Lappalainen (Principal, Y. Erlich (Principal, M. Gymrek, T. Frederick Willems, J. T. Simpson, M. D. Shriver (Principal, J. A. Rosenfeld (Principal, C. D. Bustamante (Principal, S. B. Montgomery (Principal, F. M. De La Vega (Principal, J. K. Byrnes, A. W. Carroll, M. K. DeGorter, P. Lacroute, B. K. Maples, A. R. Martin, A. Moreno-Estrada, S. S. Shringarpure, F. Zakharia, E. Halperin (Principal, Y. Baran, C. Lee (Principal, E. Cerveira, J. Hwang, A. Malhotra (Co-Projec, D. Plewczynski, K. Radew, M. Romanovitch, C. Zhang (Co-Projec, F. C. L. Hyland, D. W. Craig (Principal, A. Christoforides, N. Homer, T. Izatt, A. A. Kurdoglu, S. A. Sinari, K. Squire, S. T. Sherry (Principal, C. Xiao, J. Sebat (Principal, D. Antaki, M. Gujral, A. Noor, K. Ye, E. G. Burchard (Principal,

R. D. Hernandez (Principal, C. R. Gignoux, D. Haussler (Principal, S. J. Katzman, W. James Kent, B. Howie, A. Ruiz-Linares (Principal, E. T. Dermitzakis (Principal, S. E. Devine (Principal, G. R. Abecasis (Principal, H. Min Kang (Project L, J. M. Kidd (Principal, T. Blackwell, S. Caron, W. Chen, S. Emery, L. Fritsche, C. Fuchsberger, G. Jun, B. Li, R. Lyons, C. Scheller, C. Sidore, S. Song, E. Sliwerska, D. Taliun, A. Tan, R. Welch, M. Kate Wing, X. Zhan, P. Awadalla (Principal, A. Hodgkinson, Y. Li, X. Shi (Principal, A. Quitadamo, G. Lunter (Principal, G. A. McVean (Principal, J. L. Marchini (Principal, S. Myers (Principal, C. Churchhouse, O. Delaneau, A. Gupta-Hinch, W. Kretzschmar, Z. Iqbal, I. Mathieson, A. Menelaou, A. Rimmer, D. K. Xifara, T. K. Oleksyk (Principal, Y. Fu (Principal, X. Liu, M. Xiong, L. Jorde (Principal, D. Witherspoon, J. Xing, E. E. Eichler (Principal, B. L. Browning (Principal, S. R. Browning (Principal, F. Hormozdiari, P. H. Sudmant, E. Khurana (Principal, R. M. Durbin (Principal, M. E. Hurles (Principal, C. Tyler-Smith (Principal, C. A. Albers, Q. Ayub, S. Balasubramaniam, Y. Chen, V. Colonna, P. Danecek, L. Jostins, T. M. Keane, S. McCarthy, K. Walter, Y. Xue, M. B. Gerstein (Principal, A. Abyzov, S. Balasubramanian, J. Chen, D. Clarke, Y. Fu, A. O. Harmanci, M. Jin, D. Lee, J. Liu, X. Jasmine Mu, J. Zhang, Y. Zhang, Y. Li, R. Luo, H. Zhu, C. Alkan, E. Dal, F. Kahveci, G. T. Marth (Principal, E. P. Garrison, D. Kural, W.-P. Lee, A. N. Ward, J. Wu, M. Zhang, S. A. McCarroll (Principal, R. E. Handsaker (Project L, D. M. Altshuler, E. Banks, G. del Angel, G. Genovese, C. Hartl, H. Li, S. Kashin, J. C. Nemesh, K. Shakir, S. C. Yoon (Principal, J. Lihm, V. Makarov, J. Degenhardt, J. O. Korbel (Principal, M. H. Fritz, S. Meiers, B. Raeder, T. Rausch, A. M. Stütz, P. Flicek (Principal, F. Paolo Casale, L. Clarke, R. E. Smith, O. Stegle, X. Zheng-Bradley, D. R. Bentley (Principal, B. Barnes, R. Keira Cheetham, M. Eberle, S. Humphray, S. Kahn, L. Murray, R. Shaw, E.-W. Lameijer, M. A. Batzer (Principal, M. K. Konkel, J. A. Walker, L. Ding (Principal, I. Hall, K. Ye, P. Lacroute, C. Lee (Principal, E. Cerveira, A. Malhotra, J. Hwang, D. Plewczynski, K. Radew, M. Romanovitch, C. Zhang, D. W. Craig (Principal, N. Homer, D. Church, C. Xiao, J. Sebat (Principal, D. Antaki, V. Bafna, J. Michaelson, K. Ye, S. E. Devine (Principal, E. J. Gardner (Project L, G. R. Abecasis (Principal, J. M. Kidd (Principal, R. E. Mills (Principal, G. Dayama, S. Emery, G. Jun, X. Shi (Principal, A. Quitadamo, G. Lunter (Principal, G. A. McVean (Principal, K. Chen (Principle, X. Fan, Z. Chong, T. Chen, D. Witherspoon, J. Xing, E. E. Eichler (Principal, M. J. Chaisson, F. Hormozdiari, J. Huddleston, M. Malig, B. J. Nelson, P. H. Sudmant, N. F. Parrish, E. Khurana (Principal, M. E. Hurles (Principal, B. Blackburne, S. J. Lindsay, Z. Ning, K. Walter, Y. Zhang, M. B. Gerstein (Principal, A. Abyzov, J. Chen, D. Clarke, H. Lam, X. Jasmine Mu, C. Sisu, J. Zhang, Y. Zhang, R. A. Gibbs (Principal, F. Yu (Project L, M. Bainbridge, D. Challis, U. S. Evani, C. Kovar, J. Lu, D. Muzny, U. Nagaswamy, J. G. Reid, A. Sabo, J. Yu, X. Guo, W. Li, Y. Li, R. Wu, G. T. Marth (Principal, E. P. Garrison, W. Fung Leong, A. N. Ward, G. del Angel, M. A. DePristo, S. B. Gabriel, N. Gupta, C. Hartl, R. E. Poplin, A. G. Clark (Principal, J. L. Rodriguez-Flores, P. Flicek (Principal, L. Clarke, R. E. Smith, X. Zheng-Bradley, D. G. MacArthur (Principal, E. R. Mardis (Principal, R. Fulton, D. C. Koboldt, S. Gravel, C. D. Bustamante (Principal, D. W. Craig (Principal, A. Christoforides, N. Homer, T. Izatt, S. T. Sherry (Principal, C. Xiao, E. T. Dermitzakis (Principal, G. R. Abecasis (Principal, H. Min Kang, G. A. McVean (Principal, M. B. Gerstein (Principal, S. Balasubramanian, L. Habegger, H. Yu (Principal, P. Flicek (Principal, L. Clarke, F. Cunningham, I. Dunham, D. Zerbino, X. Zheng-Bradley, K. Lage (Principal, J. Berg Jespersen, H. Horn, S. B. Montgomery (Principal, M. K. DeGorter, E. Khurana (Principal, C. Tyler-Smith (Principal, Y. Chen, V. Colonna, Y. Xue, M. B. Gerstein (Principal, S. Balasubramanian, Y. Fu, D. Kim, A. Auton (Principal, A. Marcketta, R. Desalle, A. Narechania, M. A. Wilson Sayres, E. P. Garrison, R. E. Handsaker, S. Kashin, S. A. McCarroll, J. L. Rodriguez-Flores, P. Flicek (Principal, L. Clarke, X. Zheng-Bradley, Y. Erlich, M. Gymrek, T. Frederick Willems, C. D. Bustamante (Principal, F. L. Mendez, G. David Poznik, P. A. Underhill, C. Lee, E. Cerveira, A. Malhotra, M. Romanovitch, C. Zhang, G. R. Abecasis (Principal, L. Coin (Principal, H. Shao, D. Mittelman, C. Tyler-Smith (Principal, Q. Ayub, R. Banerjee, M. Cerezo, Y. Chen, T. W. Fitzgerald, S. Louzada, A. Massaia, S. McCarthy, G. R. Ritchie, Y. Xue, F. Yang, R. A. Gibbs (Principal, C. Kovar, D. Kalra, W. Hale, D. Muzny, J. G. Reid, J. Wang (Principal, X. Dan, X. Guo, G. Li, Y. Li, C. Ye, X. Zheng, D. M. Altshuler, P. Flicek (Principal, L. Clarke (Project L, X. Zheng-Bradley, D. R. Bentley (Principal, A. Cox, S. Humphray, S. Kahn, R. Sudbrak (Project L, M. W. Albrecht, M. Lienhard, D. Larson, D. W. Craig (Principal, T. Izatt, A. A. Kurdoglu, S. T. Sherry (Principal, C. Xiao, D. Haussler (Principal, G. R. Abecasis (Principal, G. A. McVean (Principal, R. M. Durbin (Principal, S. Balasubramaniam, T. M. Keane, S. McCarthy, J. Stalker, A. Chakravarti (Co-Chair), B. M. Knoppers (Co-Chair), G. R. Abecasis, K. C. Barnes, C. Beiswanger, E. G. Burchard, C. D. Bustamante, H. Cai, H. Cao, R. M. Durbin, N. P. Gerry, N. Gharani, R. A. Gibbs, C. R. Gignoux, S. Gravel, B. Henn, D. Jones, L. Jorde, J. S. Kaye, A. Keinan, A. Kent, A. Kerasidou, Y. Li, R. Mathias, G. A. McVean, A. Moreno-Estrada, P. N. Ossorio, M. Parker, A. M. Resch, C. N. Rotimi, Charmaine D. Royal, K. Sandoval, Y. Su, R. Sudbrak, Z. Tian, S. Tishkoff, L. H. Toji, C. Tyler-Smith, M. Via, Y. Wang, H. Yang, L. Yang, J. Zhu, W. Bodmer, G. Bedoya, A. Ruiz-Linares, Z. Cai, Y. Gao, J. Chu, L. Peltonen, A. Garcia-Montero, A. Orfao, J. Dutil, J. C. Martinez-Cruzado, T. K. Oleksyk, K. C. Barnes, R. A. Mathias, A. Hennis, H. Watson, C. McKenzie, F. Qadri, R. LaRocque, P. C. Sabeti, J. Zhu, X. Deng, P. C. Sabeti, D. Asogun, O. Folarin,

C. Happi, O. Omoniwa, M. Stremlau, R. Tariyal, M. Jallow, F. Sisay Joof, T. Corrah, K. Rockett, D. Kwiatkowski, J. Kooner, T. Tịnh Hiê`n, S. J. Dunstan, N. Thuy Hang, R. Fonnie, R. Garry, L. Kanneh, L. Moses, P. C. Sabeti, J. Schieffelin, D. S. Grant, C. Gallo, G. Poletti, D. Saleheen, A. Rasheed, L. D. Brooks, A. L. Felsenfeld, J. E. McEwen, Y. Vaydylevich, E. D. Green, A. Duncanson, M. Dunn, J. A. Schloss, J. Wang, H. Yang, A. Auton, L. D. Brooks, R. M. Durbin, E. P. Garrison, H. Min Kang, J. O. Korbel, J. L. Marchini, S. McCarthy, G. A. McVean, G. R. Abecasis, Corresponding authors, Steering committee, Production group, Baylor College of Medicine, BGI-Shenzhen, Broad Institute of MIT and Harvard, Coriell Institute for Medical Research, European Molecular Biology Laboratory, European Bioinformatics Institute, Illumina, Max Planck Institute for Molecular Genetics, McDonnell Genome Institute at Washington University, US National Institutes of Health, University of Oxford, Wellcome Trust Sanger Institute, Analysis group, Affymetrix, Albert Einstein College of Medicine, Baylor College of Medicine, BGI-Shenzhen, Bilkent University, Boston College, Broad Institute of MIT and Harvard, Cold Spring Harbor Laboratory, Cornell University, European Molecular Biology Laboratory, European Molecular Biology Laboratory, European Bioinformatics Institute, Harvard University, Human Gene Mutation Database, Illumina, Icahn School of Medicine at Mount Sinai, Louisiana State University, Massachusetts General Hospital, Max Planck Institute for Molecular Genetics, McDonnell Genome Institute at Washington University, McGill University, National Eye Institute, NIH, New York Genome Center, Ontario Institute for Cancer Research, Pennsylvania State University, Rutgers Cancer Institute of New Jersey, Stanford University, Tel-Aviv University, The Jackson Laboratory for Genomic Medicine, T. F. Scientific, Translational Genomics Research Institute, US National Institutes of Health, University of California, San Diego, University of California, San Francisco, University of California, Santa Cruz, University of Chicago, University College London, University of Geneva, University of Maryland School of Medicine, University of Michigan, University of Montréal, University of North Carolina at Chapel Hill, University of North Carolina at Charlotte, University of Oxford, University of Puerto Rico, University of Texas Health Sciences Center at Houston, University of Utah, University of Washington, Weill Cornell Medical College, Wellcome Trust Sanger Institute, Yale University, Structural variation group, BGI-Shenzhen, Bilkent University, Boston College, Broad Institute of MIT and Harvard, Cold Spring Harbor Laboratory, Cornell University, European Molecular Biology Laboratory, European Molecular Biology Laboratory, European Bioinformatics Institute, Illumina, Leiden University Medical Center, Louisiana State University, McDonnell Genome Institute at Washington University, Stanford University, The Jackson Laboratory for Genomic Medicine, Translational Genomics Research Institute, US National Institutes of Health, University of California, San Diego, University of Maryland School of Medicine, University of Michigan, University of North Carolina at Charlotte, University of Oxford, University of Texas MD Anderson Cancer Center, University of Utah, University of Washington, Vanderbilt University School of Medicine, Weill Cornell Medical College, Wellcome Trust Sanger Institute, Yale University, Exome group, Baylor College of Medicine, BGI-Shenzhen, Boston College, Broad Institute of MIT and Harvard, Cornell University, European Molecular Biology Laboratory, European Bioinformatics Institute, Massachusetts General Hospital, McDonnell Genome Institute at Washington University, McGill University, Stanford University, Translational Genomics Research Institute, US National Institutes of Health, University of Geneva, University of Michigan, University of Oxford, Yale University, Functional interpretation group, Cornell University, European Molecular Biology Laboratory, European Bioinformatics Institute, Harvard University, Stanford University, Weill Cornell Medical College, Wellcome Trust Sanger Institute, Yale University, Chromosome Y group, Albert Einstein College of Medicine, American Museum of Natural History, Arizona State University, Boston College, Broad Institute of MIT and Harvard, Cornell University, European Molecular Biology Laboratory, European Bioinformatics Institute, New York Genome Center, Stanford University, The Jackson Laboratory for Genomic Medicine, University of Michigan, University of Queensland, Virginia Bioinformatics Institute, Wellcome Trust Sanger Institute, Data coordination center group, Baylor College of Medicine, BGI-Shenzhen, Broad Institute of MIT and Harvard, European Molecular Biology Laboratory, European Bioinformatics Institute, Illumina, Max Planck Institute for Molecular Genetics, McDonnell Genome Institute at Washington University, Translational Genomics Research Institute, US National Institutes of Health, University of California, Santa Cruz, University of Michigan, University of Oxford, Wellcome Trust Sanger Institute, Samples and ELSI group, Sample collection, British from England and Scotland (GBR), Colombians in Medellín, Colombia (CLM), Han Chinese South (CHS), Finnish in Finland (FIN), Iberian Populations in Spain (IBS), Puerto Ricans in Puerto Rico (PUR), African Caribbean in Barbados (ACB), Bengali in Bangladesh (BEB), Chinese Dai in Xishuangbanna, China (CDX), Esan in Nigeria (ESN), Gambian in Western Division - Mandinka (GWD), Indian Telugu in the UK (ITU) and Sri Lankan Tamil in the UK (STU), Kinh in Ho Chi Minh City, Vietnam (KHV), Mende in Sierra Leone (MSL), Peruvian in Lima, Peru (PEL), Punjabi in Lahore, Pakistan (PJL), Scientific management, Writing group, A global reference for human genetic variation. *Nature*. **526**, 68–74 (2015).

48. N. Zaitlen, B. Paşaniuc, T. Gur, E. Ziv, E. Halperin, Leveraging genetic variability across populations for the identification of causal variants. *Am. J. Hum. Genet.* **86**, 23–33 (2010).

49. A. Mahajan, M. J. Go, W. Zhang, J. E. Below, K. J. Gaulton, T. Ferreira, M. Horikoshi, A. D. Johnson, M. C. Y. Ng, I. Prokopenko, D. Saleheen, X. Wang, E. Zeggini, G. R. Abecasis, L. S. Adair, P. Almgren, M. Atalay, T. Aung, D. Baldassarre, B. Balkau, Y. Bao, A. H. Barnett, I. Barroso, A. Basit, L. F. Been, J. Beilby, G. I. Bell, R. Benediktsson, R. N. Bergman, B. O. Boehm, E. Boerwinkle, L. L. Bonnycastle, N. Burtt, Q. Cai, H. Campbell, J. Carey, S. Cauchi, M. Caulfield, J. C. N. Chan, L.-C. Chang, T.-J. Chang, Y.-C. Chang, G. Charpentier, C.-H. Chen, H. Chen, Y.-T. Chen, K.-S. Chia, M. Chidambaram, P. S. Chines, N. H. Cho, Y. M. Cho, L.-M. Chuang, F. S. Collins, M. C. Cornelis, D. J. Couper, A. T. Crenshaw, R. M. van Dam, J. Danesh, D. Das, U. de Faire, G. Dedoussis, P. Deloukas, A. S. Dimas, C. Dina, A. S. F. Doney, P. J. Donnelly, M. Dorkhan, C. van Duijn, J. Dupuis, S. Edkins, P. Elliott, V. Emilsson, R. Erbel, J. G. Eriksson, J. Escobedo, T. Esko, E. Eury, J. C. Florez, P. Fontanillas, N. G. Forouhi, T. Forsen, C. Fox, R. M. Fraser, T. M. Frayling, P. Froguel, P. Frossard, Y. Gao, K. Gertow, C. Gieger, B. Gigante, H. Grallert, G. B. Grant, L. C. Groop, C. J. Groves, E. Grundberg, C. Guiducci, A. Hamsten, B.-G. Han, K. Hara, N. Hassanali, A. T. Hattersley, C. Hayward, A. K. Hedman, C. Herder, A. Hofman, O. L. Holmen, K. Hovingh, A. B. Hreidarsson, C. Hu, F. B. Hu, J. Hui, S. E. Humphries, S. E. Hunt, D. J. Hunter, K. Hveem, Z. I. Hydrie, H. Ikegami, T. Illig, E. Ingelsson, M. Islam, B. Isomaa, A. U. Jackson, T. Jafar, A. James, W. Jia, K.-H. Jöckel, A. Jonsson, J. B. M. Jowett, T. Kadowaki, H. M. Kang, S. Kanoni, W. H. L. Kao, S. Kathiresan, N. Kato, P. Katulanda, S. M. Keinanen-Kiukaanniemi, A. M. Kelly, H. Khan, K.-T. Khaw, C.-C. Khor, H.-L. Kim, S. Kim, Y. J. Kim, L. Kinnunen, N. Klopp, A. Kong, E. Korpi-Hyövälti, S. Kowlessur, P. Kraft, J. Kravic, M. M. Kristensen, S. Krithika, A. Kumar, J. Kumate, J. Kuusisto, S. H. Kwak, M. Laakso, V. Lagou, T. A. Lakka, C. Langenberg, C. Langford, R. Lawrence, K. Leander, J.-M. Lee, N. R. Lee, M. Li, X. Li, Y. Li, J. Liang, S. Liju, W.-Y. Lim, L. Lind, C. M. Lindgren, E. Lindholm, C.-T. Liu, J. J. Liu, S. Lobbens, J. Long, R. J. F. Loos, W. Lu, J. Luan, V. Lyssenko, R. C. W. Ma, S. Maeda, R. Mägi, S. Männistö, D. R. Matthews, J. B. Meigs, O. Melander, A. Metspalu, J. Meyer, G. Mirza, E. Mihailov, S. Moebus, V. Mohan, K. L. Mohlke, A. D. Morris, T. W. Mühleisen, M. Müller-Nurasyid, B. Musk, J. Nakamura, E. Nakashima, P. Navarro, P.-K. Ng, A. C. Nica, P. M. Nilsson, I. Njølstad, M. M. Nöthen, K. Ohnaka, T. H. Ong, K. R. Owen, C. N. A. Palmer, J. S. Pankow, K. S. Park, M. Parkin, S. Pechlivanis, N. L. Pedersen, L. Peltonen, J. R. B. Perry, A. Peters, J. M. Pinidiyapathirage, C. G. P. Platou, S. Potter, J. F. Price, L. Qi, V. Radha, L. Rallidis, A. Rasheed, W. Rathmann, R. Rauramaa, S. Raychaudhuri, N. W. Rayner, S. D. Rees, E. Rehnberg, S. Ripatti, N. Robertson, M. Roden, E. J. Rossin, I. Rudan, D. Rybin, T. E. Saaristo, V. Salomaa, J. Saltevo, M. Samuel, D. K. Sanghera, J. Saramies, J. Scott, L. J. Scott, R. A. Scott, A. V. Segrè, J. Sehmi, B. Sennblad, N. Shah, S. Shah, A. S. Shera, X. O. Shu, A. R. Shuldiner, G. Sigurðsson, E. Sijbrands, A. Silveira, X. Sim, S. Sivapalaratnam, K. S. Small, W. Y. So, A. Stančáková, K. Stefansson, G. Steinbach, V. Steinthorsdottir, K. Stirrups, R. J. Strawbridge, H. M. Stringham, Q. Sun, C. Suo, A.-C. Syvänen, R. Takayanagi, F. Takeuchi, W. T. Tay, T. M. Teslovich, B. Thorand, G. Thorleifsson, U. Thorsteinsdottir, E. Tikkanen, J. Trakalo, E. Tremoli, M. D. Trip, F. J. Tsai, T. Tuomi, J. Tuomilehto, A. G. Uitterlinden, A. Valladares-Salgado, S. Vedantam, F. Veglia, B. F. Voight, C. Wang, N. J. Wareham, R. Wennauer, A. R. Wickremasinghe, T. Wilsgaard, J. F. Wilson, S. Wiltshire, W. Winckler, T. Y. Wong, A. R. Wood, J.-Y. Wu, Y. Wu, K. Yamamoto, T. Yamauchi, M. Yang, L. Yengo, M. Yokota, R. Young, D. Zabaneh, F. Zhang, R. Zhang, W. Zheng, P. Z. Zimmet, D. Altshuler, D. W. Bowden, Y. S. Cho, N. J. Cox, M. Cruz, C. L. Hanis, J. Kooner, J.-Y. Lee, M. Seielstad, Y. Y. Teo, M. Boehnke, E. J. Parra, J. C. Chambers, E. S. Tai, M. I. McCarthy, A. P. Morris, Genome-wide trans-ancestry meta-analysis provides insight into the genetic architecture of type 2 diabetes susceptibility. *Nat. Genet.* **46**, 234–244 (2014).

50. P. Mohammadi, S. E. Castel, A. A. Brown, T. Lappalainen, Quantifying the regulatory effect size of cis-acting genetic variation using allelic fold change. *Genome Res.* **27**, 1872–1884 (2017).

51. G. Kichaev, W.-Y. Yang, S. Lindstrom, F. Hormozdiari, E. Eskin, A. L. Price, P. Kraft, B. Pasaniuc, Integrating functional data to prioritize causal variants in statistical fine-mapping studies. *PLoS Genet.* **10**, e1004722 (2014).

52. G. Kichaev, B. Pasaniuc, Leveraging Functional-Annotation Data in Trans-ethnic Fine-Mapping Studies. *Am. J. Hum. Genet.* **97**, 260–271 (2015).

53. A. M. Newman, C. B. Steen, C. L. Liu, A. J. Gentles, A. A. Chaudhuri, F. Scherer, M. S. Khodadoust, M. S. Esfahani, B. A. Luca, D. Steiner, M. Diehn, A. A. Alizadeh, Determining cell type abundance and expression from bulk tissues with digital cytometry. *Nat. Biotechnol.* **37**, 773–782 (2019).

54. J. Werner, J. Gillis, Preservation of co-expression defines the primary tissue fidelity of human neural organoids. *bioRxiv* (2023), p. 2023.03.31.535112, , doi:10.1101/2023.03.31.535112.

55. S. Kim-Hellmuth, F. Aguet, M. Oliva, M. Muñoz-Aguirre, S. Kasela, V. Wucher, S. E. Castel, A. R. Hamel, A. Viñuela, A. L. Roberts, S. Mangul, X. Wen, G. Wang, A. N. Barbeira, D. Garrido-Martín, B. B. Nadel, Y. Zou, R. Bonazzola, J. Quan, A. Brown, A. Martinez-Perez, J. M. Soria, GTEx Consortium, G. Getz, E. T. Dermitzakis, K. S. Small, M. Stephens, H. S. Xi, H. K. Im, R. Guigó, A. V. Segrè, B. E. Stranger, K. G. Ardlie, T. Lappalainen, Cell type-specific genetic regulation of gene expression across human tissues. *Science*. **369** (2020), doi:10.1126/science.aaz8528.

56. N. Aygün, A. L. Elwell, D. Liang, M. J. Lafferty, K. E. Cheek, K. P. Courtney, J. Mory, E. Hadden-Ford, O. Krupa, L. de la Torre-Ubieta, D. H. Geschwind, M. I. Love, J. L. Stein, Brain-trait-associated variants impact cell-type-specific gene regulation during neurogenesis. *Am. J. Hum. Genet.* (2021), doi:10.1016/j.ajhg.2021.07.011.

57. D. Liang, A. L. Elwell, N. Aygün, O. Krupa, J. M. Wolter, F. A. Kyere, M. J. Lafferty, K. E. Cheek, K. P. Courtney, M. Yusupova, M. E. Garrett, A. Ashley-Koch, G. E. Crawford, M. I. Love, L. de la Torre-Ubieta, D. H. Geschwind, J. L. Stein, Cell-type-specific effects of genetic variation on chromatin accessibility during human neuronal differentiation. *Nat. Neurosci.* (2021), doi:10.1038/s41593-021-00858-w.

58. B. K. Bulik-Sullivan, P.-R. Loh, H. K. Finucane, S. Ripke, J. Yang, Schizophrenia Working Group of the Psychiatric Genomics Consortium, N. Patterson, M. J. Daly, A. L. Price, B. M. Neale, LD Score regression distinguishes confounding from polygenicity in genome-wide association studies. *Nat. Genet.* **47**, 291–295 (2015).

59. F. Hormozdiari, S. Gazal, B. van de Geijn, H. K. Finucane, C. J.-T. Ju, P.-R. Loh, A. Schoech, Y. Reshef, X. Liu, L. O'Connor, A. Gusev, E. Eskin, A. L. Price, Leveraging molecular quantitative trait loci to understand the genetic architecture of diseases and complex traits. *Nat. Genet.* **50**, 1041–1047 (2018).

60. D. Demontis, R. K. Walters, J. Martin, M. Mattheisen, T. D. Als, E. Agerbo, G. Baldursson, R. Belliveau, J. Bybjerg-Grauholm, M. Bækvad-Hansen, F. Cerrato, K. Chambert, C. Churchhouse, A. Dumont, N. Eriksson, M. Gandal, J. I. Goldstein, K. L. Grasby, J. Grove, O. O. Gudmundsson, C. S. Hansen, M. E. Hauberg, M. V. Hollegaard, D. P. Howrigan, H. Huang, J. B. Maller, A. R. Martin, N. G. Martin, J. Moran, J. Pallesen, D. S. Palmer, C. B. Pedersen, M. G. Pedersen, T. Poterba, J. B. Poulsen, S. Ripke, E. B. Robinson, F. K. Satterstrom, H. Stefansson, C. Stevens, P. Turley, G. B. Walters, H. Won, M. J. Wright, ADHD Working Group of the Psychiatric Genomics Consortium (PGC), Early Lifecourse & Genetic Epidemiology (EAGLE) Consortium, 23andMe Research Team, O. A. Andreassen, P. Asherson, C. L. Burton, D. I. Boomsma, B. Cormand, S. Dalsgaard, B. Franke, J. Gelernter, D. Geschwind, H. Hakonarson, J. Haavik, H. R. Kranzler, J. Kuntsi, K. Langley, K.-P. Lesch, C. Middeldorp, A. Reif, L. A. Rohde, P. Roussos, R. Schachar, P. Sklar, E. J. S. Sonuga-Barke, P. F. Sullivan, A. Thapar, J. Y. Tung, I. D. Waldman, S. E. Medland, K. Stefansson, M. Nordentoft, D. M. Hougaard, T. Werge, O. Mors, P. B. Mortensen, M. J. Daly, S. V. Faraone, A. D. Børglum, B. M. Neale, Discovery of the first genome-wide significant risk loci for attention deficit/hyperactivity disorder. *Nat. Genet.* **51**, 63–75 (2019).

61. D. M. Howard, M. J. Adams, M. Shirali, T.-K. Clarke, R. E. Marioni, G. Davies, J. R. I. Coleman, C. Alloza, X. Shen, M. C. Barbu, E. M. Wigmore, J. Gibson, 23andMe Research Team, S. P. Hagenaars, C. M. Lewis, J. Ward, D. J. Smith, P. F. Sullivan, C. S. Haley, G. Breen, I. J. Deary, A. M. McIntosh, Genome-wide association study of depression phenotypes in UK Biobank identifies variants in excitatory synaptic pathways. *Nat. Commun.* **9**, 1470 (2018).

62. N. Mullins, A. J. Forstner, K. S. O'Connell, B. Coombes, J. R. I. Coleman, Z. Qiao, T. D. Als, T. B. Bigdeli, S. Børte, J. Bryois, A. W. Charney, O. K. Drange, M. J. Gandal, S. P. Hagenaars, M. Ikeda, N. Kamitaki, M. Kim, K. Krebs, G. Panagiotaropoulou, B. M. Schilder, L. G. Sloofman, S. Steinberg, V. Trubetskoy, B. S. Winsvold, H.-H. Won, L. Abramova, K. Adorjan, E. Agerbo, M. Al Eissa, D. Albani, N. Alliey-Rodriguez, A. Anjorin, V. Antilla, A. Antoniou, S. Awasthi, J. H. Baek, M. Bækvad-Hansen, N. Bass, M. Bauer, E. C. Beins, S. E. Bergen, A. Birner, C. Bøcker Pedersen, E. Bøen, M. P. Boks, R. Bosch, M. Brum, B. M. Brumpton, N. Brunkhorst-Kanaan, M. Budde, J. Bybjerg-Grauholm, W. Byerley, M. Cairns, M. Casas, P. Cervantes, T.-K. Clarke, C. Cruceanu, A. Cuellar-Barboza, J. Cunningham, D. Curtis, P. M. Czerski, A. M. Dale, N. Dalkner, F. S. David, F. Degenhardt, S. Djurovic, A. L. Dobbyn, A. Douzenis, T. Elvsåshagen, V. Escott-Price, I. N. Ferrier, A. Fiorentino, T. M. Foroud, L. Forty, J. Frank, O. Frei, N. B. Freimer, L. Frisén, K. Gade, J. Garnham, J. Gelernter, M. Giørtz Pedersen, I. R. Gizer, S. D. Gordon, K. Gordon-

Smith, T. A. Greenwood, J. Grove, J. Guzman-Parra, K. Ha, M. Haraldsson, M. Hautzinger, U. Heilbronner, D. Hellgren, S. Herms, P. Hoffmann, P. A. Holmans, L. Huckins, S. Jamain, J. S. Johnson, J. L. Kalman, Y. Kamatani, J. L. Kennedy, S. Kittel-Schneider, J. A. Knowles, M. Kogevinas, M. Koromina, T. M. Kranz, H. R. Kranzler, M. Kubo, R. Kupka, S. A. Kushner, C. Lavebratt, J. Lawrence, M. Leber, H.-J. Lee, P. H. Lee, S. E. Levy, C. Lewis, C. Liao, S. Lucae, M. Lundberg, D. J. MacIntyre, S. H. Magnusson, W. Maier, A. Maihofer, D. Malaspina, E. Maratou, L. Martinsson, M. Mattheisen, S. A. McCarroll, N. W. McGregor, P. McGuffin, J. D. McKay, H. Medeiros, S. E. Medland, V. Millischer, G. W. Montgomery, J. L. Moran, D. W. Morris, T. W. Mühleisen, N. O'Brien, C. O'Donovan, L. M. Olde Loohuis, L. Oruc, S. Papiol, A. F. Pardiñas, A. Perry, A. Pfennig, E. Porichi, J. B. Potash, D. Quested, T. Raj, M. H. Rapaport, J. R. DePaulo, E. J. Regeer, J. P. Rice, F. Rivas, M. Rivera, J. Roth, P. Roussos, D. M. Ruderfer, C. Sánchez-Mora, E. C. Schulte, F. Senner, S. Sharp, P. D. Shilling, E. Sigurdsson, L. Sirignano, C. Slaney, O. B. Smeland, D. J. Smith, J. L. Sobell, C. Søholm Hansen, M. Soler Artigas, A. T. Spijker, D. J. Stein, J. S. Strauss, B. Świątkowska, C. Terao, T. E. Thorgeirsson, C. Toma, P. Tooney, E.-E. Tsermpini, M. P. Vawter, H. Vedder, J. T. R. Walters, S. H. Witt, S. Xi, W. Xu, J. M. K. Yang, A. H. Young, H. Young, P. P. Zandi, H. Zhou, L. Zillich, HUNT All-In Psychiatry, R. Adolfsson, I. Agartz, M. Alda, L. Alfredsson, G. Babadjanova, L. Backlund, B. T. Baune, F. Bellivier, S. Bengesser, W. H. Berrettini, D. H. R. Blackwood, M. Boehnke, A. D. Børglum, G. Breen, V. J. Carr, S. Catts, A. Corvin, N. Craddock, U. Dannlowski, D. Dikeos, T. Esko, B. Etain, P. Ferentinos, M. Frye, J. M. Fullerton, M. Gawlik, E. S. Gershon, F. S. Goes, M. J. Green, M. Grigoroiu-Serbanescu, J. Hauser, F. Henskens, J. Hillert, K. S. Hong, D. M. Hougaard, C. M. Hultman, K. Hveem, N. Iwata, A. V. Jablensky, I. Jones, L. A. Jones, R. S. Kahn, J. R. Kelsoe, G. Kirov, M. Landén, M. Leboyer, C. M. Lewis, Q. S. Li, J. Lissowska, C. Lochner, C. Loughland, N. G. Martin, C. A. Mathews, F. Mayoral, S. L. McElroy, A. M. McIntosh, F. J. McMahon, I. Melle, P. Michie, L. Milani, P. B. Mitchell, G. Morken, O. Mors, P. B. Mortensen, B. Mowry, B. Müller-Myhsok, R. M. Myers, B. M. Neale, C. M. Nievergelt, M. Nordentoft, M. M. Nöthen, M. C. O'Donovan, K. J. Oedegaard, T. Olsson, M. J. Owen, S. A. Paciga, C. Pantelis, C. Pato, M. T. Pato, G. P. Patrinos, R. H. Perlis, D. Posthuma, J. A. Ramos-Quiroga, A. Reif, E. Z. Reininghaus, M. Ribasés, M. Rietschel, S. Ripke, G. A. Rouleau, T. Saito, U. Schall, M. Schalling, P. R. Schofield, T. G. Schulze, L. J. Scott, R. J. Scott, A. Serretti, C. Shannon Weickert, J. W. Smoller, H. Stefansson, K. Stefansson, E. Stordal, F. Streit, P. F. Sullivan, G. Turecki, A. E. Vaaler, E. Vieta, J. B. Vincent, I. D. Waldman, T. W. Weickert, T. Werge, N. R. Wray, J.-A. Zwart, J. M. Biernacka, J. I. Nurnberger, S. Cichon, H. J. Edenberg, E. A. Stahl, A. McQuillin, A. Di Florio, R. A. Ophoff, O. A. Andreassen, Genome-wide association study of more than 40,000 bipolar disorder cases provides new insights into the underlying biology. *Nat. Genet.* **53**, 817–829 (2021).

63. Y. Hou, W. Liang, J. Zhang, Q. Li, H. Ou, Z. Wang, S. Li, X. Huang, C. Zhao, Schizophrenia-associated rs4702 G allele-specific downregulation of FURIN expression by miR-338-3p reduces BDNF production. *Schizophr. Res.* **199**, 176–180 (2018).

64. N. Schrode, S.-M. Ho, K. Yamamuro, A. Dobbyn, L. Huckins, M. R. Matos, E. Cheng, P. J. M. Deans, E. Flaherty, N. Barretto, A. Topol, K. Alganem, S. Abadali, J. Gregory, E. Hoelzli, H. Phatnani, V. Singh, D. Girish, B. Aronow, R. Mccullumsmith, G. E. Hoffman, E. A. Stahl, H. Morishita, P. Sklar, K. J. Brennand, Synergistic effects of common schizophrenia risk variants. *Nat. Genet.* **51**, 1475–1485 (2019).

65. J. M. Fu, F. K. Satterstrom, M. Peng, H. Brand, R. L. Collins, S. Dong, B. Wamsley, L. Klei, L. Wang, S. P. Hao, C. R. Stevens, C. Cusick, M. Babadi, E. Banks, B. Collins, S. Dodge, S. B. Gabriel, L. Gauthier, S. K. Lee, L. Liang, A. Ljungdahl, B. Mahjani, L. Sloofman, A. N. Smirnov, M. Barbosa, C. Betancur, A. Brusco, B. H. Y. Chung, E. H. Cook, M. L. Cuccaro, E. Domenici, G. B. Ferrero, J. J. Gargus, G. E. Herman, I. Hertz-Picciotto, P. Maciel, D. S. Manoach, M. R. Passos-Bueno, A. M. Persico, A. Renieri, J. S. Sutcliffe, F. Tassone, E. Trabetti, G. Campos, S. Cardaropoli, D. Carli, M. C. Y. Chan, C. Fallerini, E. Giorgio, A. C. Girardi, E. Hansen-Kiss, S. L. Lee, C. Lintas, Y. Ludena, R. Nguyen, L. Pavinato, M. Pericak-Vance, I. N. Pessah, R. J. Schmidt, M. Smith, C. I. S. Costa, S. Trajkova, J. Y. T. Wang, M. H. C. Yu, Autism Sequencing Consortium (ASC), Broad Institute Center for Common Disease Genomics (Broad-CCDG), iPSYCH-BROAD Consortium, D. J. Cutler, S. De Rubeis, J. D. Buxbaum, M. J. Daly, B. Devlin, K. Roeder, S. J. Sanders, M. E. Talkowski, Rare coding variation provides insight into the genetic architecture and phenotypic context of autism. *Nat. Genet.* (2022), doi:10.1038/s41588-022-01104-0.

66. D. A. Lewis, T. Hashimoto, D. W. Volk, Cortical inhibitory neurons and schizophrenia. *Nat. Rev. Neurosci.* **6**, 312–324 (2005).

67. H. L. Meltzer, Lithium mechanisms in bipolar illness and altered intracellular calcium functions. *Biol. Psychiatry*. **21**, 492–510 (1986).

68. M. Wolff, K. M. Johannesen, U. B. S. Hedrich, S. Masnada, G. Rubboli, E. Gardella, G. Lesca, D. Ville, M. Milh, L. Villard, A. Afenjar, S. Chantot-Bastaraud, C. Mignot, C. Lardennois, C. Nava, N. Schwarz, M. Gérard, L. Perrin, D. Doummar, S. Auvin, M. J. Miranda, M. Hempel, E. Brilstra, N. Knoers, N. Verbeek, M. van Kempen, K. P. Braun, G. Mancini, S. Biskup, K. Hörtnagel, M. Döcker, T. Bast, T. Loddenkemper, L. Wong-Kisiel, F. M. Baumeister, W. Fazeli, P. Striano, R. Dilena, E. Fontana, F. Zara, G. Kurlemann, J. Klepper, J. G. Thoene, D. H. Arndt, N. Deconinck, T. Schmitt-Mechelke, O. Maier, H. Muhle, B. Wical, C. Finetti, R. Brückner, J. Pietz, G. Golla, D. Jillella, K. M. Linnet, P. Charles, U. Moog, E. Õiglane-Shlik, J. F. Mantovani, K. Park, M. Deprez, D. Lederer, S. Mary, E. Scalais, L. Selim, R. Van Coster, L. Lagae, M. Nikanorova, H. Hjalgrim, G. C. Korenke, M. Trivisano, N. Specchio, B. Ceulemans, T. Dorn, K. L. Helbig, K. Hardies, H. Stamberger, P. de Jonghe, S. Weckhuysen, J. R. Lemke, I. Krägeloh-Mann, I. Helbig, G. Kluger, H. Lerche, R. S. Møller, Genetic and phenotypic heterogeneity suggest therapeutic implications in SCN2A-related disorders. *Brain*. **140**, 1316–1336 (2017).

69. P. P. Zandi, A. E. Jaffe, F. S. Goes, E. E. Burke, L. Collado-Torres, L. Huuki-Myers, A. Seyedian, Y. Lin, F. Seifuddin, M. Pirooznia, C. A. Ross, J. E. Kleinman, D. R. Weinberger, T. M. Hyde, Amygdala and anterior cingulate transcriptomes from individuals with bipolar disorder reveal downregulated neuroimmune and synaptic pathways. *Nat. Neurosci.* **25**, 381–389 (2022).

70. M. Cao, H. Zheng, X. Tan, W. Xu, Y. Rui, L. Li, X. Liu, G. Xu, G. Cui, J. Xu, J. Cao, K. Ke, Q. Wu, Upregulation of CBLL1 in rat brain cortex after lipopolysaccharide treated. *J. Mol. Histol.* **44**, 135–145 (2013).

71. A. Bhattacharya, C. Jops, M. Kim, C. Wen, D. D. Vo, J. L. Hervoso, B. Pasaniuc, M. J. Gandal, Isoform-level transcriptome-wide association uncovers extensive novel genetic risk mechanisms for neuropsychiatric disorders in the human brain. *bioRxiv* (2022), , doi:10.1101/2022.08.23.22279134.

72. F. Privé, H. Aschard, A. Ziyatdinov, M. G. B. Blum, Efficient analysis of large-scale genome-wide data with two R packages: bigstatsr and bigsnpr. *Bioinformatics*. **34**, 2781–2787 (2018).

73. A. Hukku, M. Pividori, F. Luca, R. Pique-Regi, H. K. Im, X. Wen, Probabilistic colocalization of genetic variants from complex and molecular traits: promise and limitations. *Am. J. Hum. Genet.* **108**, 25–35 (2021).

74. A. Zhu, N. Matoba, E. P. Wilson, A. L. Tapia, Y. Li, J. G. Ibrahim, J. L. Stein, M. I. Love, MRLocus: Identifying causal genes mediating a trait through Bayesian estimation of allelic heterogeneity. *PLoS Genet.* **17**, e1009455 (2021).

75. P. Langfelder, S. Horvath, WGCNA: an R package for weighted correlation network analysis. *BMC Bioinformatics*. **9**, 559 (2008).

76. M. J. Gandal, J. R. Haney, N. N. Parikshak, V. Leppa, G. Ramaswami, C. Hartl, A. J. Schork, V. Appadurai, A. Buil, T. M. Werge, C. Liu, K. P. White, CommonMind Consortium, PsychENCODE Consortium, iPSYCH-BROAD Working Group, S. Horvath, D. H. Geschwind, Shared molecular neuropathology across major psychiatric disorders parallels polygenic overlap. *Science*. **359**, 693–697 (2018).

77. N. N. Parikshak, M. J. Gandal, D. H. Geschwind, Systems biology and gene networks in neurodevelopmental and neurodegenerative disorders. *Nat. Rev. Genet.* **16**, 441–458 (2015).

78. P. F. Przytycki, K. S. Pollard, CellWalker integrates single-cell and bulk data to resolve regulatory elements across cell types in complex tissues. *Genome Biol.* **22**, 61 (2021).

79. R. S. Ziffra, C. N. Kim, J. M. Ross, A. Wilfert, T. N. Turner, M. Haeussler, A. M. Casella, P. F. Przytycki, K. C. Keough, D. Shin, D. Bogdanoff, A. Kreimer, K. S. Pollard, S. A. Ament, E. E. Eichler, N. Ahituv, T. J. Nowakowski, Single-cell epigenomics reveals mechanisms of human cortical development. *Nature*. **598**, 205–213 (2021).

80. D. Zhang, S. Guelfi, S. Garcia-Ruiz, B. Costa, R. H. Reynolds, K. D'Sa, W. Liu, T. Courtin, A. Peterson, A. E. Jaffe, J. Hardy, J. A. Botía, L. Collado-Torres, M. Ryten, Incomplete annotation has a disproportionate impact on our understanding of Mendelian and complex neurogenetic disorders. *Science Advances*. **6**, eaay8299 (2020).

81. S. Das, L. Forer, S. Schönherr, C. Sidore, A. E. Locke, A. Kwong, S. I. Vrieze, E. Y. Chew, S. Levy, M. McGue, D. Schlessinger, D. Stambolian, P.-R. Loh, W. G. Iacono, A. Swaroop, L. J. Scott, F. Cucca, F. Kronenberg, M. Boehnke, G. R. Abecasis, C. Fuchsberger, Next-generation genotype imputation service and methods. *Nat. Genet.* **48**, 1284–1287 (2016).

82. A. Frankish, M. Diekhans, I. Jungreis, J. Lagarde, J. E. Loveland, J. M. Mudge, C. Sisu, J. C. Wright, J. Armstrong, I. Barnes, A. Berry, A. Bignell, C. Boix, S. Carbonell Sala, F. Cunningham, T. Di Domenico, S. Donaldson, I. T. Fiddes, C. García Girón, J. M. Gonzalez, T. Grego, M. Hardy, T. Hourlier, K. L. Howe, T. Hunt, O. G. Izuogu, R. Johnson, F. J. Martin, L. Martínez, S. Mohanan, P. Muir, F. C. P. Navarro, A. Parker, B. Pei, F. Pozo, F. C. Riera, M. Ruffier, B. M. Schmitt, E. Stapleton, M.-M. Suner, I. Sycheva, B. Uszczynska-Ratajczak, M. Y. Wolf, J. Xu, Y. T. Yang, A. Yates, D. Zerbino, Y. Zhang, J. S. Choudhary, M. Gerstein, R. Guigó, T. J. P. Hubbard, M. Kellis, B. Paten, M. L. Tress, P. Flicek, GENCODE 2021. *Nucleic Acids Res.* **49**, D916–D923 (2021).

83. A. Dobin, C. A. Davis, F. Schlesinger, J. Drenkow, C. Zaleski, S. Jha, P. Batut, M. Chaisson, T. R. Gingeras, STAR: ultrafast universal RNA-seq aligner. *Bioinformatics*. **29**, 15–21 (2013).

84. H. Ongen, A. Buil, A. A. Brown, E. T. Dermitzakis, O. Delaneau, Fast and efficient QTL mapper for thousands of molecular phenotypes. *Bioinformatics*. **32**, 1479–1485 (2016).

85. M. Kim, D. D. Vo, C. T. Jops, C. Wen, A. Patowary, A. Bhattacharya, C. X. Yap, H. Zhou, M. J. Gandal, Multivariate variance components analysis uncovers genetic architecture of brain isoform expression and novel psychiatric disease mechanisms. *bioRxiv* (2022), p. 2022.10.18.22281204, , doi:10.1101/2022.10.18.22281204.

86. C. Wen, M. Margolis, M. Gandal, *gandallab/devBrain_xQTL: zenodo v2* (Zenodo, 2023; http://dx.doi.org/10.5281/ZENODO.8336503).

87. S. Purcell, B. Neale, K. Todd-Brown, L. Thomas, M. A. R. Ferreira, D. Bender, J. Maller, P. Sklar, P. I. W. de Bakker, M. J. Daly, P. C. Sham, PLINK: a tool set for whole-genome association and population-based linkage analyses. *Am. J. Hum. Genet.* **81**, 559–575 (2007).

88. H. Zhao, Z. Sun, J. Wang, H. Huang, J.-P. Kocher, L. Wang, CrossMap: a versatile tool for coordinate conversion between genome assemblies. *Bioinformatics*. **30**, 1006–1007 (2014).

89. S. Andrews, Others, FastQC: a quality control tool for high throughput sequence data (2010).

90. P. Ewels, M. Magnusson, S. Lundin, M. Käller, MultiQC: summarize analysis results for multiple tools and samples in a single report. *Bioinformatics*. **32**, 3047–3048 (2016).

91. C. Soneson, M. I. Love, M. D. Robinson, Differential analyses for RNA-seq: transcript-level estimates improve gene-level inferences. *F1000Res.* **4**, 1521 (2015).

92. M. I. Love, W. Huber, S. Anders, Moderated estimation of fold change and dispersion for RNA-seq data with DESeq2. *Genome Biol.* **15**, 550 (2014).

93. J. T. Leek, W. E. Johnson, H. S. Parker, A. E. Jaffe, J. D. Storey, The sva package for removing batch effects and other unwanted variation in high-throughput experiments. *Bioinformatics*. **28**, 882–883 (2012).

94. B. van de Geijn, G. McVicker, Y. Gilad, J. K. Pritchard, WASP: allele-specific software for robust molecular quantitative trait locus discovery. *Nat. Methods*. **12**, 1061–1063 (2015).

95. H. Li, B. Handsaker, A. Wysoker, T. Fennell, J. Ruan, N. Homer, G. Marth, G. Abecasis, R. Durbin, 1000 Genome Project Data Processing Subgroup, The Sequence Alignment/Map format and SAMtools. *Bioinformatics*. **25**, 2078–2079 (2009).

96. T. Raj, Y. I. Li, G. Wong, J. Humphrey, M. Wang, S. Ramdhani, Y.-C. Wang, B. Ng, I. Gupta, V. Haroutunian, E. E. Schadt, T. Young-Pearse, S. Mostafavi, B. Zhang, P. Sklar, D. A. Bennett, P. L. De Jager, Integrative transcriptome analyses of the aging brain implicate altered splicing in Alzheimer's disease susceptibility. *Nat. Genet.* **50**, 1584–1592 (2018).

97. Y. I. Li, G. Wong, J. Humphrey, T. Raj, Prioritizing Parkinson's disease genes using population-scale transcriptomic data. *Nat. Commun.* **10**, 994 (2019).

98. S. Mostafavi, A. Battle, X. Zhu, A. E. Urban, D. Levinson, S. B. Montgomery, D. Koller, Normalizing RNA-sequencing data by modeling hidden covariates with prior knowledge. *PLoS One*. **8**, e68141 (2013).

99. C. Ruiz-Arenas, A. Cáceres, M. López-Sánchez, I. Tolosana, L. Pérez-Jurado, J. R. González, scoreInvHap: Inversion genotyping for genome-wide association studies. *PLoS Genet.* **15**, e1008203 (2019).

100. D. R. Zerbino, S. P. Wilder, N. Johnson, T. Juettemann, P. R. Flicek, The ensembl regulatory build. *Genome Biol.* **16** (2015), doi:10.1186/s13059-015-0621-5.

101. W. McLaren, L. Gil, S. E. Hunt, H. S. Riat, G. R. S. Ritchie, A. Thormann, P. Flicek, F. Cunningham, The ensembl variant effect predictor. *Genome Biol.* **17** (2016), doi:10.1186/s13059-016-0974-4.

102. X. Wen, Effective QTL Discovery Incorporating Genomic Annotations. *bioRxiv* (2015), , doi:10.1101/032003.

103. P. Danecek, J. K. Bonfield, J. Liddle, J. Marshall, V. Ohan, M. O. Pollard, A. Whitwham, T. Keane, S. A. McCarthy, R. M. Davies, H. Li, Twelve years of SAMtools and BCFtools. *Gigascience*. **10** (2021), doi:10.1093/gigascience/giab008.

104. H. Zhou, J. S. Sinsheimer, D. M. Bates, B. B. Chu, C. A. German, S. S. Ji, K. L. Keys, J. Kim, S. Ko, G. D. Mosher, J. C. Papp, E. M. Sobel, J. Zhai, J. J. Zhou, K. Lange, OPENMENDEL: a cooperative programming project for statistical genetics. *Hum. Genet.* **139**, 61–71 (2020).

105. D. M. Howard, M. J. Adams, T.-K. Clarke, J. D. Hafferty, J. Gibson, M. Shirali, J. R. I. Coleman, S. P. Hagenaars, J. Ward, E. M. Wigmore, C. Alloza, X. Shen, M. C. Barbu, E. Y. Xu, H. C. Whalley, R. E. Marioni, D. J. Porteous, G. Davies, I. J. Deary, G. Hemani, K. Berger, H. Teismann, R. Rawal, V. Arolt, B. T. Baune, U. Dannlowski, K. Domschke, C. Tian, D. A. Hinds, 23andMe Research Team, Major Depressive Disorder Working Group of the Psychiatric Genomics Consortium, M. Trzaskowski, E. M. Byrne, S. Ripke, D. J. Smith, P. F. Sullivan, N. R. Wray, G. Breen, C. M. Lewis, A. M. McIntosh, Genome-wide meta-analysis of depression identifies 102 independent variants and highlights the importance of the prefrontal brain regions. *Nat. Neurosci.* **22**, 343–352 (2019).

106. Y. Liu, S. Chen, Z. Li, A. C. Morrison, E. Boerwinkle, X. Lin, ACAT: A Fast and Powerful p Value Combination Method for Rare-Variant Analysis in Sequencing Studies. *Am. J. Hum. Genet.* **104**, 410–421 (2019).

107. J. P. Shaffer, Modified Sequentially Rejective Multiple Test Procedures. *J. Am. Stat. Assoc.* **81**, 826–831 (1986).

108. N. Mancuso, M. K. Freund, R. Johnson, H. Shi, G. Kichaev, A. Gusev, B. Pasaniuc, Probabilistic fine-mapping of transcriptome-wide association studies. *Nat. Genet.* **51**, 675–682 (2019).

109. Y. Zhang, R. Zhou, Y. Wang, Sashimi.py: a flexible toolkit for combinatorial analysis of genomic data. *bioRxiv* (2022), , doi:10.1101/2022.11.02.514803.

110. M. Kim, D. D. Vo, M. E. Kumagai, C. T. Jops, M. J. Gandal, GeneticsMakie.jl: A versatile and scalable toolkit for visualizing locus-level genetic and genomic data. *Bioinformatics* (2022), doi:10.1093/bioinformatics/btac786.

111. K. J. Karczewski, L. C. Francioli, G. Tiao, B. B. Cummings, J. Alföldi, Q. Wang, R. L. Collins, K. M. Laricchia, A. Ganna, D. P. Birnbaum, L. D. Gauthier, H. Brand, M. Solomonson, N. A. Watts, D. Rhodes, M. Singer-Berk, E. M. England, E. G. Seaby, J. A. Kosmicki, R. K. Walters, K. Tashman, Y. Farjoun, E. Banks, T. Poterba, A. Wang, C. Seed, N. Whiffin, J. X. Chong, K. E. Samocha, E. Pierce-Hoffman, Z. Zappala, A. H. O'Donnell-Luria, E. V. Minikel, B. Weisburd, M. Lek, J. S. Ware, C. Vittal, I. M. Armean, L. Bergelson, K. Cibulskis, K. M. Connolly, M. Covarrubias, S. Donnelly, S. Ferriera, S. Gabriel, J. Gentry, N. Gupta, T. Jeandet, D. Kaplan, C. Llanwarne, R. Munshi, S. Novod, N. Petrillo, D. Roazen, V. Ruano-Rubio, A. Saltzman, M. Schleicher, J. Soto, K. Tibbetts, C. Tolonen, G. Wade, M. E. Talkowski, Genome Aggregation Database Consortium, B. M. Neale, M. J. Daly, D. G. MacArthur, The mutational constraint spectrum quantified from variation in 141,456 humans. *Nature*. **581**, 434–443 (2020).

112. K. A. Johnson, A. Krishnan, Robust normalization and transformation techniques for constructing gene coexpression networks from RNA-seq data. *Genome Biol.* **23**, 1 (2022).

113. C. A. de Leeuw, J. M. Mooij, T. Heskes, D. Posthuma, MAGMA: generalized gene-set analysis of GWAS data. *PLoS Comput. Biol.* **11**, e1004219 (2015).

114. N. Y. A. Sey, B. Hu, W. Mah, H. Fauni, J. C. McAfee, P. Rajarajan, K. J. Brennand, S. Akbarian, H. Won, A computational tool (H-MAGMA) for improved prediction of brain-disorder risk genes by incorporating brain chromatin interaction profiles. *Nat. Neurosci.* **23**, 583–593 (2020).

115. B. S. Abrahams, D. E. Arking, D. B. Campbell, H. C. Mefford, E. M. Morrow, L. A. Weiss, I. Menashe, T. Wadkins, S. Banerjee-Basu, A. Packer, SFARI Gene 2.0: a community-driven knowledgebase for the autism spectrum disorders (ASDs). *Mol. Autism*. **4**, 36 (2013).

116. Y.-C. A. Feng, D. P. Howrigan, L. E. Abbott, K. Tashman, F. Cerrato, T. Singh, H. Heyne, A. Byrnes, C. Churchhouse, N. Watts, M. Solomonson, D. Lal, E. L. Heinzen, R. S. Dhindsa, K. E. Stanley, G. L. Cavalleri, H. Hakonarson, I. Helbig, R. Krause, P. May, S. Weckhuysen, S. Petrovski, S. Kamalakaran, S. M. Sisodiya, P. Cossette, C. Cotsapas, P. De Jonghe, T. Dixon-Salazar, R. Guerrini, P. Kwan, A. G. Marson, R. Stewart, C. Depondt, D. J. Dlugos, I. E. Scheffer, P. Striano, C. Freyer, K. McKenna, B. M. Regan, S. T. Bellows, C. Leu, C. A. Bennett, E. M. C. Johns, A. Macdonald, H. Shilling, R. Burgess, D. Weckhuysen, M. Bahlo, T. J. O'Brien, M. Todaro, H. Stamberger, D. M. Andrade, T. R. Sadoway, K. Mo, H. Krestel, S. Gallati, S. S. Papacostas, I. Kousiappa, G. A. Tanteles, K. Štěrbová, M. Vlčková, L. Sedláčková, P. Laššuthová, K. M. Klein, F. Rosenow, P. S. Reif, S. Knake, W. S. Kunz, G. Zsurka, C. E. Elger, J. Bauer, M. Rademacher, M. Pendziwiat, H. Muhle, A. Rademacher, A. van Baalen, S. von Spiczak, U. Stephani, Z. Afawi, A. D. Korczyn, M. Kanaan, C. Canavati, G. Kurlemann, K. Müller-Schlüter, G. Kluger, M. Häusler, I. Blatt, J. R. Lemke, I. Krey, Y. G. Weber, S. Wolking, F. Becker, C. Hengsbach, S. Rau, A. F. Maisch, B. J. Steinhoff, A. Schulze-Bonhage, S. Schubert-Bast, H. Schreiber, I. Borggräfe, C. J. Schankin, T. Mayer, R. Korinthenberg, K. Brockmann, G. Kurlemann, D. Dennig, R. Madeleyn, R. Kälviäinen, P. Auvinen, A. Saarela, T. Linnankivi, A.-E. Lehesjoki, M. I. Rees, S.-K. Chung, W. O. Pickrell, R. Powell, N. Schneider, S. Balestrini, S. Zagaglia, V. Braatz, M. R. Johnson, P. Auce, G. J. Sills, L. W. Baum, P. C. Sham, S. S. Cherny, C. H. T. Lui, N. Barišić, N. Delanty, C. P. Doherty, A. Shukralla, M. McCormack, H. El-Naggar, L. Canafoglia, S. Franceschetti, B. Castellotti, T. Granata, F. Zara, M. Iacomino, F. Madia, M. S. Vari, M. M. Mancardi, V. Salpietro, F. Bisulli, P. Tinuper, L. Licchetta, T. Pippucci, C. Stipa, R. Minardi, A. Gambardella, A. Labate, G. Annesi, L. Manna, M. Gagliardi, E. Parrini, D. Mei, A. Vetro, C. Bianchini, M. Montomoli, V. Doccini, C. Marini, T. Suzuki, Y. Inoue, K. Yamakawa, B. Tumiene, L. G. Sadleir, C. King, E. Mountier, S. H. Caglayan, M. Arslan, Z. Yapıcı, U. Yis, P. Topaloglu, B. Kara, D. Turkdogan, A. Gundogdu-Eken, N. Bebek, S. Uğur-İşeri, B. Baykan, B. Salman, G. Haryanyan, E. Yücesan, Y. Kesim, Ç. Özkara, A. Poduri, B. R. Shiedley, C. Shain, R. J. Buono, T. N. Ferraro, M. R. Sperling, W. Lo, M. Privitera, J. A. French, S. Schachter, R. I. Kuzniecky, O. Devinsky, M. Hegde, P. Khankhanian, K. L. Helbig, C. A. Ellis, G. Spalletta, F. Piras, F. Piras, T. Gili, V. Ciullo, A. Reif, A. McQuillin, N. Bass, A. McIntosh, D. Blackwood, M. Johnstone, A. Palotie, M. T. Pato, C. N. Pato, E. J. Bromet, C. B. Carvalho, E. D. Achtyes, M. H. Azevedo, R. Kotov, D. S. Lehrer, D. Malaspina, S. R. Marder, H. Medeiros, C. P. Morley, D. O. Perkins, J. L. Sobell, P. F. Buckley, F. Macciardi, M. H. Rapaport, J. A. Knowles, A. H. Fanous, S. A. McCarroll, N. Gupta, S. B. Gabriel, M. J. Daly, E. S. Lander, D. H. Lowenstein, D. B. Goldstein, H. Lerche, S. F. Berkovic, B. M. Neale, Ultra-Rare Genetic Variation in the Epilepsies: A Whole-Exome Sequencing Study of 17,606 Individuals. *Am. J. Hum. Genet.* **105**, 267–282 (2019).

117. D. S. Palmer, D. P. Howrigan, S. B. Chapman, R. Adolfsson, N. Bass, D. Blackwood, M. P. M. Boks, C.-Y. Chen, C. Churchhouse, A. P. Corvin, N. Craddock, D. Curtis, A. Di Florio, F. Dickerson, N. B. Freimer, F. S. Goes, X. Jia, I. Jones, L. Jones, L. Jonsson, R. S. Kahn, M. Landén, A. E. Locke, A. M. McIntosh, A. McQuillin, D. W. Morris, M. C. O'Donovan, R. A. Ophoff, M. J. Owen, N. L. Pedersen, D. Posthuma, A. Reif, N. Risch, C. Schaefer, L. Scott, T. Singh, J. W. Smoller, M. Solomonson, D. S. Clair, E. A. Stahl, A. Vreeker, J. T. R. Walters, W. Wang, N. A. Watts, R. Yolken, P. P. Zandi, B. M. Neale, Exome sequencing in bipolar disorder identifies AKAP11 as a risk gene shared with schizophrenia. *Nat. Genet.* **54**, 541–547 (2022).

118. J. Kaplanis, K. E. Samocha, L. Wiel, Z. Zhang, K. J. Arvai, R. Y. Eberhardt, G. Gallone, S. H. Lelieveld, H. C. Martin, J. F. McRae, P. J. Short, R. I. Torene, E. de Boer, P. Danecek, E. J. Gardner, N. Huang, J. Lord, I. Martincorena, R. Pfundt, M. R. F. Reijnders, A. Yeung, H. G. Yntema, S. Borras, C. Clark, J. Dean, Z. Miedzybrodzka, A. Ross, S. Tennant, T. Dabir, D. Donnelly, M. Humphreys, A. Magee, V. McConnell, S. McKee, S. McNerlan, P. J. Morrison, G. Rea, F. Stewart, T. Cole, N. Cooper, L. Cooper-Charles, H. Cox, L. Islam, J. Jarvis, R. Keelagher, D. Lim, D. McMullan, J. Morton, S. Naik, M. O'Driscoll, K.-R. Ong, D. Osio, N. Ragge, S. Turton, J. Vogt, D. Williams, S. Bodek, A. Donaldson, A. Hills, K. Low, R. Newbury-Ecob, A. M. Norman, E. Roberts, I. Scurr, S. Smithson, M. Tooley, S. Abbs, R. Armstrong, C. Dunn, S. Holden, S.-M. Park, J. Paterson, L. Raymond, E. Reid, R. Sandford, I. Simonic, M. Tischkowitz, G. Woods, L. Bradley, J. Comerford, A. Green, S. Lynch, S. McQuaid, B. Mullaney, J. Berg, D. Goudie, E. Mavrak, J. McLean, C. McWilliam, E. Reavey, T. Azam, E. Cleary, A. Jackson, W. Lam, A. Lampe, D. Moore, M. Porteous, E. Baple, J. Baptista, C. Brewer, B. Castle, E. Kivuva, M. Owens, J. Rankin, C. Shaw-Smith, C. Turner, P. Turnpenny, C. Tysoe, T. Bradley, R. Davidson, C. Gardiner, S. Joss, E. Kinning, C. Longman, R. McGowan, V. Murday, D. Pilz, E. Tobias, M. Whiteford, N. Williams, A. Barnicoat, E. Clement, F. Faravelli, J. Hurst, L. Jenkins, W. Jones, V. K. A. Kumar, M. Lees, S. Loughlin, A. Male, D. Morrogh, E. Rosser, R. Scott, L. Wilson, A. Beleza, C. Deshpande, F. Flinter, M. Holder, M. Irving, L. Izatt, D. Josifova, S. Mohammed, A. Molenda, L. Robert, W. Roworth, D. Ruddy, M. Ryten, S. Yau, C. Bennett, M. Blyth, J. Campbell, A. Coates, A. Dobbie, S. Hewitt, E. Hobson, E. Jackson, R. Jewell, A. Kraus, K. Prescott, E. Sheridan, J. Thomson, K. Bradshaw, A. Dixit, J. Eason, R. Haines, R. Harrison, S. Mutch, A. Sarkar, C. Searle, N. Shannon, A. Sharif, M. Suri, P. Vasudevan, N. Canham, I. Ellis, L. Greenhalgh, E. Howard, V. Stinton, A. Swale, A. Weber, S. Banka, C. Breen, T. Briggs, E. Burkitt-Wright, K. Chandler, J. Clayton-Smith, D. Donnai, S. Douzgou, L. Gaunt, E. Jones, B. Kerr, C. Langley, K. Metcalfe, A. Smith, R. Wright, D. Bourn, J. Burn, R. Fisher, S. Hellens, A. Henderson, T. Montgomery, M. Splitt, V. Straub, M. Wright, S. Zwolinski, Z. Allen, B. Bernhard, A. Brady, C. Brooks, L. Busby, V. Clowes, N. Ghali, S. Holder, R. Ibitoye, E. Wakeling, E. Blair, J. Carmichael, D. Cilliers, S. Clasper, R. Gibbons, U. Kini, T. Lester, A. Nemeth, J. Poulton, S. Price, D. Shears, H. Stewart, A. Wilkie, S. Albaba, D. Baker, M. Balasubramanian, D. Johnson, M. Parker, O. Quarrell, A. Stewart, J. Willoughby, C. Crosby, F. Elmslie, T. Homfray, H. Jin, N. Lahiri, S. Mansour, K. Marks, M. McEntagart, A. Saggar, K. Tatton-Brown, R. Butler, A. Clarke, S. Corrin, A. Fry, A. Kamath, E. McCann, H. Mugalaasi, C. Pottinger, A. Procter, J. Sampson, F. Sansbury, V. Varghese, D. Baralle, A. Callaway, E. J. Cassidy, S. Daniels, A. Douglas, N. Foulds, D. Hunt, M. Kharbanda, K. Lachlan, C. Mercer, L. Side, I. K. Temple, D. Wellesley, L. E. L. M. Vissers, J. Juusola, C. F. Wright, H. G. Brunner, H. V. Firth, D. R. FitzPatrick, J. C. Barrett, M. E. Hurles, C. Gilissen, K. Retterer, Deciphering Developmental Disorders Study, Evidence for 28 genetic disorders discovered by combining healthcare and research data. *Nature* (2020), doi:10.1038/s41586-020-2832-5.

119. T. Singh, T. Poterba, D. Curtis, H. Akil, M. Al Eissa, J. D. Barchas, N. Bass, T. B. Bigdeli, G. Breen, E. J. Bromet, P. F. Buckley, W. E. Bunney, J. Bybjerg-Grauholm, W. F. Byerley, S. B. Chapman, W. J. Chen, C. Churchhouse, N. Craddock, C. M. Cusick, L. DeLisi, S. Dodge, M. A. Escamilla, S. Eskelinen, A. H. Fanous, S. V. Faraone, A. Fiorentino, L. Francioli, S. B. Gabriel, D. Gage, S. A. Gagliano Taliun, A. Ganna, G. Genovese, D. C. Glahn, J. Grove, M.-H. Hall, E. Hämäläinen, H. O. Heyne, M. Holi, D. M. Hougaard, D. P. Howrigan, H. Huang, H.-G. Hwu, R. S. Kahn, H. M. Kang, K. J. Karczewski, G. Kirov, J. A. Knowles, F. S. Lee, D. S. Lehrer, F. Lescai, D. Malaspina, S. R. Marder, S. A. McCarroll, A. M. McIntosh, H. Medeiros, L. Milani, C. P. Morley, D. W. Morris, P. B. Mortensen, R. M. Myers, M. Nordentoft, N. L. O'Brien, A. M. Olivares, D. Ongur, W. H. Ouwehand, D. S. Palmer, T. Paunio, D. Quested, M. H. Rapaport, E. Rees, B. Rollins, F. K. Satterstrom, A. Schatzberg, E. Scolnick, L. J. Scott, S. I. Sharp, P. Sklar, J. W. Smoller, J. L. Sobell, M. Solomonson, E. A. Stahl, C. R. Stevens, J. Suvisaari, G. Tiao, S. J. Watson, N. A. Watts, D. H. Blackwood, A. D. Børglum, B. M. Cohen, A. P. Corvin, T. Esko, N. B. Freimer, S. J. Glatt, C. M. Hultman, A. McQuillin, A. Palotie, C. N. Pato, M. T. Pato, A. E. Pulver, D. St Clair, M. T. Tsuang, M. P. Vawter, J. T. Walters, T. M. Werge, R. A. Ophoff, P. F. Sullivan, M. J. Owen, M. Boehnke, M. C. O'Donovan, B. M. Neale, M.

J. Daly, Rare coding variants in ten genes confer substantial risk for schizophrenia. *Nature* (2022), doi:10.1038/s41586-022-04556-w.

120. A. Taylor-Weiner, F. Aguet, N. J. Haradhvala, S. Gosai, S. Anand, J. Kim, K. Ardlie, E. M. Van Allen, G. Getz, Scaling computational genomics to millions of individuals with GPUs. *Genome Biol.* **20**, 228 (2019).

121. P. F. Przytycki, K. S. Pollard, CellWalkR: an R package for integrating and visualizing single-cell and bulk data to resolve regulatory elements. *Bioinformatics*. **38**, 2621–2623 (2022).

122. S. Fischer, J. Gillis, How many markers are needed to robustly determine a cell's type? *iScience*. **24**, 103292 (2021).

Acknowledgements:

Funding:
This work was supported by the Simons Foundation (SFARI Bridge to Independence Award to M.J.G.), NIMH (R01-MH121521, R01-MH123922 to M.J.G.). Data were generated as part of the PsychENCODE Consortium, supported by: U01DA048279, U01MH103339, U01MH103340, U01MH103346, U01MH103365, U01MH103392, U01MH116438, U01MH116441, U01MH116442, U01MH116488, U01MH116489, U01MH116492, U01MH122590, U01MH122591, U01MH122592, U01MH122849, U01MH122678, U01MH122681, U01MH116487, U01MH122509, R01MH094714, R01MH105472, R01MH105898, R01MH109677, R01MH109715, R01MH110905, R01MH110920, R01MH110921, R01MH110926, R01MH110927, R01MH110928, R01MH111721, R01MH117291, R01MH117292, R01MH117293, R21MH102791, R21MH103877, R21MH105853, R21MH105881, R21MH109956, R56MH114899, R56MH114901, R56MH114911, R01MH125516, R01MH126459, R01MH129301, R01MH126393, R01MH121521, R01MH116529, R01MH129817, R01MH117406, and P50MH106934 awarded to: Alexej Abyzov, Nadav Ahituv, Schahram Akbarian, Kristin Brennand, Andrew Chess, Gregory Cooper, Gregory Crawford, Stella Dracheva, Peggy Farnham, Michael Gandal, Mark Gerstein, Daniel Geschwind, Fernando Goes, Joachim F. Hallmayer, Vahram Haroutunian, Thomas M. Hyde, Andrew Jaffe, Peng Jin, Manolis Kellis, Joel Kleinman, James A. Knowles, Arnold Kriegstein, Chunyu Liu, Christopher E. Mason, Keri Martinowich, Eran Mukamel, Richard Myers, Charles Nemeroff, Mette Peters, Dalila Pinto, Katherine Pollard, Kerry Ressler, Panos Roussos, Stephan Sanders, Nenad Sestan, Pamela Sklar, Michael P. Snyder, Matthew State, Jason Stein, Patrick Sullivan, Alexander E. Urban, Flora Vaccarino, Stephen Warren, Daniel Weinberger, Sherman Weissman, Zhiping Weng, Kevin White, A. Jeremy Willsey, Hyejung Won, and Peter Zandi. Additional data were generated from samples provided by the Joint MRC/Wellcome Trust (grant #099175/Z/12/Z) Human Developmental Biology Resource (www.hdbr.org) through grants MC/PC/13047, MR/L010674/1 and MR/L010674/2.

Author Contributions: This study was conceived and designed by MJG and CW with input from CL and KSP. Data was provided by DHG, NS, NJB, DRW, AEJ, JEK, TMH, RLW. Analyses were performed by CW, MM, RD, PZ, PFP, DDV, AB, NM, CJ, MK, ET, CH, NA, MIL, supervised by MJG, with contributions from CC, DC, HP, MG, NPD, ZW, KR, AG, BP, MAP, JLS, MIL, KSP, CL. CW and MJG wrote the manuscript, with major contributions from MM, AB and critical input from all authors. This article was prepared while Mette Peters was employed at Sage Bionetworks. The opinions expressed in this article are the author's own and do not reflect the view of the National Institute on Aging, the National Institutes of Health, the Department of Health and Human Services, or the United States government.

Competing Interests:
M.J.G. and D.H.G. receive grant funding from Mitsubishi Tanabe Pharma America. All other authors declare that they have no competing interests.

Data and Materials Availability:
Uniformly processed gene, isoform, and splicing quantifications, harmonized metadata, full xQTL summary statistics and other extended data are available at https://doi.org/10.7303/syn50897018.5. Raw genotype and RNA-seq data from the

original studies can be accessed through dbGaP with accession number phs001900 (Walker et al. 2019), the European Genome-phenome Archive under study accession EGAS00001003214 (O'Brien et al. 2018), the PsychENCODE Knowledge Portal under identifier syn21557948 at https://doi.org/10.7303/syn21557948 (Werling et al. 2020); https://www.hdbr.org/expression (HDBR, Lindsay et al. 2016); BioProject: PRJNA245228 at http://www.ncbi.nlm.nih.gov/bioproject/?term=PRJNA245228 (LIBD, Jaffe et al. 2015). All analysis code and scripts are available on GitHub at https://github.com/gandallab/devBrain_xQTL and Zenodo (*86*). An interactive web portal is available at devbrainhub.gandallab.org.

List of supplementary materials

- Materials and Methods
- Figs. S1 to S15
- Captions for Tables S1 to S7
- References *(87-122)*

Figures:

Fig. 1. The landscape of gene, splicing, and isoform regulation in the developing human brain.
(A) The number of eGenes discovered here versus sample size, compared with other human brain studies (*12–14*, *16*, *24–27*). **(B)** Overlap of eGenes between fetal brain (N = 629), GTEx v8 Brain Cortex (N = 205), and PsychENCODE (N = 1,387). **(C)** Correlation of eQTL effect size, measured by allelic fold change (aFC), between fetal and adult brain. Each dot is a shared pair of eGene-primary eQTL between fetal brain and GTEx (247 pairs) or PsychENCODE (253 pairs). **(D)** Overlap among eGenes, isoGenes, and sGenes. **(E)** Distance between the transcription start site (TSS) of each target gene of *cis*-eQTL, *cis*-isoQTL, and *cis*-sQTL SNPs. **(F)** Enrichment of *cis*-eQTL, *cis*-isoQTL, and *cis*-sQTLs within functional regions of the genome. **(G)** Loss-of-function mutation intolerance, as measured by pLI score, of eGenes, isoGenes, and sGenes. **(H)** Storey's pi1 statistic of the proportion of true associations in the discovery group of QTL (y-axis; permutation qvalue < 0.05) that are also true associations in the replication group of QTL (x-axis; all nominal Pvalues). **(I)** Number of fine-mapping credible sets versus number of conditionally independent eQTLs discovered. The size of the dots is scaled to the number of genes. **(J)** Common recurrent Inversion-QTLs in the developing brain. Inversions are displayed according to their length and the number of overlapping SNPs. Inversions with significantly associated eGenes have filled circles (FDR < 0.05). The size of the circle indicates the population frequency of the inversions.

Fig. 2. Cross-ancestry gene regulation and fine-mapping.
(A) Genotype PCA of the fetal brain samples. Sample ancestry was inferred by merging imputed genotypes with 1000 Genomes (*47*). **(B)** Comparison of eGenes discovered in the full cross-ancestry dataset ("ALL", N = 629) and in the separate sub-ancestries, EUR (N = 280), AMR (N = 162), and AFR (N = 135). **(C)** Correlation of eQTL effect sizes between AMR/AFR (top/bottom) and EUR, as measured by allelic fold change. Each dot is an AMR/AFR eGene-primary eQTL pair and colored by its nominal significance in EUR. Gray lines denote the lower and upper bounds of aFC. **(D)** Comparison of fine-mapping credible set sizes between the ancestries. **(E)** *Cis* associations for the gene *MTFR1* in the cross-ancestry, EUR, AMR, and AFR datasets.

Fig. 3. Trimester-specific patterns of gene expression and splicing regulation.
(A) Comparison of eGenes and sGenes identified in Tri1, Tri2, and the full dataset. Notably, we identify many more e/sGenes in Tri1 than Tri2 despite similar sample sizes. **(B)** An example of a trimester-specific eGene is shown for *WARS2*, where rs146862216 (G>A) is an eQTL in Tri1 (beta = -0.89, FDR = 3.88e-13) but not in Tri2 (beta = -0.03, P-value = 0.71). **(C, left)** *cis*-heritability of gene expression drops from Tri1 to Tri2 timepoints, as well as between fetal and adult (PsychENCODE) samples. Right, a similar drop is observed in splicing heritability between Tri1 and Tri2. **(D)** A sliding-window analysis of gene expression (left) and splicing (right) *cis*-heritability is shown for samples from 10-18 weeks. Each dot represents a sliding set of temporally ordered samples (N = 150), with mean age (+/- SD) on the x-axis, and median *cis*-

h^2_{SNP} (+/- SD) on the y-axis. **(E)** Comparison of gene biotype enrichment of Tri1-only and Tri2-only e/sGenes. Values associated with each gene type represent the proportion of genes classified within that category. Red boxes highlight significant post-hoc P-value. **(F)** Estimated proportion of 7 major cell classes over development, via bulk tissue cell-type deconvolution using CIBERSORTx (*53*).

Fig. 4. Integrative analysis of fetal xQTLs with neuropsychiatric GWAS.
(**A**) Quantile-quantile plot of SCZ GWAS p-values, subsetted by top *cis*-eQTLs, *cis*-isoQTLs, and *cis*-sQTLs in comparison to all background GWAS SNPs. (**B**) s-LDSC enrichment of SCZ GWAS heritability within fetal brain xQTLs and adult brain cortex eQTLs (GTEx v8), compared with background functional annotations. The proportional genomic coverage of SNPs within each annotation is shown in parentheses. (**C**) Estimated proportion (+/- SE) of GWAS h^2_{SNP} mediated by the *cis* genetic component of gene, isoform, and intron (splicing) regulation. Isoform-level QTLs mediate the greatest degree of heritability for multiple neuropsychiatric traits in the developing brain, compared with e/sQTLs. (**D**) Estimated proportion of GWAS h^2_{SNP} mediated by the *cis* genetic component of trimester-stratified gene-, isoform-, and intron (splicing)-regulation. For B, C, D: *** FDR<0.001, ** FDR<0.01, * FDR<0.05.

Fig. 5. Neuropsychiatric risk gene prioritization through colocalization and isoTWAS.
(**A**) Total number of GWAS loci exhibiting significant colocalization (CLPP>0.01) with specific fetal brain xQTL annotations. (**B**) Colocalization between SCZ GWAS and fetal brain xQTLs, ranked by CLPP and grouped by GWAS locus, as indicated by the index SNP to the right. (**C**) Top: locus plots of SCZ GWAS with *SP4* e- and sQTLs. A significant colocalization (CLPP = 0.02) is observed for SCZ GWAS with a cryptic splicing event in *SP4*. Notably, *SP4* does not have a detectable eQTL in the fetal brain. Middle: Gene structure of *SP4* with and without cryptic exon inclusion, likely resulting in nonsense mediated decay. Bottom left: sashimi plot shows the density of exon and junction read mapping for intron cluster chr7:21516925-21521542, stratified by the colocalized sQTL. Bottom right: sQTL rs10276352 (G>A) increases the contribution to cluster of annotated intron chr:21516925-21521542. The SCZ risk allele increases cryptic exon inclusion. (**D**) Fetal brain isoTWAS associations with SCZ GWAS. Each dot represents an isoform and adjusted P-value < 0.05 isoforms are colored in red. Genes of fine-mapped isoforms near a GWAS locus are labeled.

Fig. 6. Systems-level integration of risk variation with developmental gene and isoform co-expression.
(**A**) Workflow for construction of gene and isoform-level co-expression networks, followed by cell-type, pathway, and disease gene enrichment analyses. Separate gene co-expression networks were built to capture trimester and sex-specific effects. (**B**) Top: hierarchical clustering of modules from gene, isoform, trimester, and sex-stratified networks through bi-weight mid-correlation of eigengenes. Middle: heatmaps depict module-level enrichment for neuropsychiatric GWAS signal ($-\log_{10}P_{enrich}$ from s-LDSC and MAGMA) and odds ratios (OR) for rare variation and cell type enrichment (truncated at 10). Triangles indicate FDR-corrected P<0.1 significance. (**C**) Annotations for M2, a development-wide disease-associated chromatin regulation module. Center: top module ('hub') genes with circle size reflecting module membership (kME) and orange shading indicating genes with associated high-confidence neuropsychiatric disorder associated rare variants. Thin edges represent topologic overlap, solid edges indicate protein-protein interactions from the STRING database. Surrounding: circular bar plot highlighting module enrichment for cell types (purple), common (red) and rare (orange) variation, gene ontology terms (dark green), and module overlap (light green). (**D**) Annotations for M59, an ADHD-associated mitochondrial/proteasome isoform module.

Fig. 7. Module interacting eQTLs and context-specific GWAS colocalization.
(**A**) Hierarchical clustering of *cis*-eQTL enrichments among specific fetal brain cell-types as mapped by CellWalker. Outermost numbers denote results from single cell type label analysis. Inner numbers denote results from a broader, multi-level label analysis. (**B**) A schematic of module interaction ieQTL mapping and validation in cultured neurons and progenitors. (**C**) Results from module ieQTL mapping. From top to bottom, pi1 statistics depicting ieQTL overlap with eQTLs from cultured neurons or neural progenitor cells (NPCs), molecular feature (gene/isoform), number of ieQTLs, and

cell type enrichment. 62 modules with pi1>0.2 in either neurons or NPCs are shown. (**D**) Colocalization between SCZ GWAS and *BRINP2* ieQTL rs17659437 in M93 (CLPP = 0.02). (**E**) Annotation for M93, a SCZ/BIP enriched deep-layer neuronal/synaptic module. (**F**) Trajectory of M93 eigengene expression across brain development, colored by biological sex.

Science
AAAS

Supplementary Materials for

Cross-ancestry atlas of gene, isoform, and splicing regulation in the developing human brain

Cindy Wen, Michael Margolis, Rujia Dai, Pan Zhang, Pawel F. Przytycki, Daniel D. Vo, Arjun Bhattacharya, Nana Matoba, Miao Tang, Chuan Jiao, Minsoo Kim, Ellen Tsai, Celine Hoh, Nil Aygün, Rebecca L. Walker, Christos Chatzinakos, Declan Clarke, Henry Pratt, PsychENCODE Consortium, Mette A. Peters, Mark Gerstein, Nikolaos P. Daskalakis, Zhiping Weng, Andrew E. Jaffe, Joel E. Kleinman, Thomas M. Hyde, Daniel R. Weinberger, Nicholas J. Bray, Nenad Sestan, Daniel H. Geschwind, Kathryn Roeder, Alexander Gusev, Bogdan Pasaniuc, Jason L. Stein, Michael I. Love, Katherine S. Pollard, Chunyu Liu*, Michael J. Gandal*

*Corresponding author. Email: michael.gandal@pennmedicine.upenn.edu (MJG); liuch@upstate.edu (CL)

The PDF file includes:

Other Supplementary Materials for this manuscript include the following:

Materials and Methods

1: Study descriptions

Here, we integrate a large dataset of the developing human brain by combining five individual studies. The Walker (*24*) data was generated at UCLA with 219 brain cortex samples spanning 14-21 post-conception weeks (PCW). For these data, he RNA-seq library was prepared using Ribo-Zero with 60M reads per sample, and genotype data were sequenced using Illumina HumanOmni2.5 array. The O'Brien (*25*) data has 120 bulk brain samples spanning 12-19 PCW, with RNA-seq data having been generated using Ribo-Zero with 100M reads per sample, and genotype sequencing yielded approximately 710,000 SNPs using the Illumina Infinium OmniExpress-24 BeadChip array. The Werling (*12*) data has 116 DLPFC samples spanning 6-37 PCW, with RNA-seq having been generated using Ribo-Zero with 37M reads per sample. There were genotype sequenced using 30X WGS. The LIBD (*26*) data has 54 DLPFC samples spanning 14-20 PCW, with RNA-seq having been generated using Ribo-Zero with 150M reads, and genotype sequencing was performed using Illumina 1M DuoV2. The HDBR (*27*) data has 173 bulk brain samples spanning 4-20 PCW, with RNA-seq data having been prepared using PolyA with 50M reads. For this dataset, genotype sequencing was performed using Illumina HumanOmni5-4v1-B. 10 of the HDBR samples were duplicated in the O'Brien dataset, and these 10 samples were thus removed. Altogether, there are 672 unique samples. We further filtered for matching DNA-RNA and high-quality data and the final sample size is 654 (Walker n=211, O'Brien n=120, Werling n=116, LIBD n=44, HDBR n=163).

2: Genotype processing

Individual study genotype data were uniformly processed. Variants were filtered by MAF, HWE, and missingness (plink --maf 0.01 --geno 0.05 --mind 0.10 --hwe 1e-6(*87*)). Conform-gt (https://faculty.washington.edu/browning/conform-gt.html) was applied to genotype data to fix strand flips and to make it consistent with 1000 Genomes Project hg19 reference(*47*). QC-ed genotype data were imputed on the Michigan Imputation Server(*81*) (Minimac 4, phasing: Eagle v2.4) with TOPMed Freeze5(*34*) as the reference, and filtered for high imputation quality (R2 > 0.3). After imputation, individual studies were merged by intersecting the variants. Duplicated position variants (i.e. multi-allelic) were removed. TOPMed variant IDs were mapped to dbSNP151 (UCSC snp151.txt.gz) rsID (~10% variants were not mapped to rsID, and kept as hg38 CHR:POS:REF:ALT as ID). Variants were filtered (plink --maf 0.01 --geno 0.05 --hwe 1e-6) and mapped to hg19 using Crossmap (v0.5.2)(*88*). CheckVCF (https://github.com/zhanxw/checkVCF) was used for a sanity check. LD-pruned (plink --indep-pairwise 50 5 0.2) data were merged with 1000 Genomes. PCA and k-nearest-neighbors (k=50) were run to infer data ancestry. Variant QC and PCA were then conducted separately within EUR, AMR, and AFR populations. 8,420,206 variants (including 560,448 indels) were included in the final mixed ancestry data analysis (EUR 6,381,990 variants, 436,809 indels; AMR 7,290,008 variants, 493,933 indels; AFR 8,723,314 variants, 587,595 indels). Closely related subjects (plink pi_hat > 0.3) were excluded from the analysis.

3: RNA-seq processing

3.1: Alignment

Individual study RNA-seq data were acquired and uniformly processed. FastQC (v0.11.9) (*89*) was first run on FASTQ files for pre-alignment quality control. FASTQ files were then aligned to the hg19 reference genome with GENCODE v29lift37 (*82*) annotations using STAR-2.7.3a (*83*). Per-sample 2-pass mapping mode was used to improve novel junction discovery. Alignment quality control metrics were calculated using PicardTools (2.21.7) (http://broadinstitute.github.io/picard/) and compiled using MultiQC (v1.9ev0) (*90*).

3.2: Sample swap check

Sample swaps and contamination were evaluated by calling SNPs from BAM alignments and merging with the imputed genotype. Plink --genome-full was used to calculate IBD/IBS sharing of all pairs of genotype ID (including both imputed and BAM-called). PI_HAT (proportion of IBD) and Z0 (P(IBD)=0) in the plink.genome output file were checked to determine whether there were any sample swaps. Imputed/BAM-called pairs from the same subject showed high levels of

inbreeding (PI_HAT~1, Z0~0); while pairs from different subjects showed low levels of inbreeding (PI_HAT~0, Z0~1). Related subject pairs, which were removed in downstream analysis, showed high levels of IBD sharing. No unexpected sample swaps were detected.

3.3: Gene and isoform quantification

Isoform-level quantifications were calculated using Salmon (v1.0.0)(*41*) and GENCODE v33lift37(*82*) annotations and a decoy sequence-aware index. generateDecoyTranscriptome.sh provided by Salmon was used to generate the index. Sequence bias and GC bias were corrected, and selective alignment of the sequences was enabled (--validateMappings --useEM --seqBias --gcBias). All subjects' quantifications and gene-level quantifications were compiled using Tximport (1.14.0)(*91*). Raw counts, TPM, and length-scaled counts (countsFromAbundance="lengthScaledTPM") were generated for downstream analysis.

Genes/isoforms on chromosomes M, X, and Y were excluded for downstream analysis. Genes/isoforms with an expression level of TPM > 0.1 in more than 25% of subjects were included for downstream analysis. Counts were normalized and variances were stabilized using DESeq2::varianceStabilizingTransformation(*92*). Inter-subject connectivity was calculated using the R package WGCNA(*75*) and outlier subjects were excluded from the analysis (connectivity z-score < -3). Batch effects were corrected using sva::Combat(*93*). 31,947 genes and 127,986 isoforms (mapped to 31,121 genes) were included for QTL mapping.

3.4: Splicing quantification

3.4.1: Alignment

As above, FASTQ files were aligned to the hg19 reference genome using GENCODE v33lift37(*82*) annotation reference using STAR(*83*). To improve the sensitivity for discovering novel junctions, the multi-sample 2-pass mapping mode was used. At the end of the first pass of mapping, splice junctions (SJ) from all samples were filtered (excluding all MT junctions, all non-canonical SJ, SJ supported by multi-mappers-only, SJ supported by too few reads (<=2)). In the second pass, SJs from all samples were included in the mapping of all samples. WASP(*94*) filtering implemented in STAR was also applied in the second pass to reduce reference bias, and Samtools 1.9(*95*) was used to filter out reads that did not pass WASP (vW:i:[2-7]).

3.4.2: Intron quantification and normalization

Introns were quantified using Leafcutter (v0.2.7) (*42*). Bam2junc.sh and leafcutter_cluster.py scripts provided by Leafcutter were used to quantify intron usage (excision ratio). Intron clusters were generated with the following options: >50 reads per cluster, >500kb intron length, >0.001 of reads in a cluster support an intron, >5 reads per intron (--minclureads 50 --maxintronlen 500000 --mincluratio 0.001 --minreads 5). 502,571 introns from 105,700 intron clusters and 22,751 corresponding genes were detected. The leafcutter script prepare_phenotype_table.py was then used to filter introns and prepare BED files. Non-autosomal introns, introns used in <40% of subjects, or with almost no variation were filtered out. Intron usage was standardized and quantile normalized. 273,167 introns from 50,311 clusters and 14,368 corresponding genes passed the filters and were included in sQTL mapping. ComBat was applied to the normalized data to remove batch effects.

3.4.3: Intron annotation

We annotated the introns detected by Leafcutter in two slightly different ways. First, the script Gtf2leafcutter.pl was applied to the Gencode reference annotation GTF file to generate an annotation code: all_introns.bed.gz, threeprime.bed.gz, fiveprime.bed.gz, and all_exons.bed.gz. All detected introns were mapped to annotated introns, and intron clusters were mapped to the most representive gene of the introns in this cluster. Introns were annotated as follows

- "Unknown_strand": intron is in a cluster with an unknown gene strand

- "Cryptic_unanchored": intron is in a cluster with a known gene strand, but the intron does not have a known gene with 5' or 3' splice junctions
- "Cryptic_threeprime": intron is in a cluster with + gene strand, known gene on 5' end, unknown gene on 3' end OR intron is in a cluster with - gene strand, known gene on 3' end, unknown gene on 5' end
- "Cryptic_fiveprime": intron is in a cluster with + gene strand, known gene on 3' end, unknown gene on 5' end OR intron is in a cluster with - gene strand, known gene on 5' end, unknown gene on 3' end
- "Cryptic": intron is in a cluster with unknown gene strand AND intron has known gene on 5' OR 3' end
- "Annotated": intron has known gene on both ends
- "Novel annotated pair": both are annotated but never in the same junctions

Second, we followed the approach taken by GTEx (*16*) to annotate introns by matching them with annotated exons. Briefly, each intron discovered by Leafcutter was matched with annotated exons by 3' or 5' junctions; then an intron cluster was mapped to all the genes with introns for which this cluster were matched. One cluster can map to multiple genes. In this way, 71,429 out of 105,700 clusters were mapped to genes; 5,132 clusters were mapped to more than 1 gene. 263,331 out of the 273,167 introns that we tested for sQTL have mapped genes in this way. Note that GTEx filters out introns that are not mapped to any genes; however, we only used this cluster-to-gene mapping file for grouped permutation-based sQTL identification (see Section 4.4). A customized version of sqtlviztools (*96*, *97*) was used to visualize intron contribution to cluster at sQTL.

4: *cis*-xQTL mapping

4.1: Covariate selection

Age and sex information from each of the donor samples were compiled from each study. Unavailable sexes were inferred from expression of *XIST* and aggregated expression of chrY genes. To account for unknown technical and biological factors, we employed the Hidden Covariates with Prior (HCP) (*98*) method using normalized expression values with a prior informed by PicardTools sequencing QC metrics. Age, sex, the top 5 genotype PCs, and HCP factors were included as covariates in QTL mapping.

4.2: *cis*-eQTL mapping

cis-eQTL mapping was conducted using FastQTL v2.0(*84*). The *cis*-window was defined as 1 Mb up- and downstream around a gene's transcription start site (TSS). Gene expression was standard normalized (--normal). To identify the optimal number of HCP covariates to include, a nominal association for each "gene-*cis* variant" pair was calculated using FastQTL in nominal mode, and multiple test-corrected with FDR < 0.05. The number of optimal HCPs was then selected by optimizing for the number of eGenes with nominally significant eQTLs. To discover eGenes (genes with at least one significant *cis*-eQTL), FastQTL adaptive permutations (--permute 1000 10000) were then run with the optimal number of HCP. Beta-approximated permutation p-value was multiple test-corrected using Storey-Tibshirani's method(*43*), and eGenes were defined as those with a qvalue < 0.05. A nominal p-value threshold was calculated for each gene (following GTEx (*16*) and using qbeta to map the permutation adjusted p-value back to a nominal p-value threshold), and QTLtools v1.0(*44*) conditional mode was run to identify conditionally independent eQTL signals.

4.3: *cis*-isoQTL mapping

cis-isoQTLs were mapped in a similar way as *cis*-eQTL. FastQTL nominal pass mode was first run with all expressed isoforms and variants within 1 Mb of the isoforms' TSS. Then, using the optimized number of HCP factors as covariates, we first ran "naive" adaptive permutations (--permute 1000 10000), where isoforms are treated as independent from each other, and isoQTLs with a qvalue < 0.05 were identified as significant. Next, to account for the dependence between isoforms of a gene, we used grouped permutations as described in (*16*), where adaptive permutations were run jointly on all isoforms of a gene, and isoGenes were defined as those with a qvalue < 0.05.

4.4: *cis*-sQTL mapping

HCP factors were generated using normalized intron usage values and a prior derived from PicardTools metrics. FastQTL nominal pass mode was run with all introns that passed filters, using variants within 1Mb of the intron body. The default 100kb window gave low p-values near the *cis* window boundaries, so we decided to use 1 Mb, as had been done for eQTLs and isoQTLs. Adaptive permutations (--permute 1000 10000) were run with the optimal number of HCP factors, and sQTLs with qvalue < 0.05 were identified as significant. Next, to account for the dependent structure of multiple introns and intron clusters of a gene, we ran grouped permutations, and sGenes were identified as those with a qvalue < 0.05.

5: Inversion-associated eQTLs

Large-scale recurrent inversions were called in our fetal brain dataset using scoreInvHap (v1.10.0)(*99*). 17 common inversions had a sufficient number of surrounding SNPs in our QCd genotype data and could be imputed. A linear model was then fit to test for the association between each inversion and gene expression across the transcriptome. The same set of covariates was used as in *cis*-eQTL mapping. Specifically, covariates include age, sex, the top 5 genotype PCs, and 90 HCP factors. FDR correction was used to account for multiple testing within each inversion. Associations with FDR < 0.05 were reported as significant.

6: Population-specific *cis*-xQTL mapping

To investigate population-specific genetic regulation, we separated genotype and gene/isoform/splicing data into the three major populations with N >100: EUR (N = 292), AMR (N = 164), and AFR (N = 145). Among genotyped variants, MAF and HWE filters and genotype PCs calculation were then performed separately in each population. We followed the *cis*-xQTL mapping approach for the multi-ethnic dataset and mapped *cis*-e/iso/sQTL in the three populations.

7: cis-xQTL effect sizes

cis-xQTL effect sizes were measured by two metrics: allelic fold change (aFC) (*50*) and linear regression slope (beta). To compare *cis*-eQTL effect sizes between fetal and adult QTL reference panels, we calculated aFC in log2 scale for permutation-derived eGene-primary eQTL pairs in the fetal brain dataset, GTEx v8 Brain Cortex (*16*), and PsychENCODE (*13*).

8: *cis*-xQTL overlap

We investigated the overlap between *cis*-e/iso/sQTLs using Storey's pi1 statistic implemented in the qvalue R package(*43*). To estimate the proportion of eQTLs that are also truely associatiated with an isoQTL (pi1), we took the significant primary eGene-eQTL pairs passing the permutation threshold and matched them to all gene-SNP pairs' association in isoQTL. We calculated pi1 as 1-(qvalue(pval_nominal_iso))$pi0. For eGene-eQTL pairs that are missing in isoQTL, we randomly assigned a nominal p-value sampled from a uniform null distribution. We did the same for all pairs between e/iso/sQTLs. For isoQTL and sQTL nominal associations, we first mapped isoforms and introns to genes as described in previous sections, and only kept gene-SNP pairs with the lowest nominal p-value.

9: Functional enrichment of *cis*-xQTL

We generated genomic annotations using the following resources: Ensembl regulatory build (*100*) (homo_sapiens.GRCh37.Regulatory_Build.regulatory_features.20201218.gff.gz; annotations include: TF_binding_site, promoter_flanking_region, promoter, open_chromatin_region, enhancer, CTCF_binding_site), and Ensembl's Variant Effect Predictor VEP v102 (*101*) on fetal brain genotype data (GENCODE v33lift37 annotation and genome fasta; using cache in homo_sapiens/102_GRCh37/ which has GENCODE v19, only annotations supported by GENCODE v33 was selected; annotation consequences include: synonymous_variant, stop_gained, splice_region_variant, splice_donor_variant, splice_acceptor_variant, non_coding_transcript_exon_variant, missense_variant, intron_variant, frameshift_variant, 5_prime_UTR_variant, 3_prime_UTR_variant). Functional enrichment analyses were performed using torus (*102*), with

the genomic annotations, and all *cis* associations calculated by FastQTL (torus -d {fastqtl_allpairs} --fastqtl -est -annot {annot}).

10: Gene constraint

To investigate the level of intolerance to loss-of-function mutation of genes, we downloaded ExAC data from gnomAD (*36*). We filtered for autosomal protein-coding genes and used the pLI score as a measure for gene constraint.

11: Fine-mapping of *cis*-xQTL

We performed QTL fine-mapping using the Sum of Single Effects Regression (SuSiE) as implemented in the susieR_0.11.42 package (*45*). The fine-mapping was performed for each eGene, isoform with permutation-significant isoQTL, and intron with permutation-significant sQTL and variants within 1 Mb from the feature. The genotype VCF file used for QTL mapping was converted to a dosage matrix using bcftools 1.9 (*103*). Genotype dosage and gene/isoform expression or intron splicing files were residualised by the same set of covariates as those used in the FastQTL permutations. Fine-mapping was performed with the following parameters: L = 10, estimate_residual_variance = TRUE, estimate_prior_variance = TRUE, scaled_prior_variance = 0.1, compute_univariate_zscore = TRUE, min_abs_corr = 0. We then constructed credible sets (CS) for the features by extracting variants with posterior inclusion probabilities (PIPs) summing up to 95%. As described in the SuSiE paper, we used CS purity as a measure of the correlation of variants in that CS and filtered for high-purity CS for downstream analysis.

For population-specific *cis*-eQTLs, we performed SuSiE fine-mapping separately within each population. For the multi-ethnic dataset, we first performed SuSiE fine-mapping, and then to leverage population-specific linkage disequilibrium (LD), we performed multi-ethnic fine-mapping using PAINTOR (*51*, *52*), which uses genomic annotations (see Section 9) and population-specific summary statistics and genetic backgrounds. For the 982 permutation eGenes shared between EUR, AMR, and AFR, we ran PAINTOR with the *cis* variants shared by the three populations. We enumerated with 2 casuals at maximum (-enumerate 2) and constructed 95% CS based on PIPs.

12: Age specificity of genetic regulation

We stratified the EUR samples into first and second trimesters, and mapped trimester-specific *cis*-e/iso/sQTL (eQTL Tri1 N = 137, Tri2 N = 142; isoQTL Tri1 N = 136, Tri2 N = 139; sQTL Tri1 N = 141, Tri2 N = 143. The sample sizes slightly differ because gene and isoform expression outlier samples were excluded from the analysis, see Section 3.3). We used the same set of covariates as described in Section 4.1.

We estimated heritability for both gene expression and splicing phenotypes in EUR individuals by fitting a univariate variance component linear mixed model via the restricted maximum likelihood (REML) approach using the majorization-minimization (MM) algorithm implemented in the MultiResponseVarianceComponentModels.jl (*85*). We specified three variance components corresponding to genetic effects from *cis*-SNPs (defined as SNPs within 1 Mb around gene TSS and intron body), genetic effects from trans-SNPs (defined as SNPs that do not fall within the previously described *cis*-window), and residual effects. For each gene/intron, we first regressed out fixed effects covariates from the complete EUR expression files, constructed two separate classic genetic relationship matrices (GRMs) for *cis*-SNPs and trans-SNPs using SnpArrays.jl (*104*), and then estimated variance components for each trimester separately. Additionally, a sliding window of samples by age was analyzed—that is, after sorting the samples by age, variance components were estimated for batches of 150 samples with the window shifting 25 samples by batch. Heritability estimates and their standard errors were subsequently calculated using the delta method, which is built into the Julia package.

To investigate possible biological explanations to the observed heritability drop, we reanalyzed a functional genomic dataset from cultured phNPCs and their differentiated neuronal progeny (*56*) to estimate gene expression cis-heritability. We subset to individuals with RNAseq data captured from both phNPCs and neurons (n = 82). We retained

genes with TPM > 0.1 in at least 25% of samples for phNPCs and neurons respectively. We further subset to unrelated individuals, identified as samples with a relatedness < 0.2 from a GRM constructed from SNPs with a MAF > 0.05. We examined the variance in the gene expression, measured as the normalized RNAseq count from DESeq2, that can be attributed to genetic variance. If a sample was profiled more than once, the replicate with the higher RIN score was used. Similar to above, we specified three variance components corresponding to genetic effects from *cis*-SNPs (defined as SNPs within 1MB around gene body), genetic effects from trans-SNPs (defined as SNPs that do not fill within the previously described *cis*-window), and residual effects. Fixed effects covariates included in the model were 10 genotype principal components, 10 gene expression principal components, RIN, sex, age, and age^2. Heritability estimates and their standard errors were calculated with genomic restricted maximum likelihood (GREML) using GCTA.

13: GWAS summary statistics

To investigate the overlap between fetal brain xQTLs and neuropsychiatric disorder GWAS results, we downloaded GWAS summary statistics for the following traits: schizophrenia (SCZ) (*1*) (we used the European summary statistics), autism spectrum disorder (ASD) (*2*), bipolar disorder (BIP) (*62*), attention-deficit/hyperactivity disorder (ADHD) (*60*), major depression (MDD) (*105*). GWAS summary statistics were munged using munge_sumstats.py script from LD Score Regression (LDSC) (*6*, *58*).

14: MESC

We applied Mediated Expression Score Regression (MESC) (*38*) to estimate the proportion of neuropsychiatric disease heritability mediated by genes, isoforms, and introns, respectively. QTL effect sizes were estimated using individual-level expression and genotype data to reduce noise (--compute-expscore-indiv). LD scores and LD weights calculated from the 1000 Genomes Phase 3 EUR samples (*47*) were included in the analysis. By default, LD scores are computed from 1000 Genomes Phase 3 stratified over a modified version of the baselineLD model v2.0 (https://data.broadinstitute.org/alkesgroup/LDSCORE/).

15: Stratified LD score regression

To investigate the enrichment of neuropsychiatric GWAS heritability among fetal brain QTLs, we first generated the maxCPP annotation(*59*) for the following QTL datasets: *cis*-eQTLs, *cis*-isoQTLs, *cis*-sQTLs, and trimester-specific e/iso/sQTLs. To construct this probabilistic maxCPP annotation, we first ran SuSiE fine-mapping for each dataset(*45*). For each variant in the genome, we then assigned an annotation value based on the maximum fine-mapping PIP across all molecular features within which the variant lies in the SuSiE 95% CS. Variants that do not belong to any of the SuSiE CSs were assigned an annotation value of 0. We restricted to 1000 Genomes EUR HapMap3 variants for the analysis. The corresponding maxCPP annotation for GTEx v8 Brain Cortex was also downloaded (*16*, *59*).

Next, we applied stratified LD score regression (S-LDSC) (*6*) using the maxCPP annotations. S-LDSC was performed using the 1000 Genomes EUR reference panel (*47*), restricted to HapMap3 SNPs, and corresponding regression weights. We applied S-LDSC for each GWAS and QTL dataset pair, jointly with 53 baseline annotations (https://alkesgroup.broadinstitute.org/LDSCORE/). We used two metrics to measure the importance of an annotation: the enrichment and effect size z-score. The enrichment of an annotation is defined as the proportion of heritability captured by the annotation divided by the proportion of SNPs in that annotation (Pr(h2)/Pr(SNP)). The effect size z-score (Coefficient_z.score = Coefficient/Coefficient_std_error) is an estimate of how much more significantly the annotation explains the GWAS statistics on top of the other annotations in the model.

16: Isoform-level TWAS

To identify genes and their isoforms whose *cis*-regulated expression is associated with neuropsychiatric diseases, we performed an isoform-level transcriptome-wide association study (isoTWAS) (*71*). We generated SNP weights using our uniformly processed fetal brain dataset (full dataset N = 629). We used the imputed genotype data restricted to HapMap 3

variants only and expression corrected by the same set of covariates as in *cis*-isoQTL mapping (age, sex, 5 genotype PCs, and HCPs). Briefly, we built expression models using multivariate predictive methods that model all heritable isoforms of a gene jointly using either (1) multivariate elastic net, (2) multivariate SuSiE regression, or (3) multivariate LASSO regression with simultaneous covariance estimation using graphical LASSO. These multivariate methods account for the correlation between isoforms of the same gene to increase the prediction accuracy of each individual isoform, compared to methods that consider each isoform separately. Optimal model weights using all SNPs within a 1Mb window of the genes were trained by selecting the model with the best 5-fold cross-validation R^2. We filtered for isoforms for cross-validation $R^2 > 0$. A stepwise trait mapping procedure is used in isoTWAS (*71*). First, isoform associations from the same gene family to the gene-level using the aggregated Cauchy association test (*106*), and gene-level P-values are adjusted for multiple testing burden using a Bonferroni correction. Second, for isoforms of a gene that passes Bonferroni correction, the family-wise error rate for isoforms of the same gene is controlled using Shaffer's modified sequentially rejective Bonferroni correction (*107*). Through this process, we identified both gene-disease and isoform-disease associations with the LD structure calculated from our data and schizophrenia GWAS summary statistics. We then prioritized isoform-disease associations using a permutation-based test (1000 permutations of the SNP-isoform weights). This permutation test assesses whether the SNP-isoform weights add any mechanistic insight beyond the SNP-disease associations from the GWAS.

17: FOCUS

To leverage local LD and prioritize candidate isoforms for isoTWAS analysis, we performed probabilistic fine-mapping using FOCUS (*108*). FOCUS models the correlation among isoform-specific signals and estimates the posterior probability of an isoform explaining the observed isoTWAS association signal in the risk region. We generated 90% credible sets of causal isoforms for any set of isoforms that showed isoTWAS associations.

18: eCAVIAR

eCAVIAR (v2.2) (*9*) was used to prioritize likely causal variants responsible for both QTLs and GWAS. For each GWAS described in Section 13, we extracted variants within 1 Mb around the index variant for each GWAS loci. For each locus, summary statistics for variants that are also in the 1000 Genomes EUR reference panel (*47*) were extracted. Candidate target features (i.e. genes, isoforms, introns) were defined as features with at least one of the GWAS locus variants as nominal QTL (FDR < 0.05). Next, for each candidate target feature of the locus, we extracted the overlapping variants between GWAS and the feature's *cis* variants. We calculated the LD of these variants for GWAS using 1000 Genomes EUR reference panel and for the multi-ethnic fetal brain samples using in-sample genotypes. Finally, we ran eCAVIAR and calculated the colocalization posterior probability (CLPP) for each variant (a maximum of two possible causal variants for each locus was assumed: eCAVIAR -f 1 -c 2 -r 0.95). Significant colocalization was defined as CLPP > 0.01. Sashimi.py (*109*) was used to create the SP4 read density plot and GeneticsMakie.jl (*110*) was used to create the LocusZoom plots.

19: MRLocus

To estimate gene-to-trait effect sizes, MRLocus-eCAVIAR (*74*) was run on conditional fetal brain eQTL (from this study) and Schizophrenia GWAS (*1*) summary statistics (European ancestries; 53,386 cases and 77,258 controls; https://figshare.com/articles/dataset/scz2022/19426775). Gene-to-trait effect sizes were only tested within a subset of genes already shown to be associated with schizophrenia risk via TWAS. Among 199 genes discovered through TWAS, 14 genes were selected with 3 or more instruments: conditionally distinct sets of SNPs associated with those eGenes. For each signal cluster (a set of SNPs associated with gene expression, which is conditionally distinct and LD-independent from other sets), we extracted beta and standard error (SE) values from both eQTL and GWAS summary statistics. Since eQTL and GWAS were conducted within different populations, we prepared two LD matrices (*r*) based on (1) individuals enrolled in the eQTL population composed of multiple ancestries and (2) pre-calculated non-Finnish European LD matrices provided by the gnomAD v2 (*111*) for the GWAS population. Only SNPs that existed in all datasets (i.e. eQTL, GWAS and gnomAD reference panel) were used for further analysis. Running MRLocus-eCAVIAR entailed using eCAVIAR (v2.2) (*9*) to estimate posterior probabilities of colocalization within each signal cluster to choose candidate SNPs, followed by running

MRLocus (v0.0.24) gene-to-trait slope estimation over signal clusters. For signal clusters that straddled a 500kb boundary from the gene TSS, SNPs that were greater than 500kb away from TSS were filtered from the cluster before running eCAVIAR. To reduce dependency across clusters, a cluster was trimmed and not used in slope estimation if the eQTL SNP (instrument) had $r^2 > 0.05$ to any other cluster's eQTL candidate SNP, following the trimming procedure described in (*74*). Per locus p-values testing the null hypothesis of no gene-to-trait effect were corrected for multiple testing using the Benjamini-Hochberg method, providing FDR control at 20% for raw p-values less than 0.078.

20: WGCNA

20.1: Preparation of count data

We performed robust Weighted Gene Correlation Network Analysis (WGCNA) on gene-level and isoform-level quantifications in order to group fetal genes into disease-relevant networks. First, unscaled and untransformed gene- and isoform-level counts for all the samples were obtained following the procedure outlined in 3-3. Outlier sample removal and expression filtering resulted in a gene-level count matrix of 31,947 genes and 642 samples and an isoform-level count matrix of 127,986 transcripts and 639 samples. Next, a vector of each sample's study of origin was fed to ComBat-seq in the *sva* R package (version 3.35.2) to generate batch-corrected count data. CTF library normalization (*112*) was performed on the batch-corrected count data using TMM normalization factors obtained from the *edgeR* R package (version 3.36.0). Briefly, a CTF factor for each sample was generated by multiplying each sample's edgeR-derived normalization factor by the sample's library size. Then, a scaled CTF factor was obtained by dividing each CTF factor by the overall smallest CTF factor. Finally, each sample's expression was divided by the scaled CTF factor, incremented by 1, and log2 transformed, resulting in a pseudo-count matrix of normalized expression. The gene-level samples (n = 642) were subsequently split by trimester into tr1-gene (n = 212) and tr2-gene (n = 427), and by sex into xx-gene (n = 302) and xy-gene (n = 340).

20.2: Network generation

Gene- and isoform-level signed networks were generated with the WGCNA R package (version 1.69.0). First, for each log2-normalized expression matrix, a soft-threshold power was selected to minimize mean connectivity and maintain a scale free $R^2 > 0.8$. For each gene-level expression matrix, a topological overlap matrix (TOM) was robustly generated using the consensusTOM function on a vector of 100 downsampled pseudo-count matrices, each containing ⅔ of the respective samples. This robust WGCNA approach (rWGCNA) reduces the likelihood that resulting modules will capture signals corresponding to sample subpopulations instead of sample-wide biological signals (*75*). For the isoform-level expression matrix, since rWGCNA was too computationally expensive, a vector containing the single original pseudo-count matrix was processed through the consensusTOM function. Network dendrograms for each TOM were generated using average linkage hierarchical clustering of the dissimilarity TOM (1 - TOM). Modules were subsequently constructed using the cutreeHybrid function with a minimum module size of 200, deep split parameter of 4, pamStage of 1, pamRespectsDendro of 0, and cut height of 0.999. Highly correlated modules were combined with the mergeCloseModules function using a merge cut height of 0.225.

20.3: Cell Type enrichment

Within each module, genes with a kME > 0.5 were compared against known fetal brain cell markers(*39*) using over-representation analysis. The original 16 cell types were collapsed into 9 broad cell classes, corresponding to hierarchical clustering of these developmental cell populations(*65*). Fisher's exact test p-values for gene-marker overlap were collected into a table and subsequently FDR-corrected to control for multiple comparisons. Module parameters were selected to maximize cell type enrichment.

20.4: Disease enrichment

We computed each module's enrichment for common and rare disease variants to identify key disease-associated developmental modules.

For common variation, we utilized summary statistics from the largest available GWAS across major neurodevelopmental disorders (Section 13). Each module's SNP-level disease heritability was estimated with S-LDSC. First, module genes were assembled into lists, and genomic annotations were generated using a 10kb window with GENCODE v33lift37 as a reference. Then, LD scores were calculated for each set of annotation files, and partitioned heritability was used to estimate the SNP heritability for each module was jointly compared with a baseline set of 53 genomic annotations. Finally, each module's SNP heritability was divided by the proportion of SNPs annotated within that module. Significance was assessed by converting the regression coefficient (tau) z-scores into p-values. Additionally, gene-level disease heritability for each module was estimated using MAGMA(*113*). For each GWAS, SNP-level effect sizes were converted to gene-level effect sizes using the default MAGMA annotation set(*114*). For each network, a two-column file containing module membership status and gene identity was generated and run through MAGMA in gene-set analysis mode. The resulting module enrichment p-values were subsequently FDR-corrected for multiple comparisons.

For rare variation, we used compiled curated gene lists for each disorder: SFARI gene list for ASD(*115*), Epi25 for Epilepsy(*116*), BipEx for BIP(*117*), The Deciphering Developmental Disorders Study (DDD)(*118*), SCHEMA for SCZ(*119*). In addition, we downloaded TADA-based summary statistics for ASD and DDD from(*65*) and curated genes for epilepsy, as published by Polioudakis et al(*39*). A binary vector representing each gene's membership with the module (with 1 for genes in the specified module and 0 otherwise) served as the dependent variable. For gene lists without summary statistics, a binary vector representing each gene's membership in the curated gene list was used as the primary independent variable, and gene length, log10 of gene length, transcript length, and log10 of transcript length were used as covariates. For gene lists with reported p-values, a continuous vector containing -log10(p-value) for each gene measured by the study served as the primary independent variable, controlling for gene and transcript length as above. Logistic regression was then used to test for association, and the resulting odds ratios and p-values were collected into a table. All p-values were FDR-corrected to control for multiple comparisons.

20.5: Biological pathway enrichment

To place modules into biological context, GO term enrichment was performed using the gprofiler2 R package (version 0.2.1). For each module, genes were assembled into a vector, arranged from highest to lowest kME, and processed through the gost function as an ordered query. In addition, a vector consisting of all expressed genes in our fetal dataset was passed as a custom background to the gost function. The resulting GO enrichment table was filtered for significant results and term sizes smaller than 2,000, and plotted using the gostplot function.

20.6: Module interaction eQTL mapping and GWAS colocalization

To identify *cis*-eQTLs conditional on the module enrichment, we tested the interaction between genotypes and modules using a linear regression model. The formula is exp~g+m+g*m+c, where exp is the gene expression, g is the genotype, m is module eigengenes which is the first principal component of expressions of module member genes, and c is the covariate matrix that was used in bulk tissue eQTL mapping. The covariates include sex, age, genotype PCs, and HCP factors. The correlations between HCPs and module eigengenes are lower than 0.5, suggesting the HCP factors are robust to modules. TensorQTL (*120*) was used to compute the significance of the interaction term. Variants within the 1Mb window of TSS of each tested gene were included. Variants with MAF < 0.05 were removed. The phenotype input is the same matrix used in bulk tissue eQTL mapping. The top SNP with the most significant p-value for each gene was selected. P values were firstly corrected at the gene level using eigenMT. Then the genome-wide significance was computed by the Benjamini-Hochberg method. Next, we followed the eCAVIAR pipeline as described in Section 18, and ran colocalization analysis on 120 SCZ locus-isomodule-gene, and 3220 SCZ locus-genemod-gene tuples. Variant with CLPP > 0.01 was identified as significant colocalization.

To test the cell-type-specificity of module eQTLs, we used eQTLs from cultured neurons and progenitor cells as a reference (*56*). We calculated the pi1 statistic to quantify the sharing between the module and cell-type eQTLs using the qvalue

package (*43*). The nominal p values of shared eSNP-eGene pairs in reference data were used to calculate pi0 statistic. The pi1 was calculated as 1-pi0.

21: CellWalker

We used the network-based CellWalker (*78*) method to map eQTLs to specific cell types through integration with fetal single-cell chromatin accessibility data (scATAC-seq). We built and tuned a network model using CellWalkR version 0.99 (*121*) with labels derived from Polioudakis et al. (*39*) and scATAC-seq data from Ziffra et al. (*79*). Label edges were generated using the mapSnapATACToGenes function of CellWalkerR with the gene activity matrix from Ziffra et al. and log-fold change expression in marker genes from Polioudakis et al. Cell edges were computed as the Jaccard similarity of each cell's genome-wide accessibility. We selected a label edge weight parameter of 100 using the tuneEdgeWeights function with the steps parameter set to three. Once the network model was built, we used the CellWalkR labelBulk function to score all bulk and cell-type specific eQTLs for all cell types in Polioudakis et al. We called an eQTL as being specific to a cell type if it received a label score greater than two for that cell type. We then extended this scoring scheme to generate multi-level cell types by averaging the label scores of each eQTL at each branch of the hierarchy of cell types as built using the CellWalkR clusterLabels function with the "maximum" option for the distance method, and scaled by 1.5 at each level. A count of cell-type labels for the outermost nodes and how many of the multi-level label scores were greater than two for the inner nodes was used to generate a hierarchical tree of enriched cell types.

22: Cell type deconvolution with CIBERSORTx

To investigate the change in cell-type proportions during brain development, and its potential influence on the observed decrease in gene heritability, we employed CIBERSORTx (*53*) to estimate cell fractions from our bulk gene expression data. We leveraged “meta marker” genes associated with 7 major cell classes in the developing brain (Dividing_Progenitor, GABAergic, Glutamatergic, Intermediate_Progenitor, Neural_Progenitor, Non-neuronal, other) identified from an extensive meta-analysis of 2.95 million developing brain single nuclei/cells (*54*, *122*). The top 50 meta markers per cell type, along with their expression profiles derived from the meta-analysis, were used to generate the signature matrix. Our bulk gene expression, both pre- and post-HCP correction, was used to generate the mixture matrix. Cell fraction imputation was performed on CIBERSORTx web portal (https://cibersortx.stanford.edu/) with default settings.

Supplementary Figures

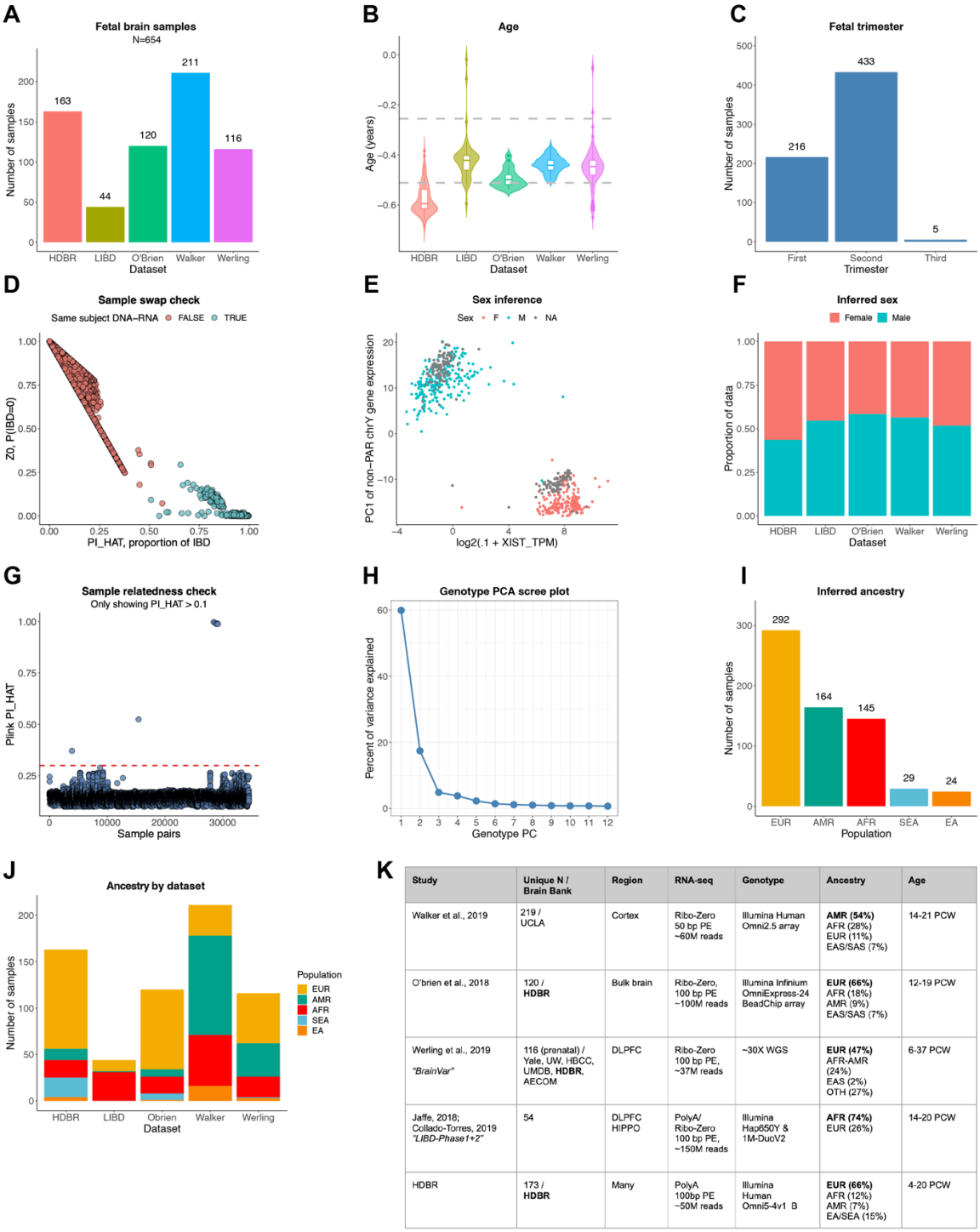

K

Study	Unique N / Brain Bank	Region	RNA-seq	Genotype	Ancestry	Age
Walker et al., 2019	219 / UCLA	Cortex	Ribo-Zero 50 bp PE ~60M reads	Illumina Human Omni2.5 array	**AMR (54%)** AFR (28%) EUR (11%) EAS/SAS (7%)	14-21 PCW
O'brien et al., 2018	120 / **HDBR**	Bulk brain	Ribo-Zero, 100 bp PE ~100M reads	Illumina Infinium OmniExpress-24 BeadChip array	**EUR (66%)** AFR (18%) AMR (9%) EAS/SAS (7%)	12-19 PCW
Werling et al., 2019 *"BrainVar"*	116 (prenatal) / Yale, UW, HBCC, UMDB, **HDBR**, AECOM	DLPFC	Ribo-Zero 100 bp PE, ~37M reads	~30X WGS	**EUR (47%)** AFR-AMR (24%) EAS (2%) OTH (27%)	6-37 PCW
Jaffe, 2018; Collado-Torres, 2019 *"LIBD-Phase1+2"*	54	DLPFC HIPPO	PolyA/ Ribo-Zero 100 bp PE, ~150M reads	Illumina Hap650Y & 1M-DuoV2	**AFR (74%)** EUR (26%)	14-20 PCW
HDBR	173 / **HDBR**	Many	PolyA 100bp PE ~50M reads	Illumina Human Omni5-4v1 B	**EUR (66%)** AFR (12%) AMR (7%) EA/SEA (15%)	4-20 PCW

Fig. S1. Compilation of developmental brain datasets.
(A) Sample sizes of fetal brain studies. **(B)** Age of fetal brain samples, spanning from 4 to 39 PCW. **(C)** Trimester of fetal brain samples (Tri1: 4-13 PCW; Tri2: 14-26 PCW; Tri3: 27-39 PCW). **(D)** Sample swap check. **(E)** *XIST* gene expression versus PC1 of chromosome Y gene expression, colored by sex of fetal brain samples. Unknown sexes are inferred. **(F)** Inferred sex of fetal brain samples by study. **(G)** Sample relatedness check, as measured by PI_HAT. PI_HAT>0.3 samples were excluded from the analysis. **(H)** Scree plot of population PCA. **(I)** Number of fetal brain samples inferred as European (EUR), American (AMR), African (AFR), Southeast Asian (SEA), and East Asian (EA). **(J)** Inferred ancestry of fetal brain samples by study. **(K)** Overview of fetal brain datasets. 654 samples with high-quality matching DNA-RNA data were kept in the analysis.

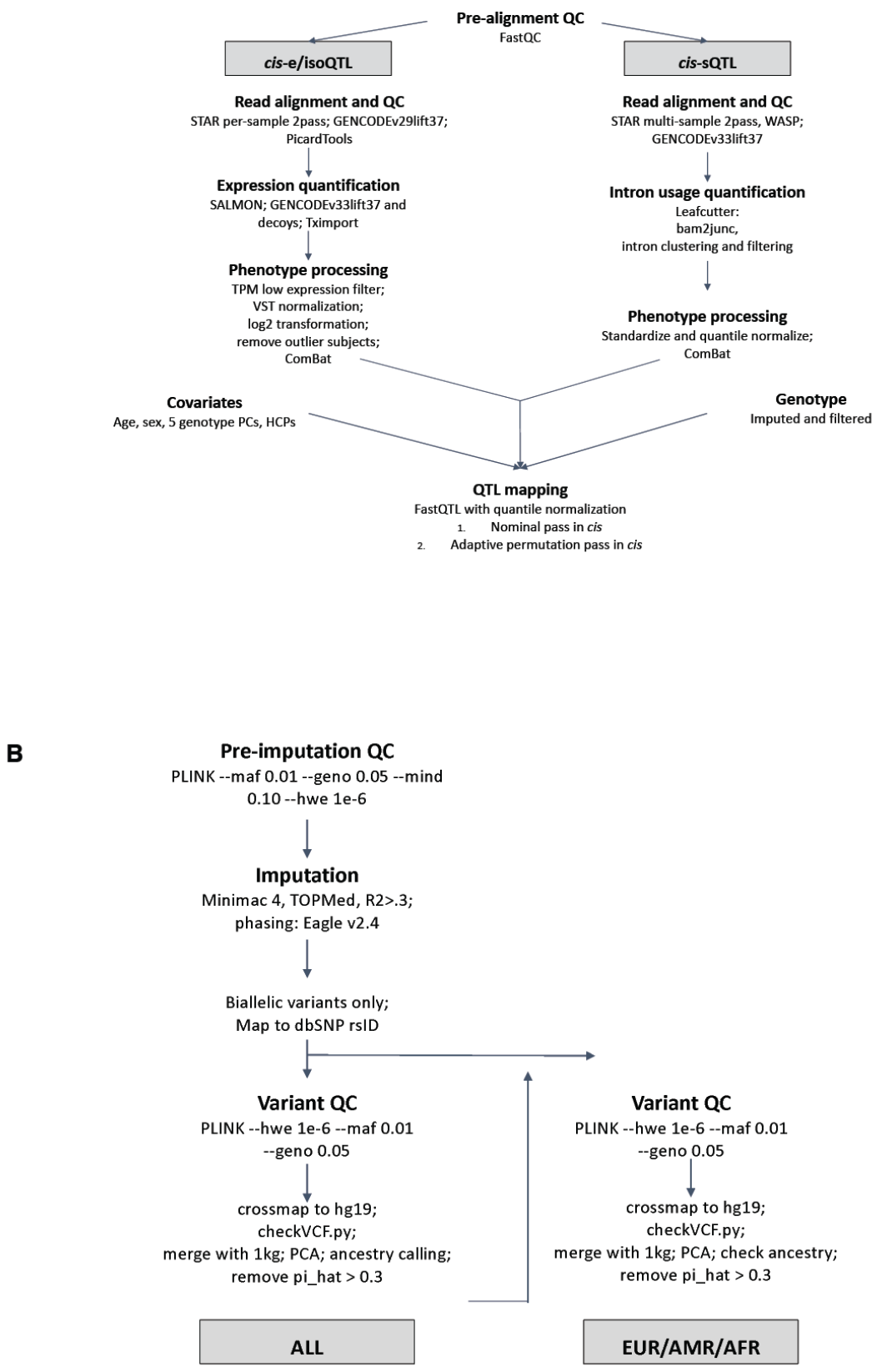

Fig. S2. Data analysis and integration pipeline.
Analysis pipeline through which RNA-seq **(A)** and genotype **(B)** data of all samples were uniformly processed.

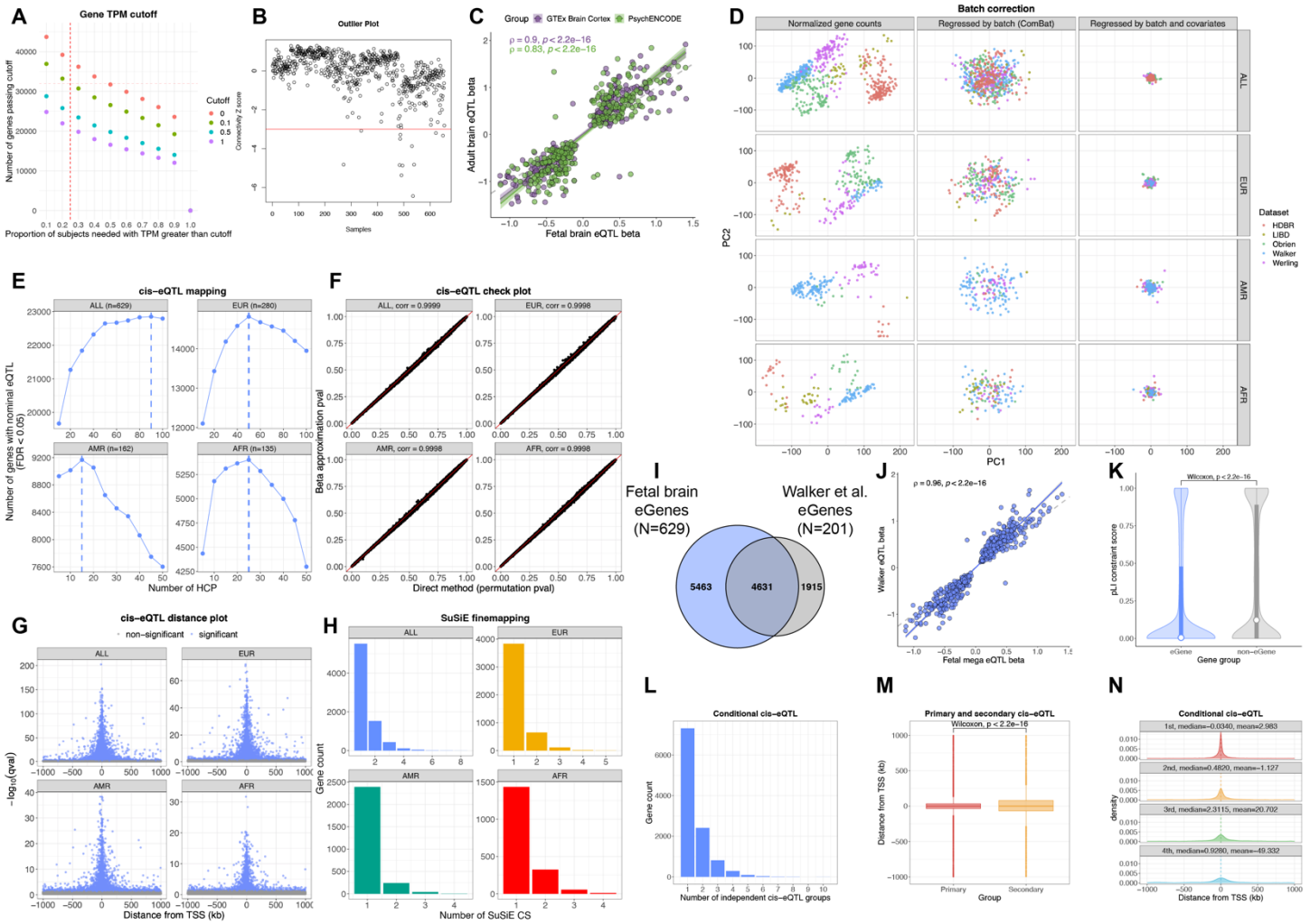

Fig. S3. *cis*-eQTL mapping and fine-mapping.

(A) Gene expression filtering. 31,947 genes with greater than 0.1 TPM in at least 25% of the samples were included in the analysis. **(B)** Gene expression outlier sample detection. Samples with connectivity Z score < -3 were excluded from the analysis. **(C)** Correlation of *cis*-eQTL effect size, measured by linear regression slope (beta), between fetal and adult brain. Each dot is a shared pair of eGene-primary eQTL between fetal brain and GTEx (247 pairs) or PsychENCODE (253 pairs). **(D)** Batch correction of gene expression. The top 2 principal components (PCs) were shown for before batch correction (left), after batch correction (middle), and after covariates correction (right). **(E)** Nominal *cis*-eQTL mapping. The optimal number of Hidden Components with Priors (HCPs) was determined by optimizing for the number of significant nominal eGenes. 90, 50, 15, and 25 HCPs were included in a permutation-based analysis for the multi-ancestry (ALL, N=629), EUR (N=280), AMR (N=162), and AFR (N=135), respectively. **(F)** Check plot of FastQTL beta approximation of permutation p value. **(G)** Distance from gene TSS of primary *cis*-eQTLs. **(H)** Number of SuSiE fine-mapping credible sets of eGenes in ALL, EUR, AMR, and AFR. **(I)** Comparison of eGenes between fetal mega-analysis dataset and Walker et al. **(J)** Correlation of *cis*-eQTL effect size measure by beta between fetal and Walker datasets. **(K)** pLI score of eGenes and non-eGenes in the fetal dataset. **(L)** Number of conditionally independent *cis*-eQTL groups. **(M)** Comparison of distances from gene TSSs between primary and secondary *cis*-eQTLs. **(N)** Comparison of distances from gene TSSs between the 1st to 4th ranks of *cis*-eQTLs.

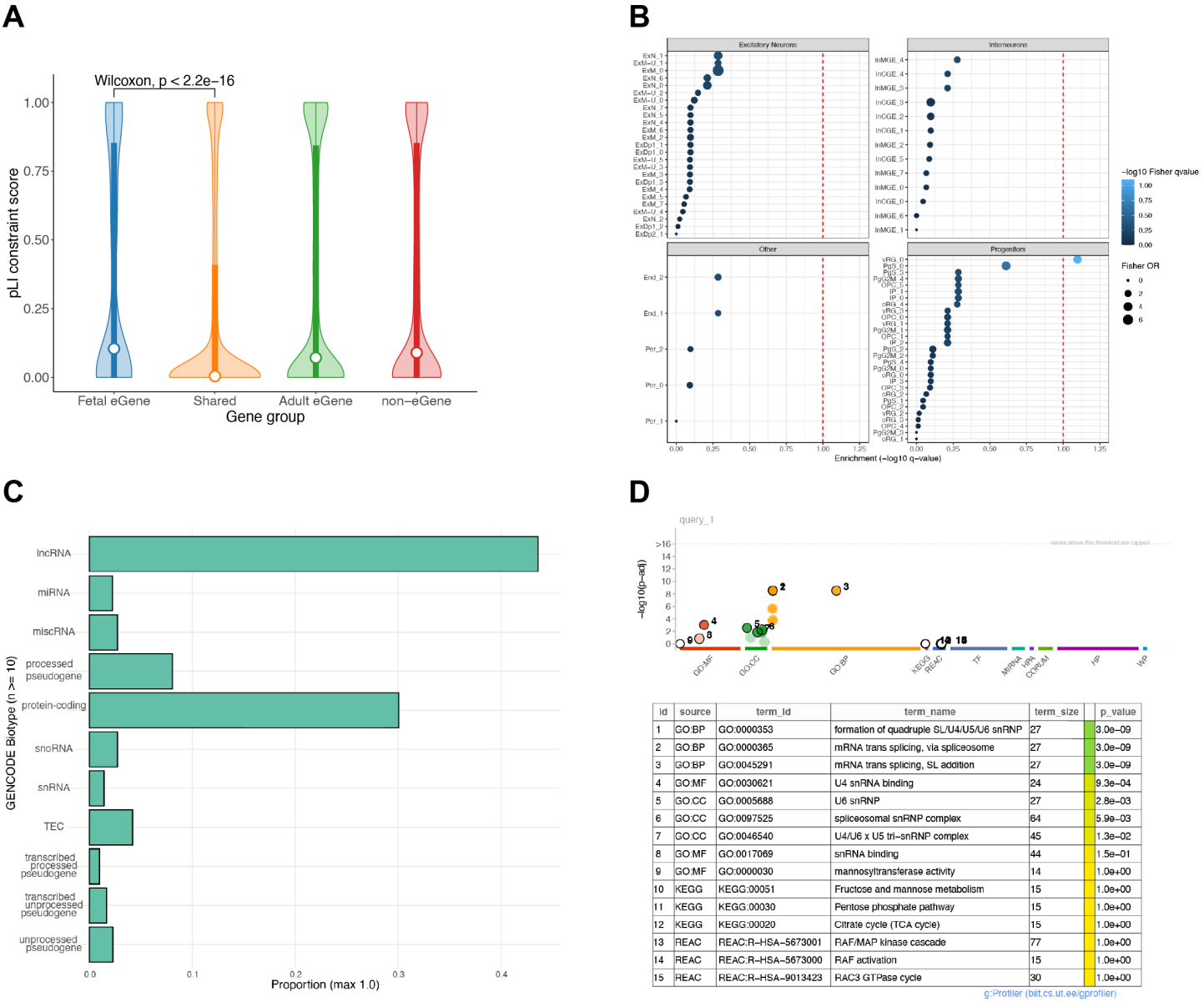

id	source	term_id	term_name	term_size	p_value
1	GO:BP	GO:0000353	formation of quadruple SL/U4/U5/U6 snRNP	27	3.0e−09
2	GO:BP	GO:0000365	mRNA trans splicing, via spliceosome	27	3.0e−09
3	GO:BP	GO:0045291	mRNA trans splicing, SL addition	27	3.0e−09
4	GO:MF	GO:0030621	U4 snRNA binding	24	9.3e−04
5	GO:CC	GO:0005688	U6 snRNP	27	2.8e−03
6	GO:CC	GO:0097525	spliceosomal snRNP complex	64	5.9e−03
7	GO:CC	GO:0046540	U4/U6 x U5 tri−snRNP complex	45	1.3e−02
8	GO:MF	GO:0017069	snRNA binding	44	1.5e−01
9	GO:MF	GO:0000030	mannosyltransferase activity	14	1.0e+00
10	KEGG	KEGG:00051	Fructose and mannose metabolism	15	1.0e+00
11	KEGG	KEGG:00030	Pentose phosphate pathway	15	1.0e+00
12	KEGG	KEGG:00020	Citrate cycle (TCA cycle)	15	1.0e+00
13	REAC	REAC:R−HSA−5673001	RAF/MAP kinase cascade	77	1.0e+00
14	REAC	REAC:R−HSA−5673000	RAF activation	15	1.0e+00
15	REAC	REAC:R−HSA−9013423	RAC3 GTPase cycle	30	1.0e+00

g:Profiler (biit.cs.ut.ee/gprofiler)

Fig. S4. Characteristics of 2,488 fetal-specific eGenes.

(A) Tolerance to loss-of-function mutations, as measured by pLI score, of fetal-specific eGenes, adult-specific eGenes, shared eGenes, and non-eGenes. **(B)** Cell type enrichment of fetal-specific eGenes. **(C)** Proportion of gene types of fetal-specific eGenes. **(D)** GO pathway enrichment of fetal-specific eGenes.

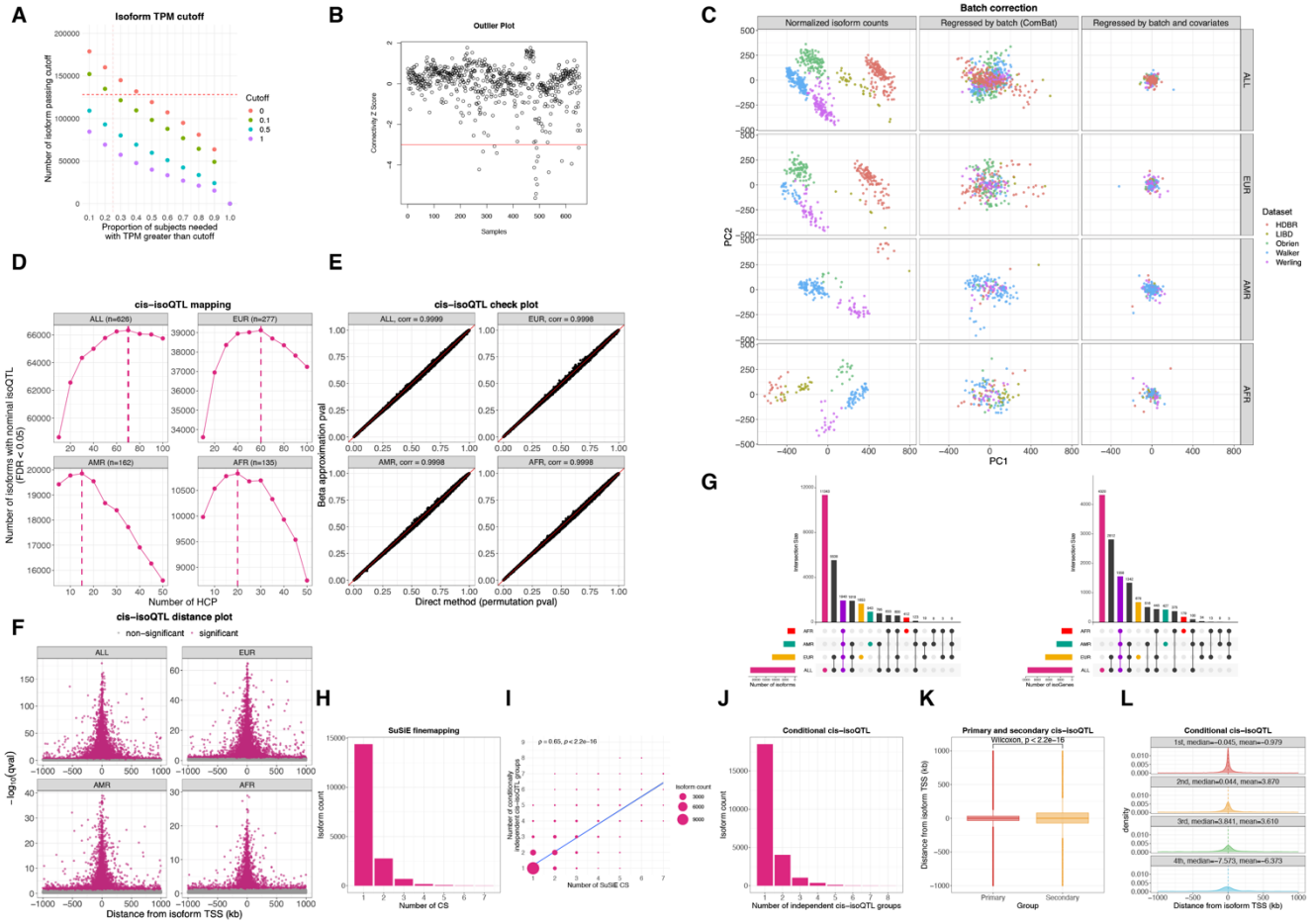

Fig. S5. *cis*-isoQTL mapping and fine-mapping.

(A) Isoform expression filtering. 127,987 isoforms with greater than 0.1 TPM in at least 25% of the samples were included in the analysis. **(B)** Isoform expression outlier sample detection. Samples with connectivity Z score < -3 were excluded from the analysis. **(C)** Batch correction of isoform expression. The top 2 principal components (PCs) were shown for before batch correction (left), after batch correction (middle), and after covariates correction (right). **(D)** *cis*-isoQTL nominal mapping. The optimal number of Hidden Components with Priors (HCPs) was determined as when the number of isoforms with nominal *cis*-isoQTLs was maximized. 70, 60, 15, and 20 HCPs were included in a permutation-bsed analysis for the multi-ancestry (ALL, N=626), EUR (N=277), AMR (N=162), and AFR (N=135) datasets, respectively. **(E)** Check plot of FastQTL beta approximation of permutation p value. **(F)** Distances from isoform TSSs of primary *cis*-isoQTLs. **(G)** Comparison of isoforms (left) and genes (right) identified with *cis*-isoQTLs discovered in ALL, EUR, AMR, and AFR. **(H)** Number of SuSiE fine-mapping credible sets of isoforms. **(I)** Number of fine-mapping credible sets versus number of conditionally independent *cis*-isoQTLs discovered. The size of the dots is scaled to designate the number of isoforms. **(J)** Number of conditionally independent *cis*-isoQTL groups. **(K)** Comparison of distances from isoform TSSs between primary and secondary *cis*-isoQTLs. **(L)** Comparison of distances from isoform TSSs between the 1st to 4th ranks of *cis*-isoQTLs.

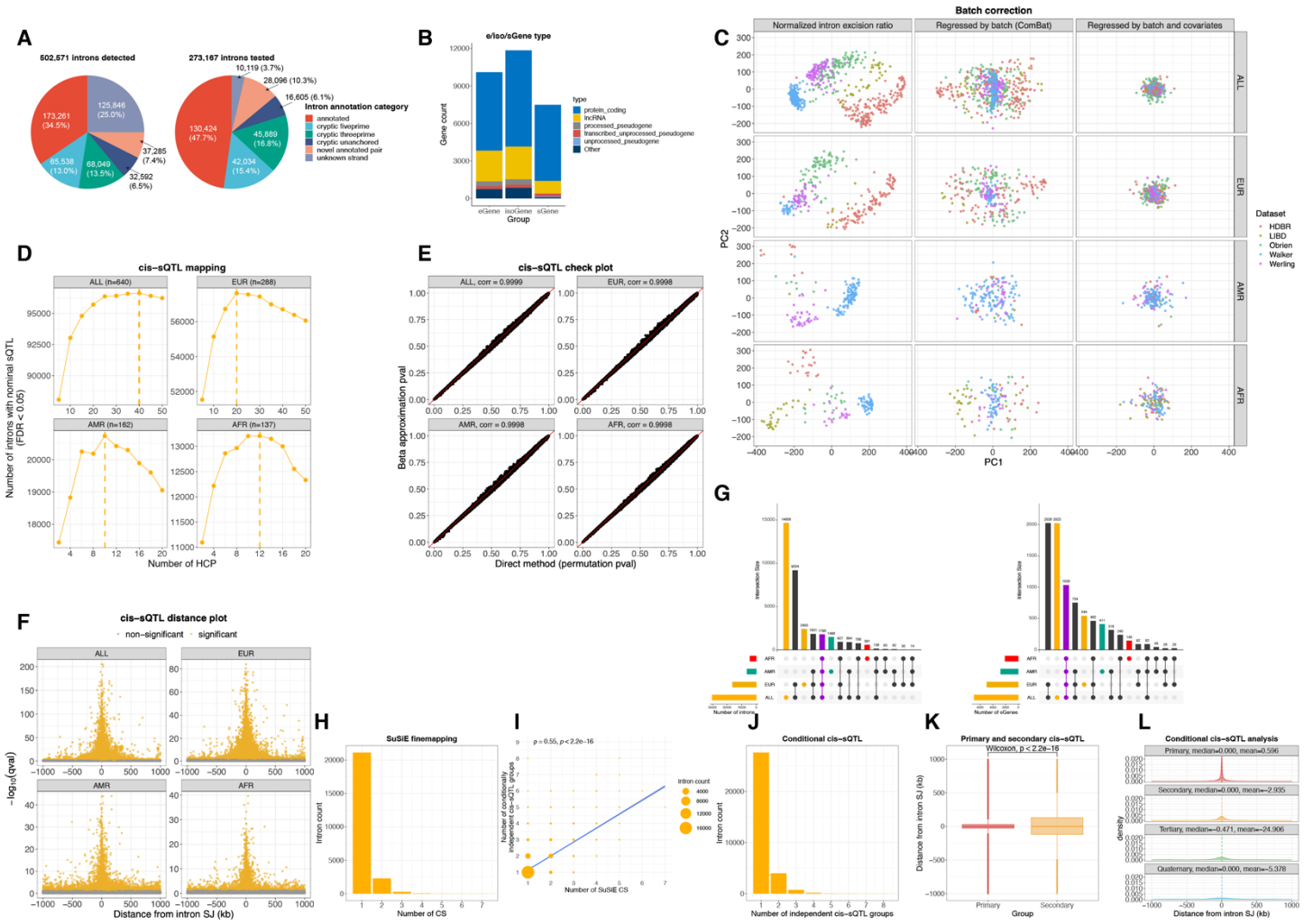

Fig. S6. *cis*-sQTL mapping and fine-mapping.

(**A**) GENCODE (v33) annotations of the 502,571 introns detected by Leafcutter (left), and the 273,167 introns that passed filters and were used to map sQTL (right). (**B**) Gene types of *cis*-eGenes, isoGenes, and sGenes. (**C**) Batch correction of intron quantification. The top 2 principle components (PCs) were shown for before batch correction (left), after batch correction (middle), and after covariates correction (right). (**D**) *cis*-sQTL nominal mapping. The optimal number of Hidden Components with Priors (HCPs) was determined as when the number of introns with nominal *cis*-sQTLs was maximized. 40, 20, 10, and 12 HCPs were included in permutation analysis for the multi-ancestry (ALL, N=640), EUR (n=288), AMR (n=162), and AFR (n=137) datasets, respectively. (**E**) Check plot of FastQTL beta approximation of permutation p value. (**F**) Distances from intron of primary *cis*-sQTLs. (**G**) Comparison of introns (left) and genes (right) identified with *cis*-sQTLs discovered in ALL, EUR, AMR, and AFR. (**H**) Number of SuSiE fine-mapping credible sets of introns. (**I**) Number of fine-mapping credible sets versus number of conditionally independent *cis*-sQTLs discovered. The size of the dots is scaled to designate the number of introns. (**J**) Number of conditionally independent *cis*-sQTL groups. (**K**) Comparison of distances from intron between primary and secondary *cis*-sQTLs. (**L**) Comparison of distances from introns between the 1st to 4th ranks of *cis*-sQTLs.

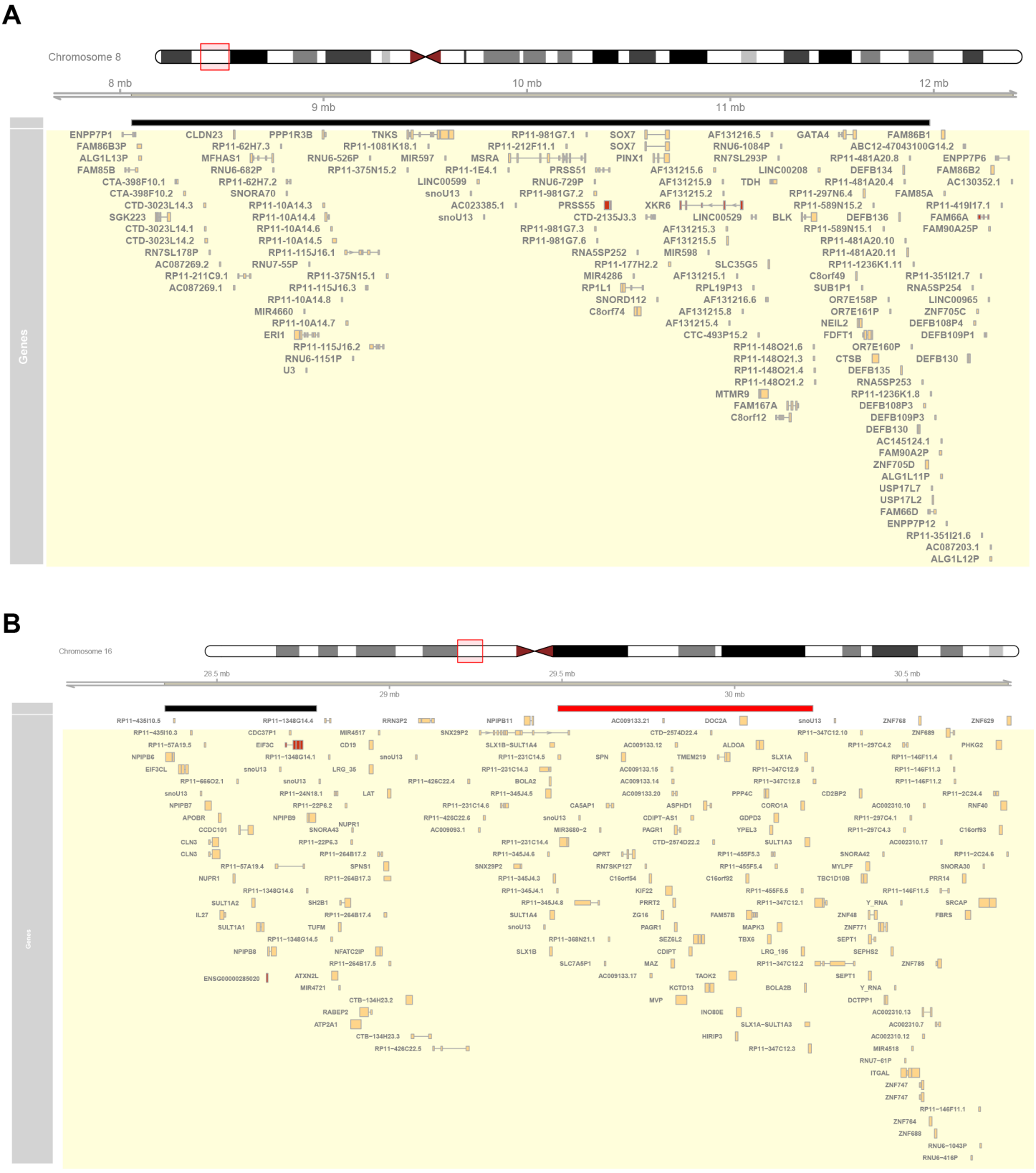

Fig. S7. Inversion eQTL.

Genomic location of inversion (black bar) and their eGenes *in cis* (red colored genes) for regions at **(A)** 8p23.1 and **(B)** 16p11.2. At 16p11.2 a rare CNV region near the inversion is highlighted with red bar.

A

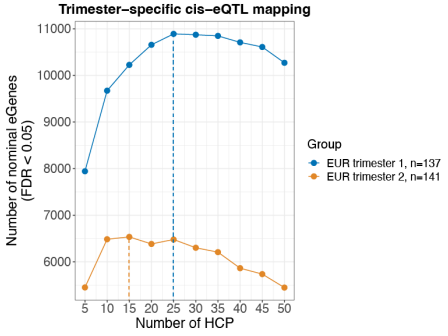

B

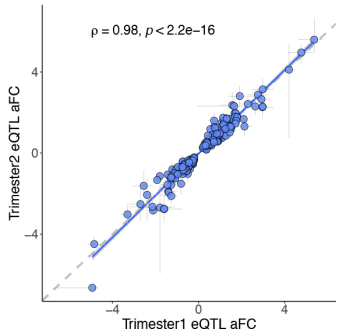

C

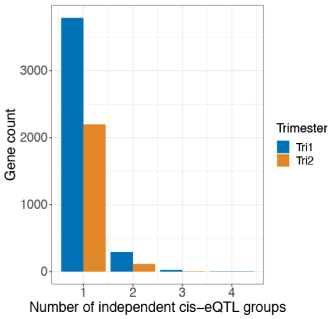

D

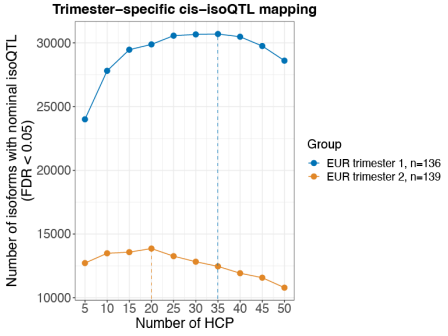

E

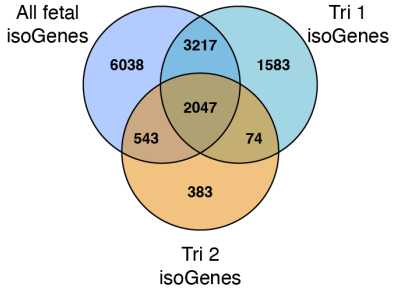

F

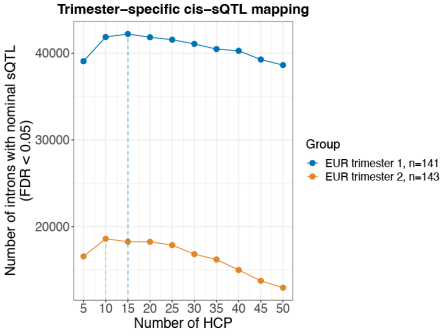

G

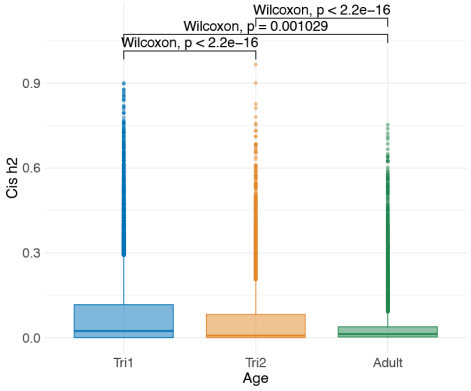

H

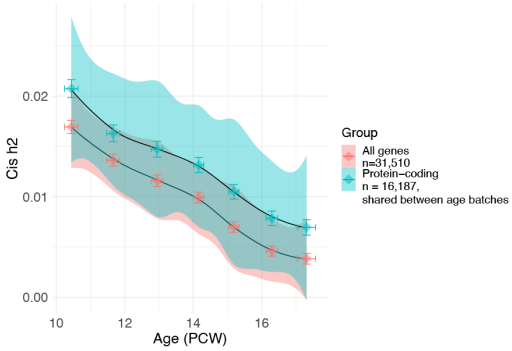

I

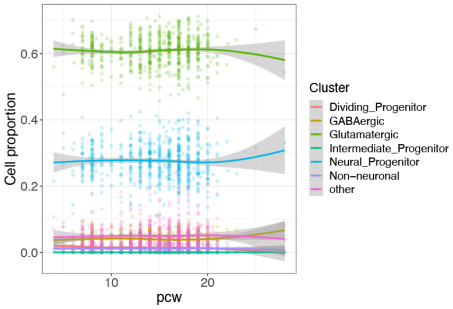

J

Correlation between cell fractions and cis-h2

cell_type	cor.est	pvalue	p.FDR
Dividing_Progenitor	0.9555435	0.0007813918	0.005469742
Glutamatergic	-0.9406919	0.0015933063	0.005576572
Neural_Progenitor	0.7524515	0.0509846339	0.118964146
other	0.6916683	0.0851565673	0.149023993
GABAergic	-0.3573895	0.4312702259	0.603778316
Intermediate_Progenitor	-0.1502767	0.7477531618	0.747753162
Non_neuronal	0.1768330	0.7044704811	0.747753162

K

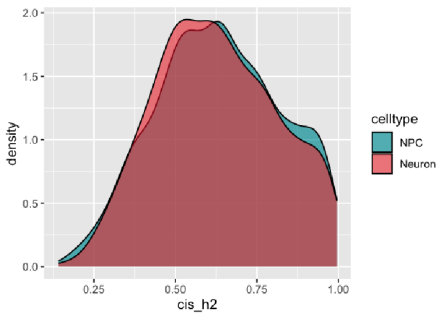

L

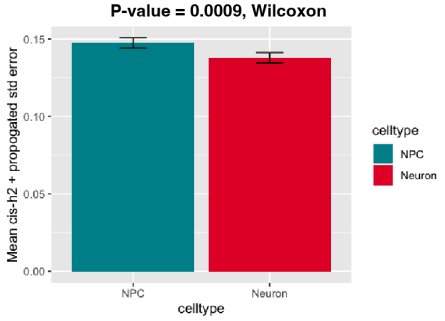

Fig. S8. Trimester-specific xQTL mapping and heritability analysis.
(A) Trimester-specific *cis*-eQTL nominal mapping. 25 and 15 HCPs maximized the number of nominal eGenes and were included in a permutation-based analysis for the first and second trimesters, respectively. Note: trimester sample sizes differ slightly for e/iso/sQTL as gene and isoform expression outliers were removed from e/isoQTL mapping. In sQTL mapping, only genotype-related samples were removed. **(B)** Correlation of eQTL effect sizes between the two trimesters, as measured by allelic fold change (aFC) between the two trimesters. **(C)** Trimester 1 and 2 conditional eQTL mapping. **(D)** Trimester-specific *cis*-isoQTL nominal mapping. 20 and 35 HCPs maximized the number of isoforms with nominal isoQTLs and were included in a permutation-based analysis for the first and second trimesters, respectively. (**E**) Comparison of isoGenes discovered in Tri1, Tri2, and the full dataset. **(F)** Trimester-specific *cis*-sQTL nominal mapping. 15 and 10 HCPs maximized the number of introns with nominal sQTLs and were included in a permutation-based analysis for the first and second trimesters, respectively. (**G**) *cis*-heritability of protein-coding gene expression drops from Tri1 to Tri2 timepoints, and between fetal and adult (PsychENCODE) samples. (**H**) *cis*-heritability of protein-coding gene expression across 10-18 post-conception weeks (PCW) in fetal brain EUR samples. Each dot represents a sliding set of temporally ordered samples (N = 150), with mean age (+/- SD) on the x-axis, and median *cis*-h2SNP (+/- SD) on the y-axis. (**I**) Estimated cell proportion from bulk tissue cell-type deconvolution using CIBERSORTx. HCP-factors that were used for eQTL and heritability calculations were removed from gene expression profiles. As shown, regression of HCP factors attenuates cell proportion shifts over development, indicating that these hidden factors control for cell proportion changes across samples. (**J**) Pearson correlations between average *cis*-h^2_{SNP} over 10-20 weeks post-conception and mean estimated cell-type proportions from CIBERSORTx deconvolution. (**K**) and (**L**) Gene expression *cis*-heritability decreases with neuronal differentiation in homogenous cell culture system. Primary human neural progenitor cells (phNPCs) and differentiated neurons were derived from a matched set of donors (n=72).

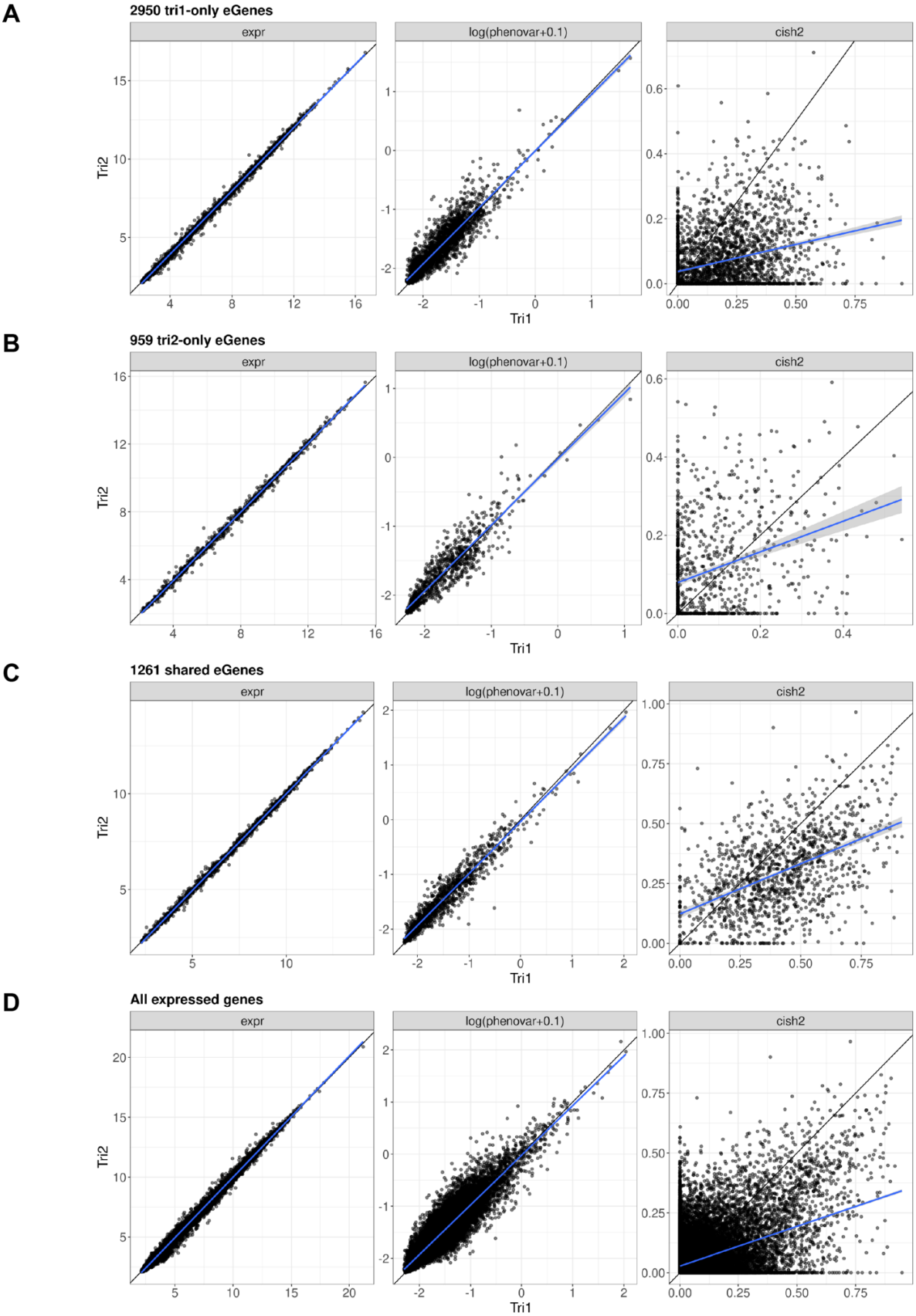

Fig. S9. Trimester heritability analysis of (**A**) trimester 1-only eGenes, (**B**) trimester 2-only eGenes, (**C**) trimester shared eGenes, and (**D**) all expressed genes. Gene expression level, phenotypic variance, and cish2 estimates in trimesters 1 and 2 are shown on the x and y axes, respectively.

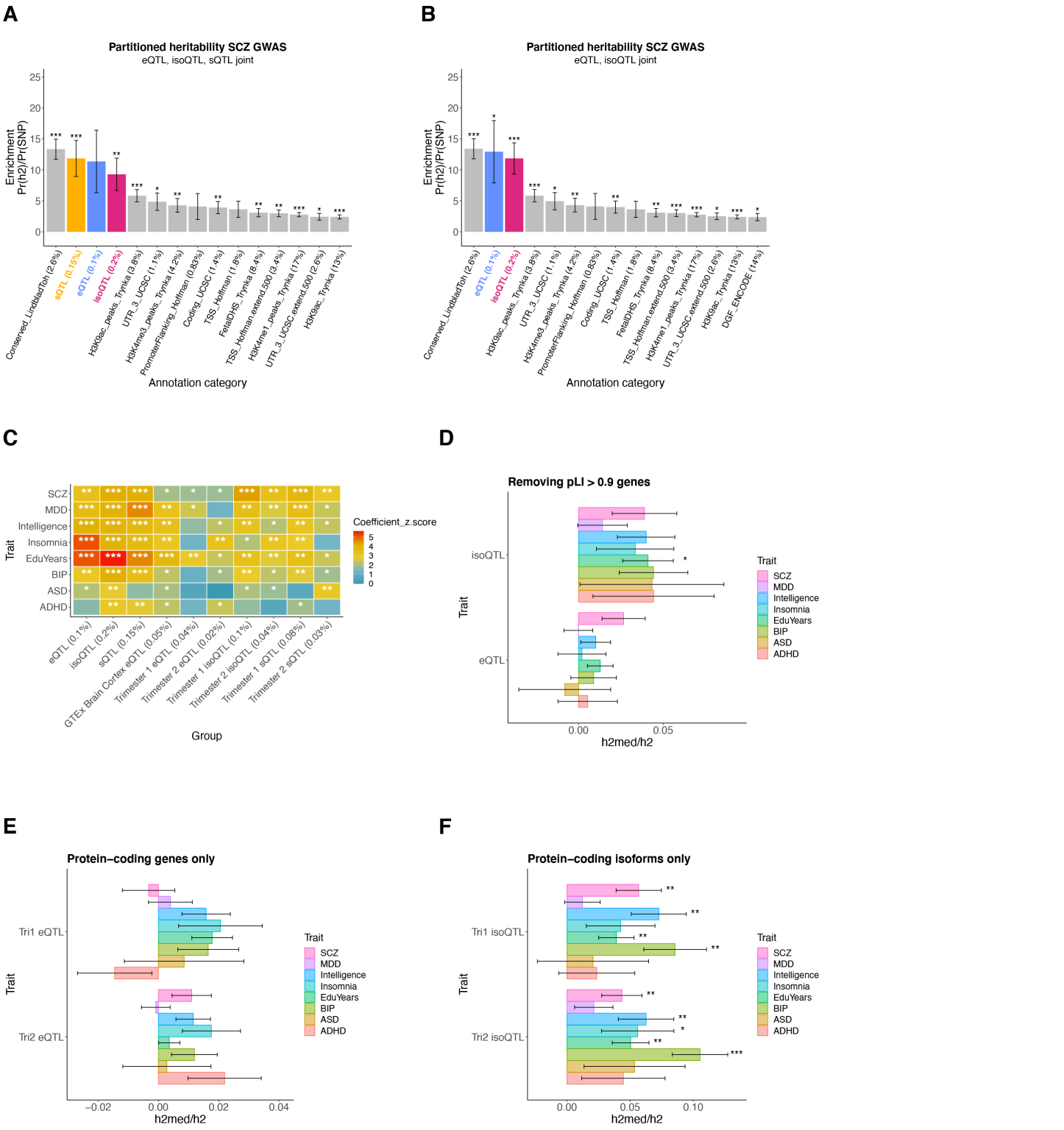

Fig. S10. S-LDSC and MESC analysis.

(A) S-LDSC enrichment of SCZ GWAS risk in fetal brain eQTL, isoQTL, sQTL, and background functional annotations, estimated jointly. For A, B, C: *** FDR<0.001, ** FDR<0.01, * FDR<0.05. In parentheses are the proportion of SNP of each annotation. **(B)** S-LDSC enrichment of SCZ GWAS risk in eQTL, isoQTL, and background annotations, estimated jointly. **(C)** S-LDSC coefficient z-scores of GWAS traits in various groups of brain QTLs. **(D)** MESC analysis of estimated proportion (+/- SE) of GWAS h2SNP mediated by *cis* eQTL and isoQTL while removing pLI > 0.9 genes. **(E)** MESC analysis of estimated proportion (+/- SE) of GWAS h2SNP mediated by *cis* trimester eQTL and isoQTL **(F)** while limiting to protein-coding genes and their isoforms.

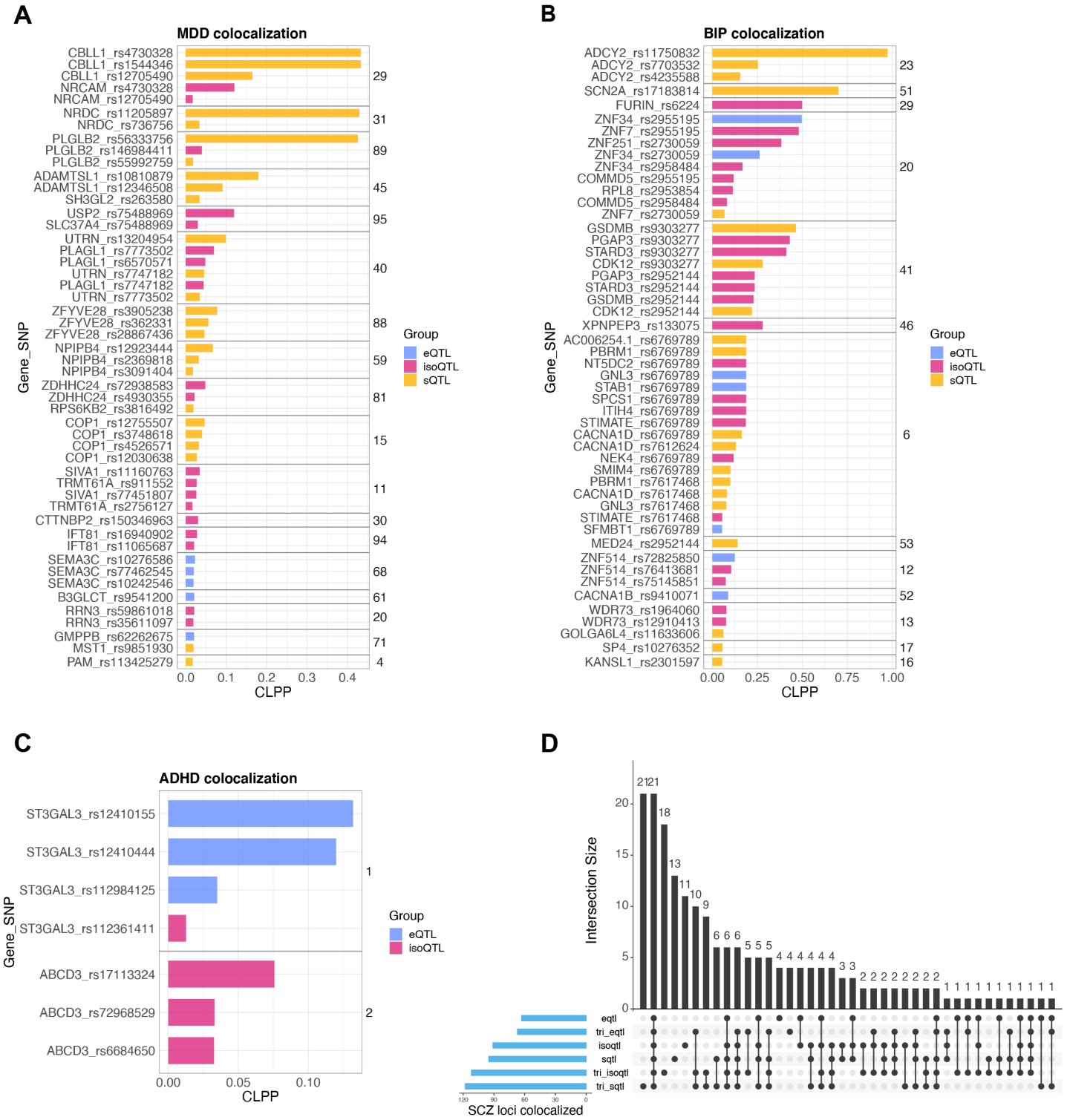

Fig. S11. Colocalization.

Top CLPP results for (**A**) MDD, (**B**) BIP, and (**C**) ADHD. Results are colored by QTL annotation. Numbers on the right represent GWAS loci. (**D**) Overlap of SCZ loci colocalized with bulk and trimester-specific e/iso/sQTL.

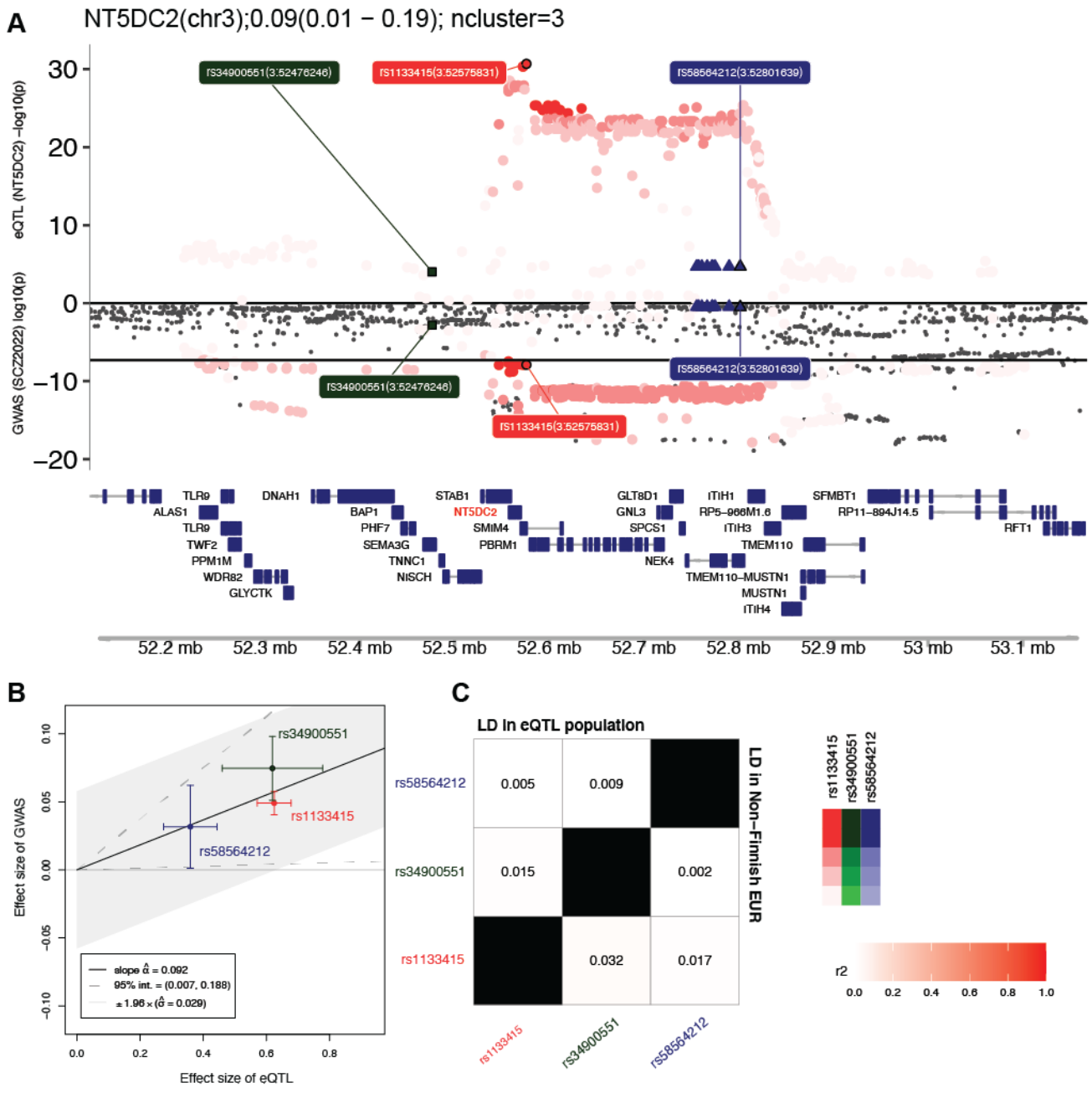

Fig. S12. MRLocus for NT5DC2 locus.

(**A**) NT5DC2 eQTL and SCZ GWAS associations are shown with a LocusZoom plot. Variants are colored by the 3 conditionally independent eQTL groups. (**B**) eQTL and GWAS effect sizes of the eCAVIAR-selected variants in the 3 eQTL groups. Bars represent the standard error of eQTL and GWAS effect sizes. (**C**) LD between the 3 eCAVIAR-selected variants, calculated in the multi-ancestry fetal brain dataset (left top) or non-Finnish EUR (right bottom), showing that these eQTL variants are nearly independent.

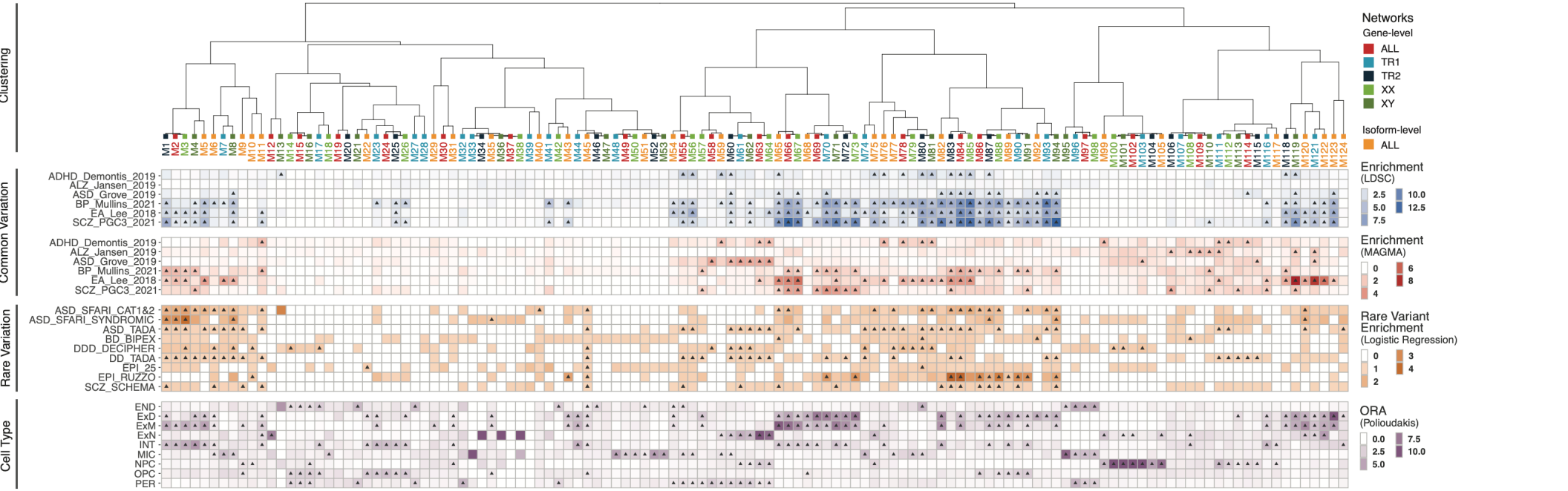
Clustering
Common Variation
ADHD_Demontis_2019
ALZ_Jansen_2019
ASD_Grove_2019
BP_Mullins_2021
EA_Lee_2018
SCZ_PGC3_2021
Rare Variation
ASD_SFARI_CAT1&2
ASD_SFARI_SYNDROMIC
ASD_TADA
BD_BIPEX
DDD_DECIPHER
DD_TADA
EPI_25
EPI_RUZZO
SCZ_SCHEMA
Cell Type
END
ExD
ExM
ExN
INT
MIC
NPC
OPC
PER
Networks
Gene-level
ALL
TR1
TR2
XX
XY
Isoform-level
ALL
Enrichment
(LDSC)
2.5
5.0
7.5
10.0
12.5
Enrichment
(MAGMA)
0
2
4
6
8
Rare Variant
Enrichment
(Logistic Regression)
0
1
2
3
4
ORA
(Polioudakis)
0.0
2.5
5.0
7.5
10.0

Fig. S13. Hierarchical clustering and risk variation for all gene and isoform co-expression modules.
Top: hierarchical clustering of modules from gene, isoform, trimester, and sex-stratified networks through bi-weight mid-correlation of eigengenes. Middle: heatmaps depict module-level enrichment for neuropsychiatric GWAS signal ($-\log_{10}P_{enrich}$ from s-LDSC and MAGMA) and odds ratios (OR) for rare variation and cell type enrichment (truncated at 10). Triangles indicate FDR-corrected $P<0.1$ significance.

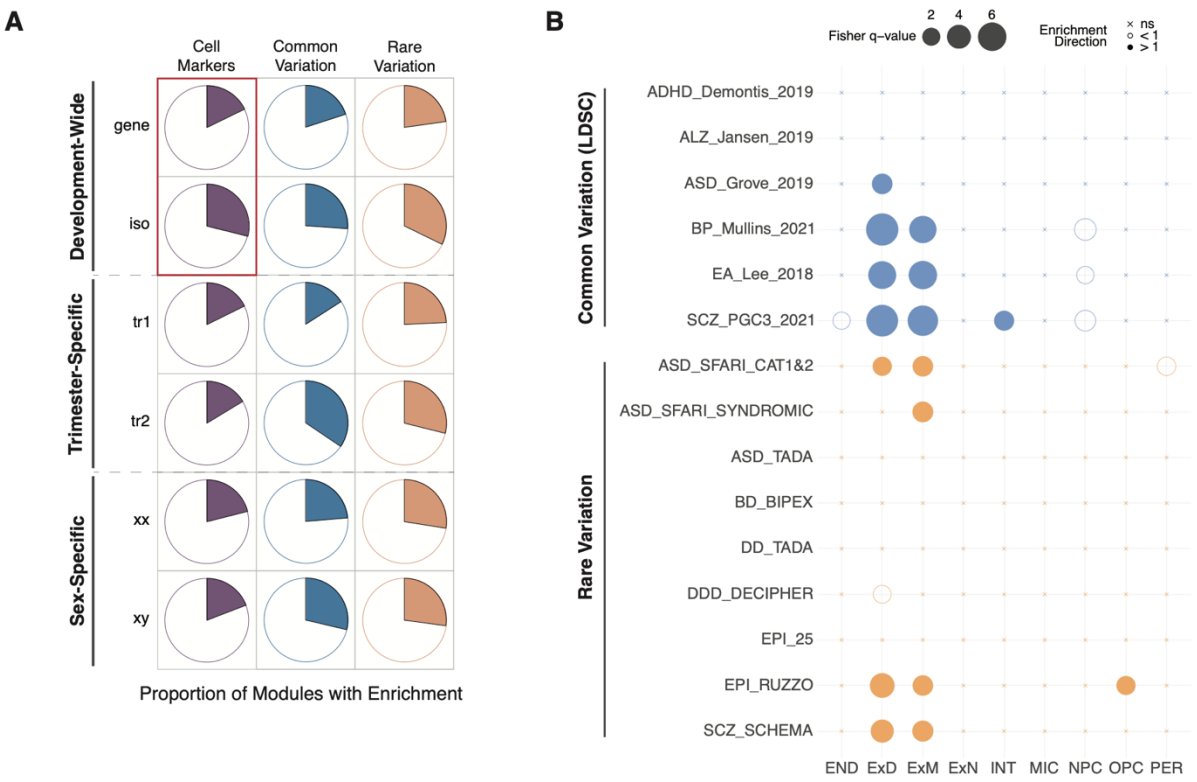

Fig. S14. Broad enrichments for co-expression modules identified by WGCNA.
(**A**) Proportion of modules exhibiting cell marker enrichment (purple), common variation enrichment (blue), and rare variation enrichment (orange), wherein red indicates statistically significant shifts in proportions. **(B)** Association of rare variant-enriched modules with cell type markers.

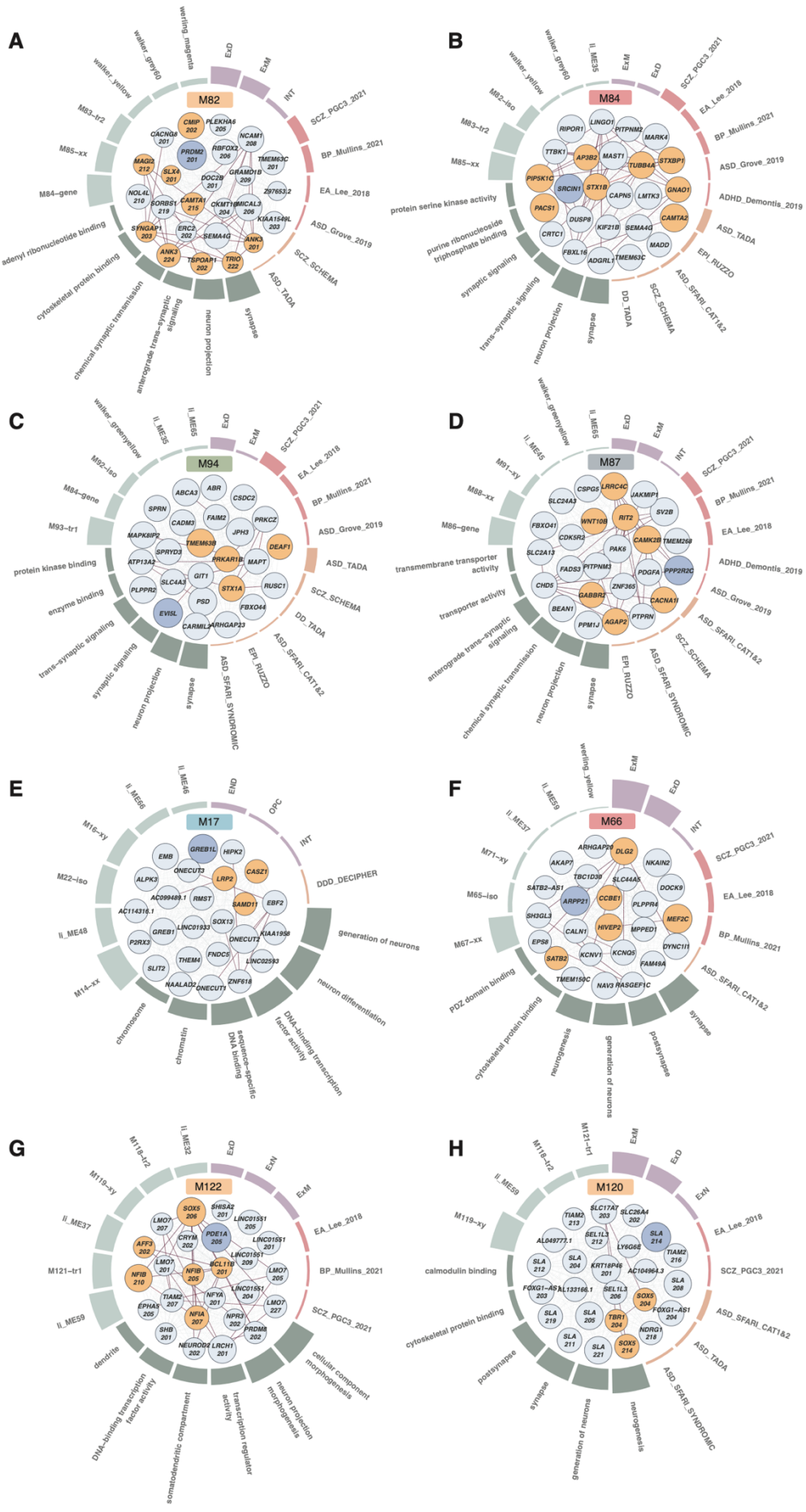
A
M82
werling_magenta
ExD
ExM
INT
SCZ_PGC3_2021
BP_Mullins_2021
EA_Lee_2018
ASD_Grove_2019
SCZ_SCHEMA
ASD_TADA
synapse
neuron projection
anterograde trans−synaptic signaling
chemical synaptic transmission
cytoskeletal protein binding
adenyl ribonucleotide binding
M84−gene
M85−xx
M83−tr2
walker_yellow
walker_green60
CMIP 202
PLEKHA6 205
CACNG8 201
NCAM1 208
PRDM2 201
RBFOX3 206
TMEM63C 201
MAGI2 212
SLX4 201
DOC2B 201
GRAMD1B 209
Z97653.2
NOL4L 210
SORBS1 219
CAMTA1 215
QKI 204
MICAL3 206
KIAA1549L 203
SYNGAP1 203
ERC2 202
SEMA4G
ANK3 201
ANK3 224
TSPOAP1 202
TRIO 222
B
M84
ll_ME35
ExM
ExD
SCZ_PGC3_2021
EA_Lee_2018
BP_Mullins_2021
ASD_Grove_2019
ADHD_Demontis_2019
ASD_TADA
EPI_RUZZO
ASD_SFARI_CAT1&2
SCZ_SCHEMA
DD_TADA
synapse
neuron projection
trans−synaptic signaling
synaptic signaling
purine ribonucleoside triphosphate binding
protein serine kinase activity
M85−xx
M83−tr2
M82−iso
walker_yellow
walker_green60
RIPOR1
LINGO1
PITPNM2
MARK4
TTBK1
AP3B2
MAST1
TUBB4A
STXBP1
PIP5K1C
SRCIN1
STX1B
CAPN5
LMTK3
GNAO1
PACS1
DUSP8
KIF21B
SEMA4G
CAMTA2
CRTC1
FBXL16
ADGRL1
TMEM63C
MADD
C
M94
ll_ME65
ExD
ExM
SCZ_PGC3_2021
EA_Lee_2018
BP_Mullins_2021
ASD_Grove_2019
ASD_TADA
SCZ_SCHEMA
DD_TADA
ASD_SFARI_CAT1&2
EPI_RUZZO
ASD_SFARI_SYNDROMIC
synapse
neuron projection
synaptic signaling
trans−synaptic signaling
enzyme binding
protein kinase binding
M93−tr1
M84−gene
M92−iso
walker_greenyellow
ll_ME65
ABCA3
ABR
CSDC2
SPRN
FAIM2
CADM3
PRKCZ
MAPK8IP2
JPH3
TMEM63B
DEAF1
SPRYD3
PRKAR1B
MAPT
ATP13A2
SLC4A3
GIT1
STX1A
RUSC1
PLPPR2
PSD
FBXO44
EVI5L
CARMIL2
ARHGAP23
D
M87
ll_ME65
ExD
ExM
INT
SCZ_PGC3_2021
BP_Mullins_2021
EA_Lee_2018
ADHD_Demontis_2019
ASD_Grove_2019
ASD_SFARI_CAT1&2
SCZ_SCHEMA
EPI_RUZZO
ASD_SFARI_SYNDROMIC
synapse
neuron projection
chemical synaptic transmission
anterograde trans−synaptic signaling
transporter activity
transmembrane transporter activity
M86−gene
M88−xx
M91−xy
ll_ME45
walker_greenyellow
CSPG5
LRRC4C
IAKMIP1
SLC24A3
SV2B
WNT10B
RIT2
FBXO41
CAMK2B
TMEM260
CDK5R2
PAK6
SLC2A13
FADS3
PITPNM3
PPP2R2C
PDGFA
CHD5
ZNF365
GABBR2
CACNA1I
BEAN1
PTPRN
PPM1J
AGAP2
E
M17
ll_ME46
END
OPC
INT
DDD_DECIPHER
generation of neurons
neuron differentiation
DNA−binding transcription factor activity
sequence−specific DNA binding
chromatin
chromosome
M14−xx
ll_ME48
M22−iso
M16−xy
ll_ME66
GREB1L
HIPK2
EMB
ONECUT3
CASZ1
ALPK3
LRP2
AC099489.1
RMST
SAMD11
EBF2
AC114316.1
GREB1
LINC01933
SOX13
P2RX3
ONECUT2
KIAA1958
FNDC5
THEM4
LINC02593
SLIT2
NAALAD2
ONECUT1
ZNF618
F
M66
ll_ME59
ExM
ExD
INT
SCZ_PGC3_2021
EA_Lee_2018
BP_Mullins_2021
ASD_SFARI_CAT1&2
synapse
postsynapse
generation of neurons
neurogenesis
cytoskeletal protein binding
PDZ domain binding
M67−xx
M65−iso
M71−xy
ll_ME57
werling_yellow
ARHGAP26
DLG2
AKAP7
NKAIN2
TBC1D30
SLC44A5
DOCK9
SATB2−AS1
ARPP21
CCBE1
PLPPR4
MEF2C
SH3GL3
CALN1
HIVEP2
MPPED1
DYNC1I1
EPS8
KCNV1
KCNQ5
FAM49A
SATB2
TMEM150C
NAV3
RASGEF1C
G
M122
ll_ME32
ExD
ExN
ExM
EA_Lee_2018
BP_Mullins_2021
SCZ_PGC3_2021
cellular component morphogenesis
neuron projection morphogenesis
transcription regulator activity
somatodendritic compartment
DNA−binding transcription factor activity
dendrite
M121−tr1
ll_ME59
ll_ME37
M119−xy
M118−tr2
SOX5 206
SHISA2 201
LINC01551 205
LMO7 207
PDE1A 205
CRYM 202
LINC01551 201
AFF3 202
LINC01551 209
BCL11B 201
LMO7 205
NFIB 210
NFIB 205
LMO7 201
LINC01551 204
TIAM2 207
NFYA 201
LMO7 227
EPHA5 205
NFIA 207
NPR3 202
SHB 201
PRDM8 202
NEUROD2 202
LRCH1 201
H
M120
ll_ME59
ExM
ExD
ExN
EA_Lee_2018
SCZ_PGC3_2021
ASD_SFARI_CAT1&2
ASD_TADA
ASD_SFARI_SYNDROMIC
neurogenesis
generation of neurons
synapse
postsynapse
cytoskeletal protein binding
calmodulin binding
M119−xy
M118−tr2
M121−tr1
SLC17A7 203
SLC26A4 202
TIAM2 213
SLA 214
SEL1L3 212
AL049777.1
LY6G6E
TIAM2 216
SLA 212
SLA 204
KRT18P46 201
AC104964.3
FOXG1−AS1 203
AL133166.1
SEL1L3 206
SOX5 204
SLA 208
FOXG1−AS1 204
SLA 219
SLA 205
TBR1 204
NDRG1 218
SLA 211
SLA 221
SOX5 214

Fig. S15. Highlighted gene and isoform-level co-expression modules with enrichment.
(**A**) Annotations for M82, a SCZ/BIP-associated deep layer neuron-projection isoform module. Center: top module ('hub') genes with circle size reflecting module membership (kME) and orange shading indicating genes with associated high-confidence neuropsychiatric disorder associated rare variants. Thin edges represent topologic overlap, solid edges indicate protein-protein interactions from the STRING database. Surrounding: circular bar plot highlighting module enrichment for cell types (purple), common (red) and rare (orange) variation, gene ontology terms (dark green), and module overlap (light green). (**B**) Annotations for M84, a development-wide gene module. (**C**) Annotations for M94, an XY module. (**D**) Annotations for M87, a trimester 2 module. (**E**) Annotations for M17, a trimester 1 module. (**F**) Annotations for M66, a gene module. (**G**) Annotations for M122, an isoform module. (**H**) Annotations for M120, an isoform module.

Supplementary Tables

Table S1. Metadata and xQTL summary statistics.

- README
- ST1-1-metadata: Metadata of 654 distinct, high-quality samples
- ST1-2-eGene: Sum stats of 10094 permutation eGenes and their primary *cis*-eQTL
- ST1-3-isoGene: Sum stats of 11845 group permutation isoGenes and their primary *cis*-isoQTL
- ST1-4-sGene: Sum stats of 7490 group permutation sGenes and their primary *cis*-sQTL
- ST1-5-torus-funcEnrich: Torus functional enrichment of *cis*-e/iso/sQTL
- ST1-6-conditional: Sum stats of conditional *cis*-eQTL mapping, for detailed descriptions of columns, see https://qtltools.github.io/qtltools/
- ST1-7-fetalOnlyeGene-CellTypeEnrich: Cell type enrichment for 2488 fetal only eGenes. "apprach" column denotes whether the cell types are defined as broad, cluster, or sub-cluster
- ST1-8-inv-eQTL: Sum stats of significant inversion eQTL
- ST1-9-torus-compare: Nominal pvalues of testing the difference of functional enrichment between e/iso/sQTLs

Table S2. Population specific xQTL and fine-mapping.

- README
- ST2-1-EUR-eGenes: Sum stats of 5296 EUR permutation eGenes and their primary *cis*-eQTL
- ST2-2-AMR-eGenes: Sum stats of 3242 EUR permutation eGenes and their primary *cis*-eQTL
- ST2-3-AFR-eGenes: Sum stats of 1876 EUR permutation eGenes and their primary *cis*-eQTL
- ST2-4-EUR-isoGenes : Sum stats of 11672/6885 isoforms/isoGenes with permutation *cis*-isoQTL in EUR
- ST2-5-AMR-isoGenes: Sum stats of 5747/3989 isoforms/isoGenes with permutation *cis*-isoQTL in AMR
- ST2-6-AFR-isoGenes: Sum stats of 3719/2682 isoforms/isoGenes with permutation *cis*-isoQTL in AFR
- ST2-7-EUR-sGenes: Sum stats of 16277/4963 introns/sGenes with permutation *cis*-sQTL in EUR
- ST2-8-AMR-sGenes: Sum stats of 6324/2772 introns/sGenes with permutation *cis*-sQTL in AMR
- ST2-9-AFR-sGenes: Sum stats of 4337/2069 introns/sGenes with permutation *cis*-sQTL in AFR

Table S3. Trimester xQTL summary statistics.

- README
- ST3-1-tri1-eGene: Sum stats of 4211 permutation eGenes in Tri1
- ST3-2-tri2-eGene: Sum stats of 2220 permutation eGenes in Tri2
- ST3-3-tri1-isoGene: Sum stats of 10881/6921 isoforms/isoGenes with permutation *cis*-isoQTL in Tri1
- ST3-4-tri2-isoGene: Sum stats of 4179/3047 isoforms/isoGenes with permutation *cis*-isoQTL in Tri2
- ST3-5-tri1-sGene: Sum stats of 14193/5312 introns/sGenes with permutation *cis*-sQTL in Tri1
- ST3-6-tri2-sGene: Sum stats of 5348/2318 introns/sGenes with permutation *cis*-sQTL in Tri2
- ST3-7-triOnly-biotype: Counts of gene types of tri1 and tri2-only e/sGenes
- ST3-8-triOnly-cellTypeEnrich: Cell type enrichment of tri1 and tri2-only e/sGenes

Table S4. S-LDSC and MESC results.

- README
- ST4-1-sLDSC: S-LDSC of background and various brain QTL annotations (e/iso/sQTL, GTEx brain cortex eQTL, tri e/iso/sQTL)
- ST4-2-sLDSC-e/iso/sQTL-joint: S-LDSC jointly running background annotations, and e+iso+sQTL, top enrichment 15 annotations
- ST4-3-sLDSC-e/isoQTL-joint: S-LDSC jointly running background annotations, and e+isoQTL, top enrichment 15 annotations

- ST4-4-MESC: h2med results for all expressed genes/isoforms/introns in the full dataset, and trimester specific datasets

Table S5. isoTWAS and colocalization.

- README
- ST5-1a-isoTWAS-preFOCUS: isoTWAS statistics of isoforms that are permutation significant
- ST5-1b-isoTWAS-finemapped: isoTWAS statistics of isoforms that are in 90% FOCUS credible sets
- ST5-2 to ST5-29: eCAVIAR significant colocalization results for various neuropsychiatric GWAS and fetal brain QTLs
- ST5-30: MRLOCUS summary statistics

Table S6. Network analyses.

- README
- ST6-1-Module-Genes: Membership of genes and transcripts to each of the modules
- ST6-2-All-Enrichment: Compiled module enrichment data from ST6-3, ST6-4, and ST6-5
- ST6-3-Cell-Enrichment: Cell type enrichment of modules using Polioudakis fetal brain marker genes
- ST6-4-Common-Enrichment: Common variation enrichment of modules using sLDSC and MAGMA
- ST6-5-Rare-Enrichment: Rare variation enrichment of modules using logistic regression
- ST6-6-Module-Overlap: Overlap of fetal modules with other fetal modules in the dataset or modules from Walker et al. (walker_), Werling et al. (werling_), and Li et al. (li_)

Table S7. CellWalker and module interacting eQTL summary statistics.

- README
- ST7-1-CellWalker-single-label: CellWalker mapping of bulk eQTL SuSiE results to single cell type labels. Corresponds to Fig 7A
- ST7-2-CellWalker-ML-strict: CellWalker mapping of bulk eQTL SuSiE results to multi-level ("ML") cell type labels. Filtered for number of cell types. See methods for details